

Theoretical and Experimental Investigation of the Thermodynamics
of the Thermally Choked Ram Accelerator

by
Carl Knowlen


A dissertation submitted in partial fulfillment
of the requirements for the degree of

Doctor of Philosophy

University of Washington

1991

Approved by



(Chairperson of Supervisory Committee)

Program Authorized
to Offer Degree

Aeronautics and Astronautics

Date

April 10, 1991

Doctoral Dissertation

In presenting this dissertation in partial fulfillment of the requirements for the Doctoral degree at the University of Washington, I agree that the Library shall make its copies freely available for inspection. I further agree that extensive copying of this dissertation is allowable only for scholarly purposes, consistent with "fair use" as prescribed in the U.S. Copyright Law. Requests for copying or reproduction of this dissertation may be referred to University Microfilms, 300 North Zeeb Road, Ann Arbor, Michigan 48106, to whom the author has granted "the right to reproduce and sell (a) copies of the manuscript in microform and/or (b) printed copies of the manuscript made from microform."

Signature _____

Date _____

University of Washington

Abstract

**Theoretical and Experimental Investigation of the Thermodynamics
of the Thermally Choked Ram Accelerator**

by Carl Knowlen

Chairperson of the supervisory Committee: Professor Abraham Hertzberg
Dept. of Aeronautics and Astronautics

A Hugoniot analysis of the quasi-one-dimensional ram accelerator propulsive modes is presented which relates the thermodynamic properties of the stationary propellant gas to the end state conditions that exist after projectile passage. In general, a ram accelerator propulsive mode is any adiabatic aerothermodynamic cycle established by the interaction of a subcaliber projectile traveling supersonically through a gaseous combustible mixture in a stationary tube. The quasi-steady theoretical approach determines the differences between the inlet and outlet properties of a supersonic propellant gas that enters a control volume with a specified mass and momentum flux, and then leaves the control volume with the same mass flux, a new chemical composition, and a different momentum flux. Regions of potentially accessible thermodynamic end states were identified, which indicate that there are no fundamental reasons why a properly shaped projectile cannot operate at or above the Chapman-Jouguet detonation velocity.

Consequences of operating a ram accelerator propulsive cycle that results in the flow being in chemical equilibrium at the thermal choking point are that the net thrust and heat release become independent, to a high degree, of projectile geometry. The velocity

and acceleration histories predicted by the Hugoniot analysis for the thermally choked ram accelerator cycle are shown to correlate very well with the experiments. Theoretical predictions for the pressure at the thermal choking point match the tube wall pressure data, collected from behind the combustion zone at the projectile base, up to the C-J velocity of the propellant mixture. The good agreement between theory and experiment for their performance profiles and choke point pressures strongly supports the assumption that projectiles are accelerated with a thermally choked propulsive cycle while they are operating in the subdetonative velocity regime.

TABLE OF CONTENTS

	Page
List of Figures	v
List of Tables	vii
Nomenclature	viii
Chapter 1: Introduction	1
1.1 Conventional Supersonic Airbreathing Ramjet	2
1.2 General Ram Accelerator Concept	4
1.3 Subsonic Combustion Ram Accelerator Propulsive Modes	5
1.4 Theoretical Approach	8
Chapter 2: Global Model of the Ram Accelerator Process	11
2.1 Ram Accelerator Hugoniot	15
2.2 Generalized Raleigh Flow	23
2.3 Sonic Point Along Ram Accelerator Hugoniot	27
2.4 Generalized Fanno Flow	30
2.5 Mach Number Limits of Ram Accelerator Operation	34
2.6 Discussion of Ram Accelerator Hugoniot Analysis	37
2.7 Mach Number Effects on Impulse of TCRA Propulsive Cycle.....	40
2.7.1 Iterative Method for Impulse.....	41
2.7.2 Analytical Solution for Impulse.....	42
Chapter 3: Detailed Model of Thermally Choked Ram Accelerator Flowfield.....	46
3.1 Ideal TCRA Propulsive Cycle	47

3.2	Discussion of Thermally Choked Propulsive Cycles	51
3.3	Component Models of the Detailed TCRA Flowfield	53
3.3.1	Base Total Pressure Drop	55
3.3.2	Diffuser Total Pressure Drop	56
3.3.3	Normal Shock Location	58
Chapter 4:	Experimental Facility	62
4.1	Ram Accelerator Test Section Instrumentation	65
4.1.1	Electromagnetic Sensors	66
4.1.2	Pressure Transducers	66
4.1.3	Optical Fiber Probes	67
4.2	Propellant Gas handling Procedures	68
4.2.1	Propellant Gas Mixing	68
4.2.2	Gas Handling Procedure for Experiments	70
4.3	Experimental Projectile Configuration	71
4.3.1	Nose Cone	71
4.3.2	Body Configuration.....	73
4.4	Data Reduction Technique	74
Chapter 5:	Experimental Results and Discussion	81
5.1	Performance Profiles of TCRA Propulsive Mode.....	83
5.2	Sensor Data from Coaxial Instrumentation Ports.....	90
5.2.1	Identification of Thermal Choking Point	94
5.2.2	Pressure Profile of Detailed TCRA Flowfield	95
5.2.3	Discussion of Experimental and Theoretical Pressure Profiles	97

5.3	Pressure-Velocity Profiles in Ram Accelerator	99
5.3.1	Throat Pressure Ratio vs Velocity	99
5.3.2	Experimental Pressure Ratios at Thermal Choking Point	101
5.3.3	Peak Combustion Pressure Ratio vs Velocity	103
5.3.4	Normal Shock Location vs Velocity	105
Chapter 6:	Summary and Conclusions	110
	Bibliography	114
Appendix A:	Derivation of Experimental Uncertainty Relations	119

LIST OF FIGURES

Number		Page
1.1	Schematic of supersonic airbreathing ramjet	2
1.2	Schematic of mechanically choked ram accelerator propulsive mode	6
1.3	Schematic of thermally choked ram accelerator propulsive mode	7
2.1	Control volume for general ram accelerator process	14
2.2	Regions of allowable end states in P-V plane	19
2.3	Effects of impulse generation on RA Hugoniots	22
2.4	Generalized Raleigh lines in P-V plane	25
2.5	Generalized Fanno curves in P-V plane	32
2.6	Comparison of iterative and analytical impulse-Mach number profiles	44
3.1	Schematic of detailed TCRA flowfield model	47
3.2	P-V cycle of TCRA mode at maximum thrust Mach number	48
3.3	P-V cycle of TCRA mode at $M_1=4.65$	50
3.4	Diffuser and base total pressure ratio-velocity profiles	58
3.5	Effect of component total pressure loss on normal shock location	60
4.1	Schematic of ram accelerator test facility	63
4.2	Schematic of experimental projectile	72

4.3	Experimental data from coaxial EM sensors	76
4.4	Relative uncertainty in velocity and acceleration measurements	79
5.1	Time-distance profile of experiment and global TCRA theory	84
5.2	Velocity-distance profile of experiment and global TCRA theory	86
5.3	Acceleration-velocity profile of experiment and global TCRA theory	87
5.4	Impulse-Mach number profile for 3 experiments and global TCRA theory	89
5.5	Pressure, EM and luminosity data from coaxial instrumentation ports	91
5.6	Experimental and theoretical throat pressure ratio vs velocity.....	100
5.7	Experimental and theoretical thermal choke point pressure ratio.....	102
5.8	Experimental peak combustion pressure ratio vs velocity	104
5.9	Experimental and theoretical normal shock location vs velocity	106

LIST OF TABLES

Number		Page
2.1	C-J Detonation Parameters of Various Mixtures.....	42
5.1	Variations in Experimental Parameters.....	88

NOMENCLATURE

A	tube cross-sectional area
c	acoustic speed
c_p	constant pressure specific heat capacity
F	thrust
H	static enthalpy normalized to initial static enthalpy (h_1)
h	static enthalpy
h_f	enthalpy of formation at 0 degree Kelvin
I	impulse $I=F/(p_1A)$
M	Mach number
m_p	projectile mass
P	pressure normalized to fill pressure (p_1)
P_f	pressure ratio along generalized Fanno curves
p	static pressure
p_t	total pressure
Q	non-dimensional heat parameter $Q=(h_{f1}-h_{f6})/(c_{p1}T_1)$
s	entropy
T	static temperature

t	time coordinate
u	projectile velocity
\bar{u}	mean velocity between instrument stations
V	specific volume normalized to initial specific volume (v_1)
v	specific volume
\bar{x}	average separation distance of instrument stations
\ddot{x}	acceleration
\ddot{x}_0	average acceleration between instrument stations

Greek Symbols

χ	grouping of terms involving M_1 and Q (defined for Eq. 3.1)
Φ	grouping of terms involving M_6 (defined for Eq. 2.24)
γ	specific heat ratio

ACKNOWLEDGMENTS

I would like to express my deepest appreciation to Professor Abraham Hertzberg for his dauntless support and imaginative ideas that have made my years as a graduate student very stimulating. Professor Adam Bruckner has been an excellent mentor and his thorough review of this manuscript was very helpful. Thanks to Professor Tom Mattick for also reviewing my dissertation and for his wonderful "black boxes" which have enhanced our ability to collect data. David Bogdanoff has provided me with superb tutelage in all manners of engineering science and experimental techniques, it is much appreciated. The assistance of Jian-guo Li in reducing data and conducting experiments has been a great help. I would also like to thank the machinists Malcolm Saynor, Dennis Peterson and Bill Lowe for their patience and advice over the years.

Not enough can be said about the tireless effort and attention to detail that the senior graduate students Edward Burnham, Alan Kull and Gilbert Chew have brought to the experiments. The diligence of the group of good-natured graduate students who have conducted the high-speed (~2500 m/sec) experiments is of high merit, thank-you all: Jackie Auzias de Turenne, Barbrina Dunmire, John Hinkey, Amy Prochko, Robert McIntosh, Matthew Jardin, Andrew Berschauer, Erik Christofferson, Peter Kaloupis, Al Alvares, Kelly Scott and Dai Morakami. In the days when 2000 m/sec just a gleam in our eyes, Dean Brackett and Dale Barr worked incredibly hard to help shake down the operating procedures for ram experimentation. The legacies of Carl Englebreck and Ivan Stonich are still around the lab, these graduate students contributed immensely to the construction of the original facility. I would also like to acknowledge Keith McFall, he has participated in everything from the sand bucket brigades to ignitor testing, and his reviewing of publications and theoretical modeling is much appreciated.

Ramo Ergo Sum

For my sons,
Myzar and Aerial

CHAPTER 1

INTRODUCTION

A concept for accelerating projectiles through a tube filled with a gaseous combustible mixture, known as the "ram accelerator," is being developed at the University of Washington. Ram accelerator propulsive cycles have the potential to accelerate a relatively low speed projectile to near orbital velocities as it travels through a stationary tube, utilizing only the heat evolved from combustible propellant mixtures. The basic principle involves combustion processes which release energy around and/or behind the projectile; however, there are no propellants carried aboard the projectile as there are with a rocket. Energy releasing processes are constrained to travel with the projectile which enable the ram accelerator concept to propel a projectile with high ballistic efficiency* as it is operating at very high velocities. Projectiles are accelerated by aerothermodynamic propulsive cycles similar to those of conventional supersonic airbreathing ramjets using either subsonic or supersonic combustion.¹ Brief descriptions of the subsonic combustion ram accelerator propulsive modes are presented in this chapter along with a comparison with the propulsive cycle of the conventional supersonic airbreathing, subsonic combustion ramjet. Descriptions of the ram accelerator modes involving oblique detonation and supersonic combustion processes can be found in the cited references 1-6. The focus of this dissertation is on the theoretical aspects of the

* Ballistic efficiency is defined here as the ratio of the rate of change of kinetic energy to the rate of chemical energy release. This is an instantaneous efficiency that varies as the projectile velocity increases.^{1,2}

subsonic combustion mode of ram acceleration utilizing thermal choking of the reacted propellant mixture and how the theory correlates with the results of current experimental investigations.

1.1 Conventional Supersonic Airbreathing Ramjet

The gasdynamic principles of the ram accelerator propulsive modes utilizing subsonic heat addition processes are similar to those of a conventional supersonic ramjet with subsonic combustion. Shown in Fig. 1.1 is the schematic of a representative airbreathing ramjet configuration which consists of a straight-walled outer cowl and an internal centerbody comprising a conical supersonic diffuser, a constant area combustion

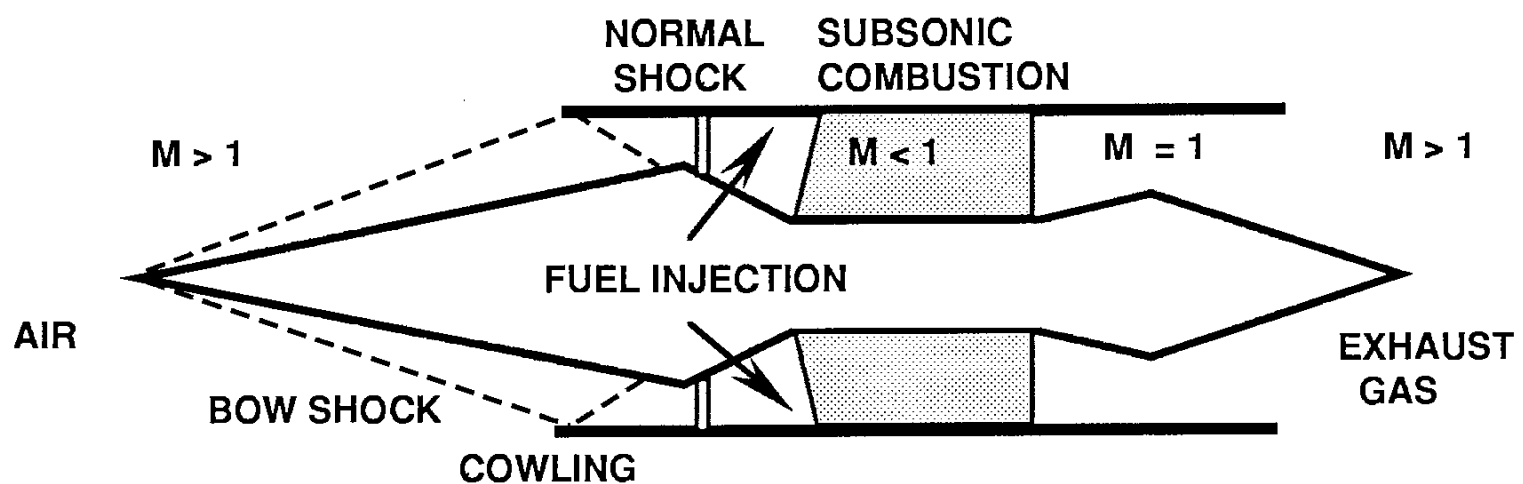


Fig. 1.1 Schematic of supersonic airbreathing ramjet.

section and a convergent-divergent nozzle. This configuration was chosen for illustration purposes because of its similarity to the in-tube-ramjet analogy of the ram accelerator concept.³⁴ The performance of such a ramjet configuration flying through the atmosphere can be readily calculated.^{7,8} Supersonic air is first compressed by the conical shock system generated by the area contraction of the diffuser and then passed through a normal shock before expanding subsonically into the combustion section. Fuel is carefully injected and mixed with the ram compressed air and the combustion is stabilized behind flame-holding recirculation zones. The subsonic exhaust gas is then mechanically choked by the nozzle throat and re-expanded supersonically back to ambient conditions. Choking of the flow at the nozzle throat maintains subsonic flow throughout the combustion region by stabilizing the normal shock on the rear half of the diffuser.

Fixed geometry ramjets with subsonic combustion can operate effectively in the Mach number range of about 3-6.⁸ The lower Mach number limit is determined by the minimum incoming mass flow rate that the fixed diffuser geometry can accept, and the upper Mach number limit primarily results from the inefficiencies of diffusing gas flows having a high supersonic velocity and the temperature limitations of the materials lining the interior flow passages.⁸ The high static temperature of the burned fuel-air mixture also limits the high Mach number performance of the ramjet because of the severe dissociation losses in the combustor.¹⁹ The thrust generating ability of the ramjet is limited by the oxygen content of the atmosphere and its density, whereas the velocity range of operation is limited by the speed of sound of the incoming air which, in turn, is fixed by both the composition and temperature of the atmosphere at the flight altitude.

1.2 General Ram Accelerator Concept

In general, a ram accelerator propulsive mode is defined as any adiabatic aerothermodynamic cycle established by the interaction of a supersonic projectile with a stationary gaseous propellant mixture and a tube wall. The net result of such cycles is to produce a change in the static pressure and momentum flux (with respect to the projectile) of the propellant mixture after it reacts, returns to the full tube area and ceases to communicate with the projectile. Supersonic projectiles influence the stationary propellant mixture with shock waves, area variations and heat addition as the result of chemical reactions.* The geometric configuration and the velocity of the projectile determine the history of thermodynamic states that the propellant gas undergoes as it passes around the projectile. The desired effect of any ram accelerator propulsive cycle is to generate a high pressure and high temperature exhaust gas which moves away from the projectile at sonic or supersonic velocities relative to the projectile. To prevent expansion waves from overtaking the projectile and affecting the established flow conditions, the exhaust gas must move away from the projectile at velocities greater than or equal to the local acoustic speed.

All ram accelerator propulsive concepts require an initial launcher, such as a conventional powder or light gas gun, to send the projectile into the ram accelerator tube at a prescribed entrance velocity. The straight-walled tube acts as the outer cowling of the conventional ramjet and the projectile has an area profile resembling that of the

* Using electrical energy input from external sources to power an in-tube-ramjet was independently conceived by Wilbur et al. [39] who dubbed their concept the "Electrothermal Ramjet." The non-dimensional formulation of the energy input presented in this dissertation applies to both electrical and chemical heat addition processes.

centerbody of the ramjet. The only propellants required by the ram accelerator are the premixed gaseous fuel and oxidizer mixtures which are loaded in the accelerator tube at the desired pressure level. The acceleration and Mach number histories of the projectile can be tailored by adjusting the fill pressure and the composition of the propellant mixture along the length of the accelerator tube.^{1,9,34} Since the fuel and oxidizer are premixed, the difficulties in obtaining rapid and complete mixing that are encountered in supersonic airbreathing ramjets are circumvented. The cone angle of the projectile is such that the initial conical shocks do not pre-ignite the propellant mixture as the projectile passes through it at supersonic velocities. The combustion process is stabilized in the vicinity of the projectile with either high strength shocks³ or flame holders as described in U.S. Patent No. 4,938,112 [Ref. 34].

1.3 Subsonic Combustion Ram Accelerator Propulsive Modes

Ram accelerator propulsive modes utilizing subsonic heat addition processes require a region of sonic flow (choked) with respect to the projectile to stabilize a shock system that can render the flow subsonic over some part of the projectile. A nozzle formed by the aftbody of the projectile provides the means for choking the reacted subsonic flow in the mechanically choked ram accelerator (MCRA) propulsive mode, shown in Fig. 1.2. The axisymmetric projectile passes through the propellant mixture at supersonic velocities and ram compresses the gas through a series of conical shocks followed by a normal shock. The subsonic flow then reacts around the midbody of the projectile. Combustion is stabilized by flame holders placed at the entrance to its combustor section as in the conventional atmospheric ramjet.¹ The heat release evolved

by the subsonic combustion activity accelerates the flow in the constant area waist section of the projectile, and the area constriction of the nozzle further accelerates the subsonic flow to establish a choked flow condition at the nozzle throat. The exhaust products then supersonically expand back to the full tube area and cease to communicate with the projectile (if the flow is assumed inviscid).

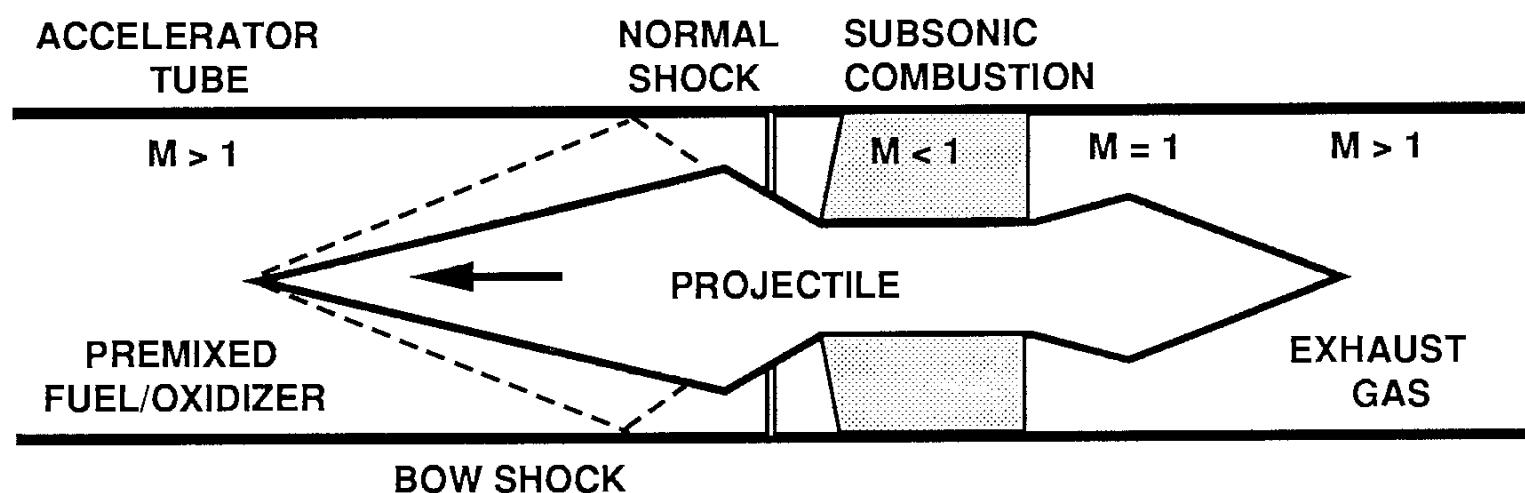


Fig. 1.2 Schematic of mechanically choked ram accelerator propulsive mode.

Another ram accelerator propulsive cycle utilizing subsonic combustion is shown in Fig. 1.3. This mode differs from the MCRA propulsive mode in that the combustion activity occurs at full tube area and releases sufficient chemical energy to thermally choke the flow downstream of the projectile. This aerothermodynamic cycle is referred to as the

thermally choked ram accelerator (TCRA) propulsive mode. Combustion activity is attached to the projectile by the flame-holding ability of the flat base of the projectile, and the thermal choking point isolates the combustion region from expansion waves originating behind the projectile. Because of the relative simplicity of igniting the propellant mixture in the region of interest (behind the projectile)³⁵ and its low minimum operating Mach number limit, the TCRA mode has been the first ram accelerator propulsive mode to be investigated experimentally.^{1,2,11}

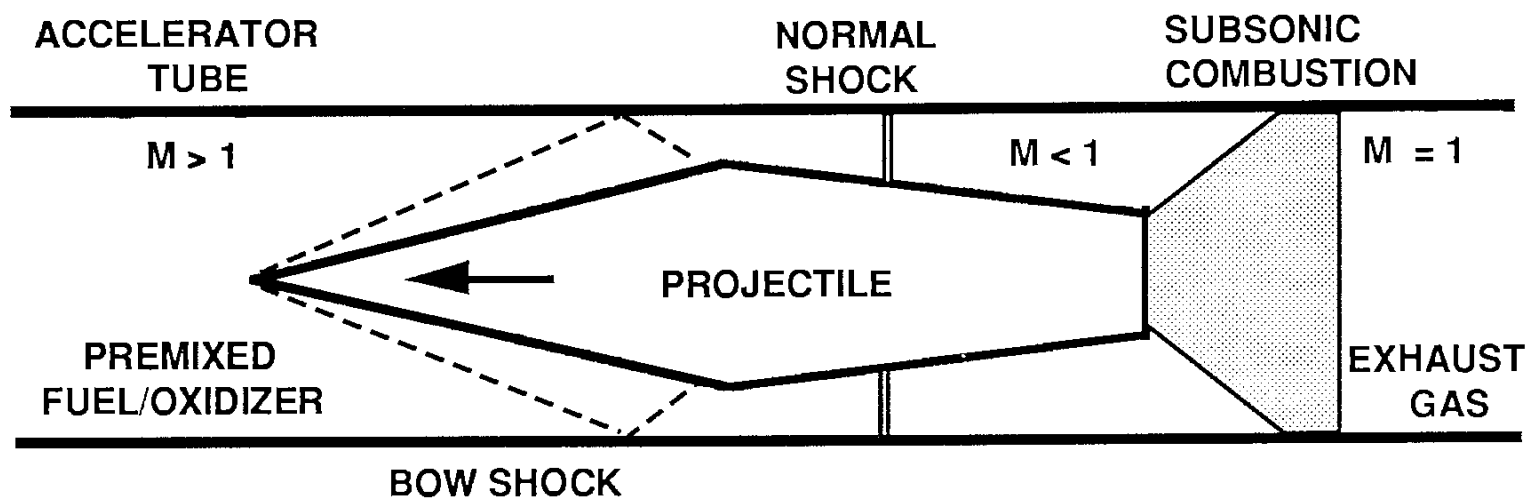


Fig. 1.3 Schematic of thermally choked ram accelerator propulsive mode.

Lower operating Mach number limits of both the MCRA and TCRA propulsive modes are, ideally, those which correspond to the minimum mass flow that the throat of

the conical diffusers can accept. Ideal upper operating Mach number limits are governed by the thermodynamic properties of the propellant gas (heat release and heat capacity) and the nozzle expansion ratio. Actual operating Mach number limits are governed by the manner in which the details of the projectile geometry affect the ignition of the propellant mixture and the flame stabilization processes. For example, projectiles with small throat diameters can accept flows at low Mach numbers, but they have only a limited ability to contain the high pressure region between the normal shock and the choking point; thus, the lower operating Mach number limit is governed by how much heat release the projectile is able to contain rather than how much mass flow it can accept. The experimental upper Mach number limit of projectiles operating in the TCRA propulsive mode is often determined by the pre-ignition of the propellant mixture at one of the reflected conical shock waves or at the normal shock.^{9,11,12} Similar Mach number limiting phenomena can be expected to occur while projectiles are operating in the MCRA propulsive mode. The TCRA propulsive mode has successfully accelerated projectiles in the velocity range of 700 to 2650 m/sec at fill pressures up to 44 atm, and experiments are currently being undertaken at the University of Washington to demonstrate operational capabilities of over 3000 m/sec.^{1,9,13,14}

1.4 Theoretical Approach

Governing equations of the TCRA process are similar to those of a Chapman-Jouguet (C-J) detonation wave. The C-J detonation velocity can be defined as the steady-state velocity at which a supersonic combustion wave travels through a reactive gas mixture with the reaction products moving at sonic velocity with respect to the wave.^{15,16}

The C-J detonation wave problem can be stated as follows: for a given temperature and density of a particular combustible gas mixture, what is the steady-state velocity at which an adiabatic combustion wave front can proceed when the flow behind it reaches chemical equilibrium at sonic velocity relative to the front of the wave? The steady flow restriction requires the momentum of the flow entering and leaving the detonation wave to be equal for a one-dimensional inviscid process. The gasdynamic conservation equations of mass, momentum and energy along with an equation of state provide enough equations to solve for the unknown detonation wave velocity for specified initial conditions of the reactive gas mixture.¹⁵⁻¹⁷

The problem statement for the TCRA propulsive mode can be stated in a similar manner as follows: for a given temperature and density of a particular combustible gas mixture, with a body passing through it at a given velocity, what is the resultant force upon the body when the flow behind it reaches chemical equilibrium at sonic velocity relative to the body? Prescribing the initial velocity for an inviscid, adiabatic one-dimensional flow and the condition of thermal choking at constant area behind the body results in the energy and mass conservation equations being sufficient (along with an equation of state) to solve for the chemical equilibria at the thermal choking point for steady flow conditions. The sum of the static pressure and momentum flux gained by the flow at the thermal choking point is then proportional to the maximum resultant force that can be applied to the body. If the resulting acceleration experienced by a free-flying body is not too high, the flowfield can adjust to the changing projectile velocity fast enough to maintain the end state conditions predicted by the steady flow analysis.⁹ Thus, the thermodynamics of the TCRA process can be analyzed with the governing equations of

the C-J detonation wave problem, if the momentum equation is generalized to allow for non-zero thrust solutions.

A generalized Hugoniot analysis of the overall ram accelerator concept is presented in the global theory section (Chapter 2) which provides insight into the acceleration potential of all ram accelerator propulsive modes. The Hugoniot approach lays the theoretical groundwork for the solution technique to the TCRA problem described above. A detailed quasi-one-dimensional model of the projectile flowfield in the TCRA mode has been developed which determines some of the effects of non-isentropic flow phenomena (Chapter 3). This detailed model incorporates total pressure losses between various flow regions of the projectile and provides a first order look at the effects on the pressure field and normal shock location due to diffuser shocks and sudden flow area expansion at the base. A description of the ram accelerator experimental facility and the accompanying instrumentation is presented in Chapter 4, along with an error analysis of the experiments. In Chapter 5 the results from several representative experiments are compared with the acceleration and velocity predicted by the ram accelerator Hugoniot theory for the TCRA propulsive mode. In addition, the experimental pressure versus velocity histories measured at various points about the projectile are compared with those determined by the detailed TCRA flowfield model.

CHAPTER 2

GLOBAL MODEL OF THE RAM ACCELERATOR PROCESS

The fundamental thermodynamic properties and the one-dimensional performance potential of all possible ram accelerator propulsive modes can be determined in a general manner. This theoretical approach is inviscid, with the stationary propellant mixture transformed to a reference frame where it is a quasi-steady* supersonic flow passing around a stationary projectile that is centered in a straight-walled tube. In the projectile reference frame, a ram accelerator propulsive mode is any adiabatic aerothermodynamic cycle established by the interaction of the projectile and tube wall with the incoming supersonic flow of a reactive gas mixture. The net result of such cycles is to produce a change in the stream thrust (defined here as the sum of the momentum flux and static pressure) of the propellant mixture after it reacts and returns to the full tube area. The increase in the stream thrust of the reacted propellant gas, after it passes over the projectile and ceases to communicate with it, corresponds to the maximum amount of force that can be applied to accelerate the projectile.⁷

Ram accelerator propulsive modes operating in a quasi-steady manner can be characterized in 1-D channel flow by the area ratio at which the heat addition process

* The condition of quasi-steady flow assumes that the flowfield about the projectile can adjust on a time scale much smaller than the time scale at which the flow is changing velocity. Thus, the instantaneous flowfield about an accelerating projectile is assumed to be that predicted from the analysis of a projectile traveling at the corresponding steady flow velocity.

occurs, the flow Mach number after heat addition, and the final Mach number of the exhaust gas when it reaches full tube area. If all the heat addition occurs in the flow region between the sides of the projectile and the tube wall, the flow will eventually expand back to full tube area at supersonic velocities (if the back pressure is sufficiently low). If the flow remains supersonic throughout the heat addition process, such as in the supersonic combustion and oblique detonation modes of operation,^{4,18} then the exit Mach number of the gas will increase continuously with respect to the projectile as the Mach number of the incoming flow increases.

Supersonic projectiles can have a region of subsonic heat addition if there is a point where the flow is choked after the heat addition zone. In the detailed theoretical models of the MCRA and TCRA propulsive modes, the transition of the flow from supersonic to subsonic velocity is assumed to occur across a single normal shock, whose strength is determined by the mass flux requirement of the choking point. A nozzle provides the means for choking the reacted subsonic flow in the MCRA propulsive mode (Fig. 1.2). For inviscid, chemically frozen flow through an isentropic nozzle, the throat-to-tube area ratio governs the exhaust Mach number of the flow and results in a constant exit Mach number for the operating velocity range of this propulsive cycle, if the specific heat ratio of the burned propellant gas is also assumed to be constant at all flight Mach numbers. The minimum area expansion ratio of a nozzle for the choked flow stabilized ram accelerator propulsive modes is unity, which corresponds to a propulsive cycle that constrains the final part of the heat addition process to occur at full tube area followed by a region of thermal choking (Fig. 1.3). The TCRA propulsive mode has a subsonic combustion zone which releases sufficient chemical energy to thermally choke the flow behind the projectile at full tube area. Thermal choking of the flow stabilizes a normal

shock system on the projectile, and the thermal choking point isolates the combustion zone from expansion waves originating behind the projectile.

Thermodynamic properties of the end state gas resulting from all quasi-one-dimensional ram accelerator processes can be determined from the differences in the properties of a supersonic gaseous propellant mixture that enters a control volume (shown in Fig. 2.1), with a specified mass and momentum flux, and leaves the control volume with a different chemical composition at some sonic or supersonic velocity with the same mass flux but different momentum flux. Since the inviscid flow does not exchange momentum with the straight tube walls, there must be a body within the control volume to absorb the changes in momentum. Restriction to steady flow implies that the position of the body relative to the tube is held fixed in a manner that does not disturb the flow about the body.²⁰ Details of the flowfield around the body, such as the oblique and normal shock systems, area contours and heat addition zones are not included in this analysis. The body is assumed to be configured in a manner that induces the flow to go from its original supersonic condition to a chemically reacted state traveling away from the body at or above the local speed of sound when the flow reaches full tube area again. Details of potential body configurations will be discussed later.

Since there are not any length scales associated with the quasi-one-dimensional flow processes occurring within the control volume, the arbitrary ram accelerator processes can be viewed as thin supersonic combustion waves across which the composition and thermodynamic properties of the flow change abruptly. The "global" properties of these ram accelerator waves are independent of body geometry and represent only the limiting performance potential of a given ram accelerator process. Actual performance limitations are determined by the details of the body configuration

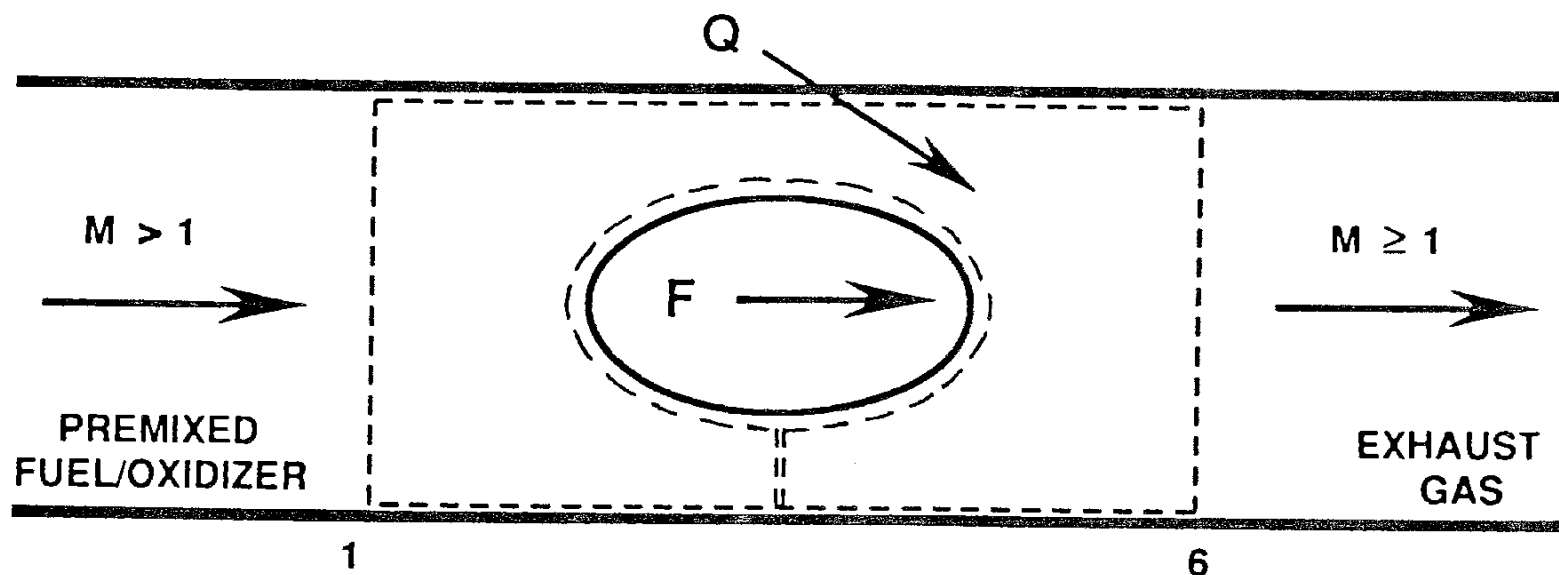


Fig. 2.1 Control volume for the general ram accelerator process.

and the chemical kinetic rates of the propellant gas. From the laboratory reference frame, the ram accelerator wave is seen to accelerate down the stationary tube at a rate proportional to the force exerted on the control volume by the change in stream thrust of the flow.

Variations in the thermodynamic properties of the end states of a general ram accelerator process, with respect to changes in the mass flux of the flow (i.e., entrance Mach number), are determined as a succession of quasi-steady solutions. These solutions do not account for the unsteady effects of the time rate of change of the mass, momentum and energy flux experienced by the accelerating body; however, the unsteady effects may be assumed to be negligible in the situation of a gradual rate of change of mass flux.⁹ The analysis proceeds as if the control volume and body were fixed in the test section of a blow-down supersonic wind tunnel capable of delivering the propellant mixture at the

appropriate flow velocity and enthalpy that would be experienced by a body traveling at the same velocity in the stationary gas. With such an ideal experimental apparatus, the pressure and temperature profiles around a given body and the resultant forces upon it can be measured at a given mass flux and correlated with quasi-steady theoretical models. Applicability of the quasi-steady analysis to unrestrained and accelerating projectiles is demonstrated for the TCRA propulsive mode by the close agreement in the velocity-distance profiles of experiments with those predicted by theory while the projectile is operating below the C-J detonation velocity.

2.1 Ram Accelerator Hugoniot

Analysis of the thermodynamics of the general ram accelerator process proceeds in a manner similar to that used for conventional one-dimensional shock and detonation waves.^{15-17,20} The conservation equations of gasdynamics are applied across the control volume shown in Fig. 2.1, which consists of an entrance plane, an exit plane and side walls to which an arbitrary body is attached. The gaseous propellant mixture, both before and after combustion, is assumed to behave as an ideal gas with temperature dependent heat capacities. Jump conditions across the control volume for the mass, energy, and momentum conservation equations are:

$$\frac{u_1}{v_1} = \frac{u_6}{v_6} \quad (2.1)$$

$$h_1 + \frac{u_1^2}{2} + h_{f1} = h_6 + \frac{u_6^2}{2} + h_{f6} \quad (2.2)$$

$$p_1 + \frac{u_1^2}{v_1} + \frac{F}{A} = p_6 + \frac{u_6^2}{v_6} \quad (2.3)$$

where v is the specific volume, u is the flow velocity, h is the static enthalpy, h_f is the enthalpy of formation for the gas mixture (at zero degrees Kelvin), p is the static pressure, A is the cross sectional area of the tube, and F is the axial force exerted on the flow by the body within the control volume. Final states (6) of the flow allowable from any initial state (1) in the pressure-specific volume plane are determined from this system of equations for any steady flow process (i.e., ram accelerator propulsive cycle) that occurs within a straight-walled tube. This includes processes involving chemical reactions that occur in a region of reduced flow area, somewhere within the control volume, which eventually result in a change in the momentum flux when the flow is brought back to the original flow area (such as in the supersonic combustion and the MCRA propulsive modes).

Initial and final flow velocities may be written in terms of a non-dimensional thrust parameter or 'impulse' defined as: $I = F/(p_1 A_1)$, and the initial and final propellant gas pressure and specific volume by combining the mass and momentum equations to yield:

$$u_1^2 = v_1^2 \left[\frac{p_6 - p_1(I+1)}{v_1 - v_6} \right] \quad (2.4)$$

$$u_6^2 = v_6^2 \left[\frac{p_6 - p_1(I+1)}{v_1 - v_6} \right] \quad (2.5)$$

Substituting the above expressions for the flow velocities into the energy equation and rearranging terms provides the ram accelerator Hugoniot equation for steady flow:

$$h_6 - h_1 = h_{f1} - h_{f6} + \frac{v_1 + v_6}{2} (p_6 - p_1(I + 1)) \quad (2.6)$$

This equation has the impulse (I) as a parameter and is completely independent of the choice of the equation of state or of the process occurring between stations 1 and 6 for steady flow. All of the quasi-steady ram accelerator propulsive cycles have end states that lie on a ram accelerator Hugoniot curve. The state of the propellant mixture at full tube area, after it is processed by any combination of area contractions and variable area heat interactions, is uniquely determined by the total amount of heat evolved from chemical reactions, the resultant non-dimensional force acting upon the projectile body, and the exiting gas velocity of the flow.

For an ideal gas, the pressure and specific volume are related to the constant pressure heat capacity (c_p) and temperature (T) as follows:

$$pv = \frac{\gamma - 1}{\gamma} c_p T \quad (2.7)$$

where γ is the ratio of specific heat capacities. Defining a non-dimensional heat parameter as: $Q = (h_{f1} - h_{f6}) / c_{p1} T_1$, and normalizing the intensive thermodynamic variables at station 6 to those of station 1, allows the ram accelerator Hugoniot to be put into a non-dimensional form for an ideal gas as follows:

$$H - 1 = Q + \frac{\gamma_1 - 1}{2\gamma_1} (V + 1)(P - (I + 1)) \quad (2.8)$$

where $H = h_6/h_1$, $P = p_6/p_1$ and $V = v_6/v_1$. By expressing the enthalpy ratio in terms of P , V and the specific heat ratios, further algebraic manipulation of Eq. 2.8 results in the following expression for the pressure ratio of the combustion products leaving the control volume:

$$P = \frac{\frac{2\gamma_1}{\gamma_1 - 1} (Q + 1) - (V + 1)(I + 1)}{V \left(\frac{2\gamma_6}{\gamma_6 - 1} - 1 \right) - 1} \quad (2.9)$$

In the derivations of Eqs. 2.8 and 2.9 the gas is assumed to be calorically perfect before and after combustion (i.e., $h_1(T_1) = c_{p1}T_1$ and $h_6(T_6) = c_{p6}T_6$); thus, the specific heat ratios must be determined in a manner consistent with this assumption for the highest degree of accuracy. Equation 2.9 represents the locus of end states of an arbitrary one-dimensional flow process in which heat is added by chemical reactions and momentum is gained or lost. The detonation Hugoniot is recovered from this equation when the momentum change is zero, and the normal shock Hugoniot results when both I and Q are set equal to zero.

Allowable regions of possible thermodynamic end states that an arbitrary ram accelerator process may produce are indicated in Fig. 2.2 for a propellant mixture having a constant specific heat ratio ($\gamma_1 = \gamma_6 = 1.4$), and a non-dimensional heat parameter value of $Q = 6$. The one-dimensional gasdynamic conservation equations constrain the

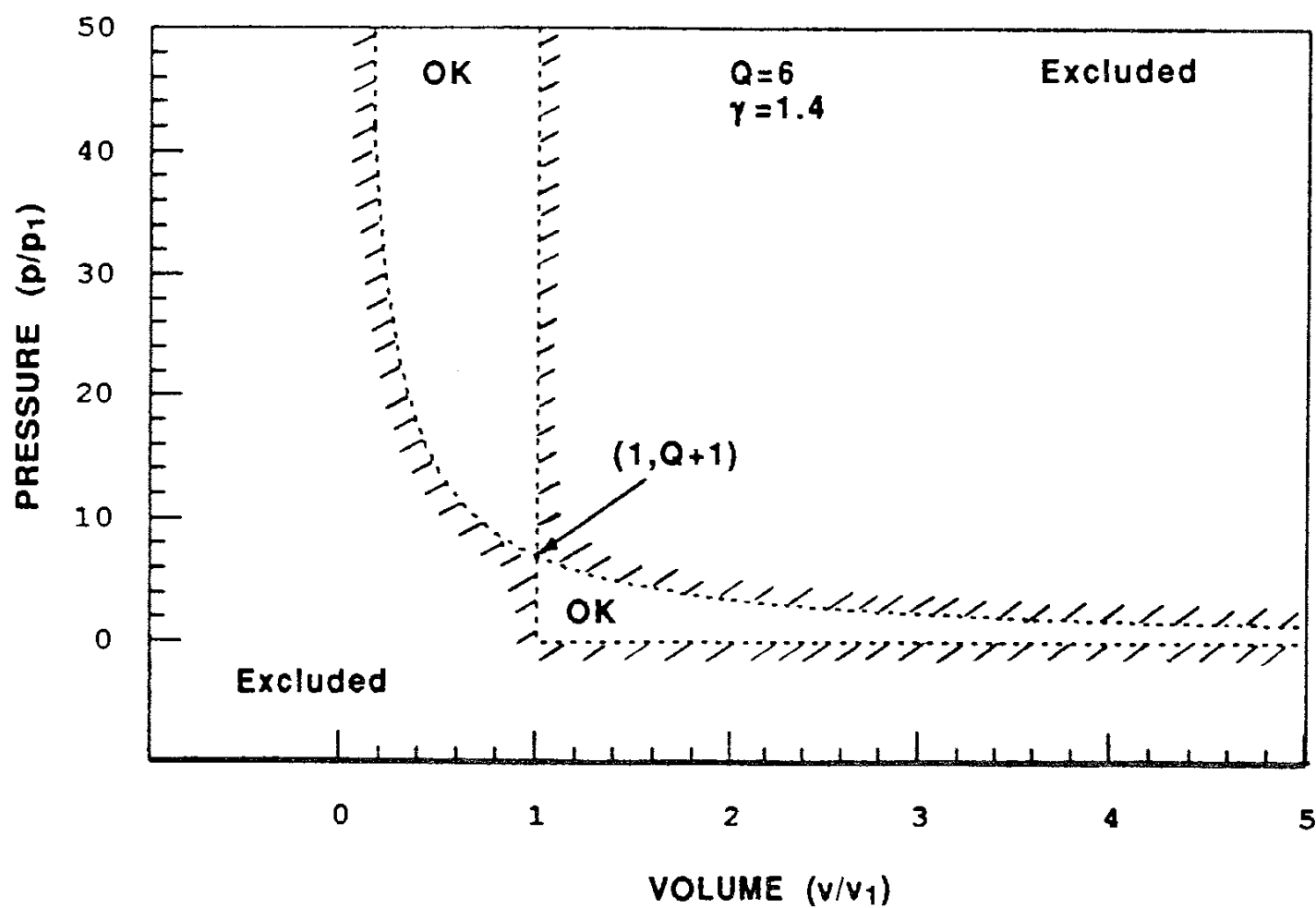


Fig. 2.2 Regions of allowable end states in the pressure-specific volume plane for an arbitrary ram accelerator process

end states produced by a ram accelerator propulsive cycle, operating in the specified propellant mixture, to lie within the boundaries indicated, regardless of the amount of impulse generated. As the denominator of Eq. 2.9 approaches zero, the pressure ratio (P) approaches infinity, just as in a 1-D shock or detonation wave, and the specific volume ratio tends to a finite limit: $V_{\min} = (\gamma_6 - 1) / (\gamma_6 + 1)$. This is the minimum specific volume (maximum compression) ratio possible for processes involving heat and momentum interaction with a steady flow that enters and leaves the control volume with the same mass flux.

The necessity of having positive values for the squares of the entrance and exit velocities (Eqs. 2.4 and 2.5) constrains the end state pressure ratio to be greater or less than the quantity $I+1$, when the end state specific volume ratio decreases or increases, respectively. A curve is shown in Fig. 2.2 that divides the P-V plane into two regions on each side of the $V=1$ line, all points within the regions indicated as "OK" are accessible end states for a ram accelerator process. This bounding curve can be determined in the P-V plane by setting $I+1=P$ in Eq. 2.9 and solving for the limiting value of the pressure ratio (P_{lim}) as a function of Q , V and the specific heat ratios, which results in the following expression:

$$P_{lim} = \frac{\gamma_1}{\gamma_6} \frac{\gamma_6 - 1}{\gamma_1 - 1} \frac{Q + 1}{V}$$

This is the equation for a hyperbola that asymptotically approaches the $P=0$ and $V=0$ lines. When the end state specific volume is less than one, the hyperbola forms the leftmost boundary of allowable end states in the P-V plane up to the point where it intersects the $V=V_{min}$ line. On the right hand side of the $V=1$ line, the bounding hyperbola represents the maximum pressure ratio that can result from a ram accelerator process that increases the specific volume of the propellant mixture.

The singularities that exist in Eqs. 2.4 and 2.5, when there is a constant specific volume heat addition process involved, result in the $V=1$ line being the asymptotic limit for infinite mass flux. This asymptote applies for all ram accelerator Hugoniot except the one which results in an end state pressure ratio of $P=I+1$. The impulse which

characterizes this particular Hugoniot is found from Eq. 2.9, and it can be shown to depend on the properties of the propellant mixture as follows:

$$I = \frac{\gamma_1(\gamma_6 - 1)}{\gamma_6(\gamma_1 - 1)}(Q + 1) - 1 \quad (2.10)$$

Note that this relation indicates that $I = Q$ for a constant γ gas. Thus, the P-V plane can be divided into two different regions of allowable states, each of which include the point $(1, Q+1)$ in their respective sets (Fig. 2.2). The existence of a point in the P-V plane where the zero of the numerator, in the equation for the pressure ratio along the ram accelerator Hugoniot (Eq. 2.9), cancels the pole at its intersection point with the $V=1$ line implies that, in principle, it is possible to continuously operate a ram accelerator process from one side of the constant specific volume line to the other. This can happen only if the net impulse generated by the propulsive cycle was equal to that determined by Eq. 2.10 under conditions which result in a constant specific volume end state.

Ram accelerator Hugoniots are represented in the P-V plane by contours of constant heat release (Q) and constant impulse (I), as shown in Fig. 2.3. The composition of the end state gas and the amount of heat release are determined by the conditions at which the propellant mixture combusts. Displaying the P-V relations of the propellant as if it always achieved the same chemical equilibria (constant Q) provides a relatively straightforward way to compare the effects of different ram accelerator propulsive cycles operating in the same propellant gas. Each ram accelerator Hugoniot contour represents the end states of a variety of ram accelerator propulsive cycles that generate the same level of impulse for the given amount of heat release. The P-V history

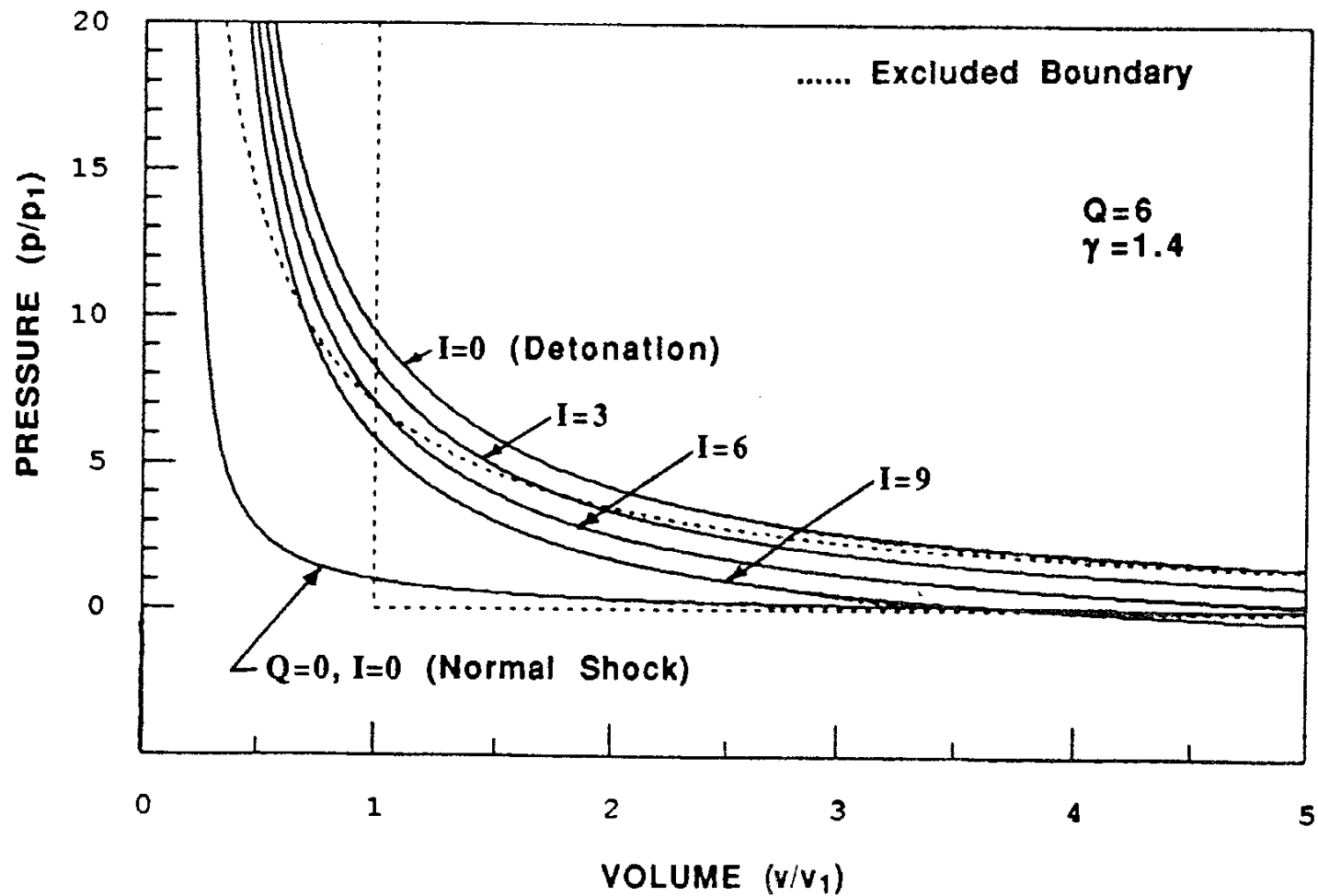


Fig. 2.3 Effects of impulse generation on ram accelerator Hugoniot curves of a given propellant mixture.

of the end states of a particular propulsive cycle can be determined by connecting the points along the different Hugoniot curves which indicate the end states that are generated by the propulsive cycle, as it accelerates a projectile through the propellant gas. (This point will be elaborated on in Sec. 2.4)

Three ram accelerator Hugoniot curves ($I=3$, $I=6$, $I=9$), based on the same amount of heat release ($Q=6$), have been plotted in Fig. 2.3 along with the normal shock ($I=Q=0$) and detonation ($I=0, Q=6$) Hugoniot curves to illustrate the effects of momentum change. The

propellant mixture is assumed to have a constant specific heat ratio ($\gamma_1 = \gamma_6 = 1.4$) and a heat release parameter of $Q=6$ for these sample cases. The boundaries for the regions of allowable end states are also included. End state pressure ratios of the ram accelerator process tend to decrease as more impulse is generated in a propellant mixture having a given amount of heat release. It is apparent from Fig. 2.3 that ram accelerator Hugoniot curves characterized by values of impulse greater and less than the value of the non-dimensional heat parameter have portions of their curves lying within the allowable end state regions. The portions of the curves that are in the excluded regions of the P-V plane represent end states that are impossible to attain for a ram accelerator propulsive cycle using a propellant mixture having the specified Q . It will be shown in the following sections that additional portions of the ram accelerator Hugoniot curves can be eliminated as possible end states of a ram accelerator process by further consideration of the governing conservation equations.

2.2 Generalized Rayleigh Flow

A steady transformation from state 1 to state 6 of a truly one-dimensional flow is restricted to occur through states which lie on a straight line connecting the initial and final conditions in the P-V plane. The equation for this line is determined from the mass and momentum conservation equations (with $I=0$) and is commonly referred to as the *Rayleigh line*. End states of a steady flow that is acted upon by an intermediate process that changes its momentum before allowing the flow to continue in the same direction with the same mass flux lie along a straight line in the P-V plane that will be referred to as the "generalized Rayleigh line." The equation for this line has the impulse (I) as a parameter and is given by the following:

$$P_r = I + 1 + \gamma_1 M_1^2 (1 - V) \quad (2.11)$$

where the subscript 'r' designates the pressure ratio along a generalized Rayleigh line and M_1 is the Mach number of the flow entering the control volume.

All quasi-steady ram accelerator propulsive cycles that are modeled with the 1-D control volume shown in Fig. 2.1 can be characterized by the exit Mach number of the flow. The entrance and exit Mach numbers (M_1 and M_6) of the flow through the control volume are related by the mass conservation equation ($\gamma_1 M_1^2 V = \gamma_6 M_6^2 P$) and can be determined along the generalized Rayleigh line as follows:

$$M_1^2 = \frac{I + 1 - P}{\gamma_1 (V - 1)} \quad (2.12)$$

$$M_6^2 = \frac{V(I + 1 - P)}{\gamma_6 P (V - 1)} \quad (2.13)$$

Examples of some generalized Rayleigh lines are illustrated in Fig. 2.4 for a gas having constant specific heat ratios ($\gamma_1 = \gamma_6 = 1.4$), along with the corresponding ram accelerator Hugoniot curve. The non-dimensional heat parameter for the Hugoniot curve has a value of $Q=6$ and the impulse parameter has a value of $I=3$. Two generalized Rayleigh lines are shown that result from adding the same impulse to the flow at different incoming flow Mach numbers ($M_1 = 4.65$ and $M_1 = 6$). Boundaries of the corresponding

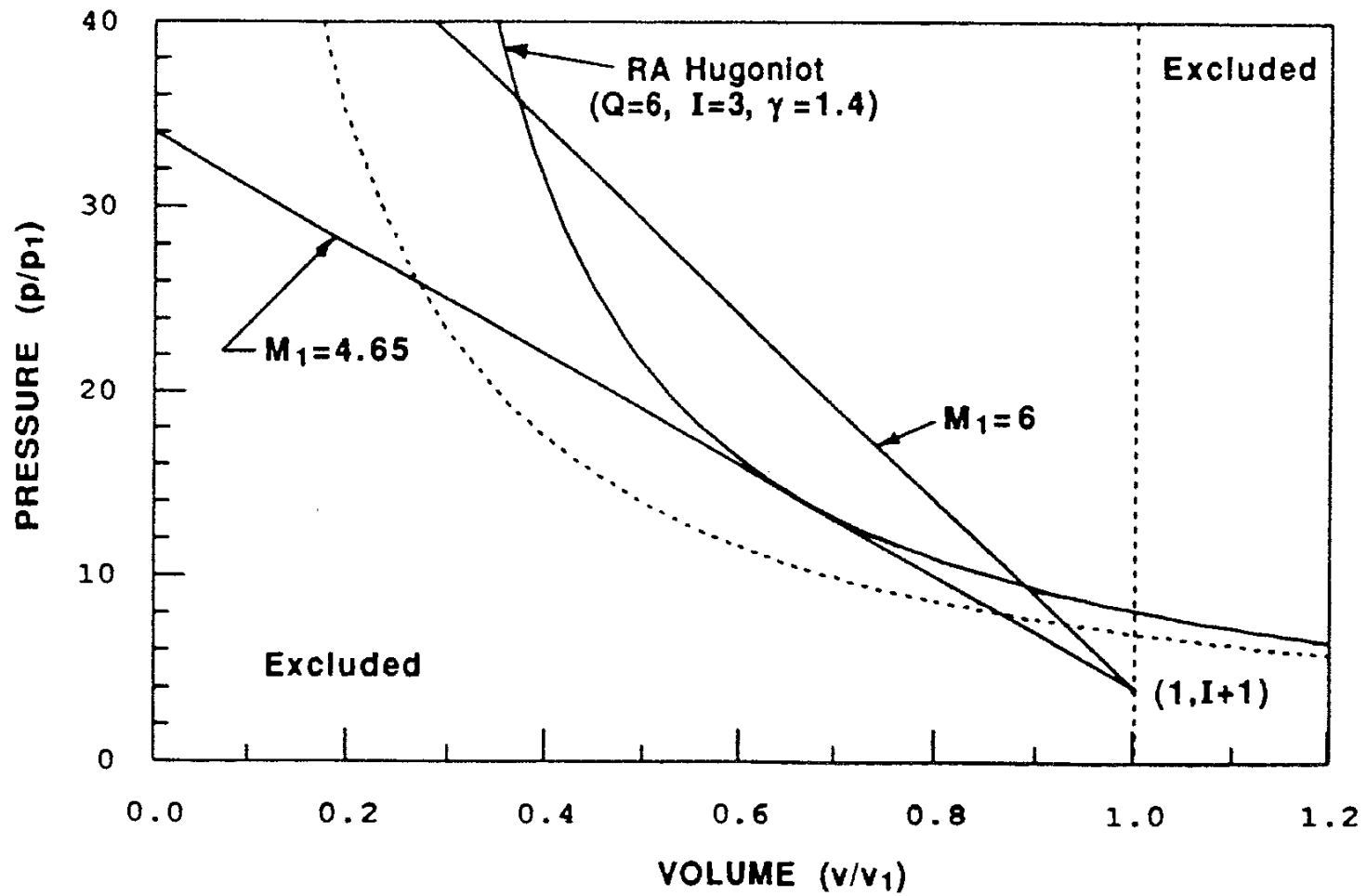


Fig. 2.4 Generalized Rayleigh lines in the pressure-specific volume plane corresponding to two different ram accelerator propulsive cycles.

excluded regions of the P-V end states of the general ram accelerator process are also included. The points of intersection of the ram accelerator Hugoniot curve with the generalized Rayleigh lines determine the end state pressure and specific volume ratios established by the corresponding ram accelerator propulsive cycles. Incoming and exiting Mach numbers of the flow at each of these intersection points can be determined from Eqs. 2.12 and 2.13. The upper and lower intersection points of the generalized Rayleigh lines indicate the end state conditions of a process that has the flow leaving the control volume at subsonic and supersonic Mach numbers, respectively.

Analysis of Eq. 2.11 shows that the generalized Rayleigh line intercepts the $V=1$ line at the point $(1, I+1)$ and has a slope that depends on the initial state of the gas and the square of the incoming Mach number of the flow; i.e., $dP/dV = -\gamma_1 M_1^2$. The minimum operating Mach number of a ram accelerator process that generates a specified amount of impulse is determined from the generalized Rayleigh line that is tangent to the corresponding ram accelerator Hugoniot (the minimum Mach number for the example in Fig. 2.4 is: $M_1 = 4.65$). The incoming flow velocity and corresponding mass flux increase as the generalized Rayleigh line becomes more vertical in the P-V plane, as indicated in Fig. 2.4. The $V=1$ line represents a flow having an infinite mass flux which corresponds to infinite slope. Thus, the intersection point of the ram accelerator Hugoniot curve with the $V=1$ line indicates the minimum pressure ratio that could result from a ram accelerator propulsive cycle that reduces the specific volume of the propellant gas.

Note that the generalized Rayleigh line given by Eq. 2.11 does not pass through the initial point $(1,1)$ when $I \neq 0$ (see Fig. 2.4). The inability of the flow to make a transition continuously from the initial state to its end state along a path in the P-V plane represented by a straight line, when there is a momentum change, indicates that there must be intermediate processes involved which are not strictly one-dimensional to bring about the necessary changes in the steady flow. If the total amount of heat release occurs at a reduced flow area (i.e., on the body), then the intersection point of the generalized Rayleigh line and the ram accelerator Hugoniot indicates the end state of the process after the flow has returned to full tube area.

Only the branch of the generalized Rayleigh line that is above its upper intersection point with the ram accelerator Hugoniot indicates the history of P-V states

that the propellant gas undergoes (after the impulse has been added to the flow) as it chemically reacts at full tube area, because this branch corresponds to a subsonic heat addition process. The branch below the lower intersection point indicates a P-V history that is physically unrealizable because it corresponds to supersonic flow leaving the projectile at full tube area, before the total amount of heat release has been added. In this situation, the effects of heat addition, in the uniform supersonic flow behind the projectile, cannot change the impulse of the flow (constant area heat addition), which means that the thrust on the projectile was generated with only a fraction of the available Q. Thus, the lower branch of the generalized Rayleigh line represents only the end states of ram accelerator propulsive cycles that have supersonic exit flows, not the P-V history of a process which couples the heat release to the impulse of the propulsive cycle.

2.3 Sonic Point Along Ram Accelerator Hugoniot

The minimum allowable velocities of a propellant mixture entering the control volume, for a specified value of impulse, are shown graphically to be those which result in generalized Rayleigh lines that lie tangent to the ram accelerator Hugoniots and pass through the point (1, I+1) as shown in Fig. 2.4. This point of tangency corresponds to the end state of a propulsive cycle which results in the exhaust gas traveling at sonic velocity with respect to the projectile. The tangency point of the ram accelerator Hugoniot and the generalized Rayleigh line can be shown to correspond exactly to sonic flow at station 6 by first differentiating Eq. 2.6 for constant initial conditions at station 1:

$$dh_6 = \frac{1}{2} [(v_6 + v_1) dp_6 + (p_6 - p_1(I+1)) dv_6] \quad (2.14)$$

Since the ram accelerator Hugoniot curve represents a set of thermodynamic states of a gas, the entropy for every point along this curve can be written as:

$$T_6 ds_6 = dh_6 - v_6 dp_6$$

where s_6 is the entropy per unit mass of the exhaust gas mixture. Combining the above two equations results in the following expression for the entropy along the ram accelerator Hugoniot curve:

$$T_6 ds_6 = \frac{1}{2} [(p_6 - p_1(I+1))dv_6 - (v_6 - v_1)dp_6] \quad (2.15)$$

It follows from Eq. 2.15 that:

$$T_6 \left(\frac{ds_6}{dv_6} \right)_{\text{hug}} = \frac{1}{2} (v_6 - v_1) \left[\frac{p_6 - p_1(I+1)}{v_6 - v_1} - \left(\frac{dp_6}{dv_6} \right)_{\text{hug}} \right] \quad (2.16)$$

where the subscript 'hug' designates that the derivatives are taken along the ram accelerator Hugoniot curve. From the thermodynamics of shock waves and detonation waves it can be shown that somewhere along the ram accelerator Hugoniot curve there will be a point where the isentrope passing through that point is also tangent to the Hugoniot.¹⁷ At this tangency point, ds_6 must be zero and Eq. 2.16 becomes:

$$\left[\left(\frac{dp_6}{dv_6} \right)_{\text{hug}} \right]_s = \frac{p_6 - p_1(I+1)}{v_6 - v_1} \quad (2.17)$$

or expressed non-dimensionally:

$$\left[\left(\frac{dP}{dV} \right)_{\text{hug}} \right]_s = \frac{P - (I+1)}{V - 1} \quad (2.18)$$

By differentiating Eq. 2.11, the slope of the generalized Rayleigh line is found to be:

$$\left(\frac{dP}{dV} \right)_{\text{ray}} = \frac{P - (I+1)}{V - 1}$$

which is exactly the same as Eq. 2.18, this establishes that at the minimum allowable flow velocity, the ram accelerator Hugoniot curve and generalized Rayleigh line are tangent to the isentrope curve that passes through their tangency point. From the isentrope curve, the acoustic velocity of the burned gas (c_6) can be written as:

$$c_6^2 = -v_6^2 \left(\frac{dp_6}{dv_6} \right)_s \quad (2.19)$$

Since the representation of the order of differentiation on the left-hand side of Eq. 2.17 can be reversed, its right-hand side can be substituted into Eq. 2.19 to yield the following:

$$c_6^2 = -v_6^2 \left(\frac{p_6 - p_1(I+1)}{v_6 - v_1} \right)$$

Comparing this expression with Eq. 2.5 confirms that the tangency point of the ram accelerator Hugoniot and generalized Rayleigh line corresponds to a flow which is leaving the control volume at sonic velocity. Since the slopes of the generalized Rayleigh lines that intercept the ram accelerator Hugoniot above the sonic point are less than the slope of the ram accelerator Hugoniot itself, the flow leaving the control volume must be subsonic.¹⁷ Similar considerations show that the flow leaving the control volume must be supersonic at all points along the ram accelerator Hugoniot curve lying below the sonic point in the P-V plane.

2.4 Generalized Fanno Flow

Thermodynamic end state histories in the P-V plane that a particular one-dimensional ram accelerator propulsive mode will generate, as it accelerates a projectile through a given velocity range, can be determined from the mass and energy conservation equations (Eqs. 2.1 and 2.2). The term *Fanno flow* is often associated with steady adiabatic flow in a constant area duct that experiences a change in momentum flux due to frictional effects in the absence of internal heat generation. By combining the ideal gas equation of state with the conservation equations of mass and energy, while leaving a heat release term in the energy equation, a relation can be derived for a curve in the P-V plane which represents the history of end states over the operating velocity range of a ram accelerator propulsive cycle that has a constant exiting Mach number. The equation for

this "generalized Fanno curve" which has the exiting Mach number and non-dimensional heat release as parameters is as follows:

$$P_f = \frac{\frac{\gamma_1(\gamma_6 - 1)}{\gamma_6(\gamma_1 - 1)} V(Q + 1)}{V^2 \left(1 + \frac{\gamma_6 - 1}{2} M_6^2 \right) - \frac{\gamma_6 - 1}{2} M_6^2} \quad (2.20)$$

where the subscript 'f' designates the pressure ratio along the generalized Fanno curve.

A series of generalized Fanno curves can be drawn, using various exit Mach numbers as a parameter, which represent the history of P-V states that different nozzle-stabilized ram accelerator propulsive cycles produce while operating in the same propellant gas. Examples of three generalized Fanno curves which represent the end states generated throughout the potential operating ranges of the TCRA propulsive mode ($M_6=1$) and two possible cases of the MCRA mode are shown in Fig. 2.5. Curves labeled by $M_6=2$ and $M_6=3$ correspond to projectile geometries operating in the MCRA propulsive mode which have the nozzle throat-to-tube area ratios required to accelerate the reacted propellant mixture ($\gamma_6 = 1.4$) to exit Mach numbers of 2 and 3, respectively. The non-dimensional heat parameter for all curves in this figure has a value of $Q=6$.

All of the generalized Fanno curves intersect the $V=1$ line at the same point that the ram accelerator Hugoniot characterized by $I=Q$ does, which indicates that end state conditions generated by any propulsive cycle will be the same at the constant specific volume point of operation (Fig. 2.5). Details of the body configuration within the control volume must be considered to determine the feasibility of any ram accelerator propulsive mode actually generating a level of impulse equal to the non-dimensional heat

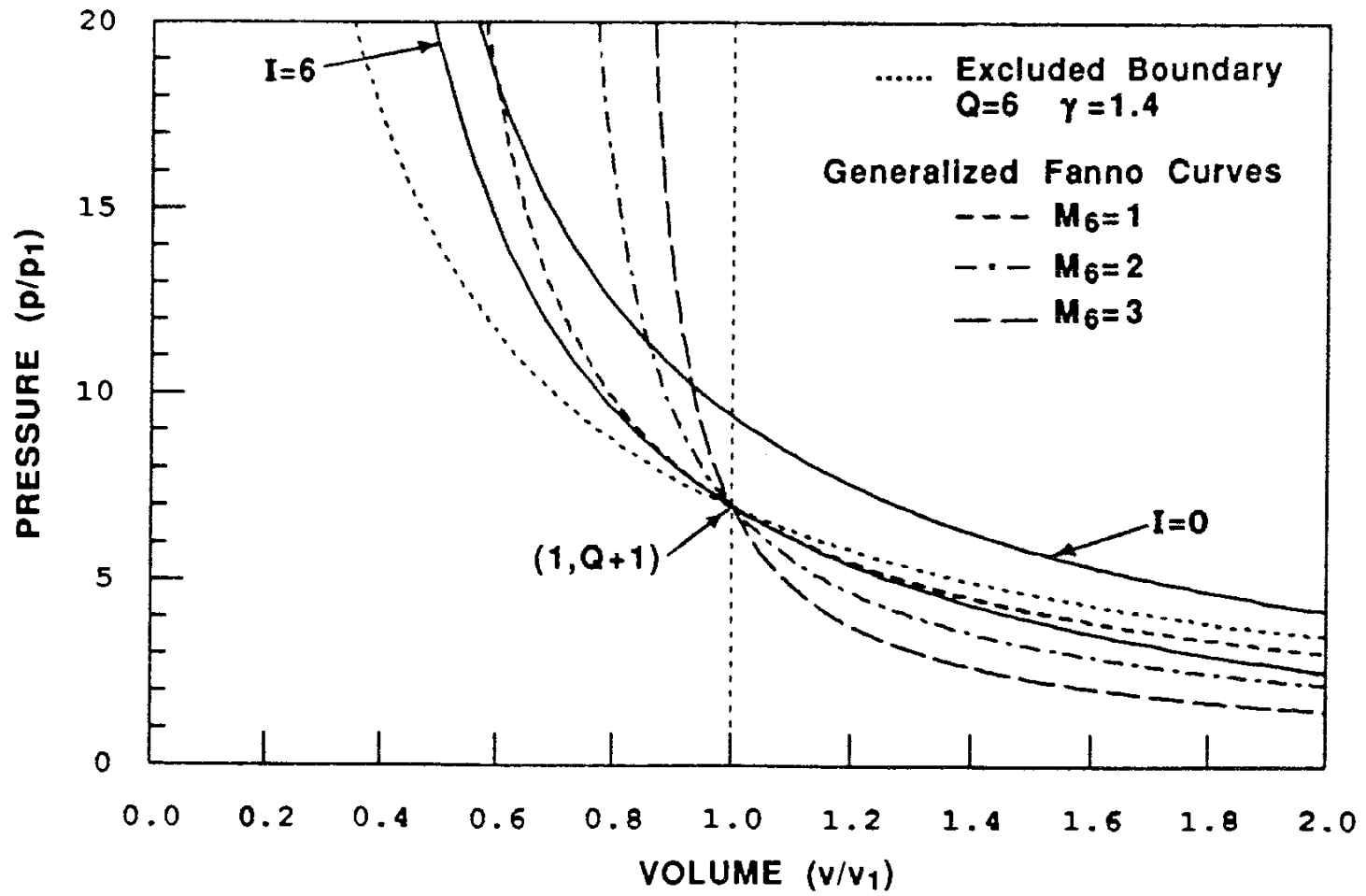


Fig. 2.5 Generalized Fanno curves representing the histories of end states in the pressure-specific volume plane of ram accelerator propulsive cycles having different exit Mach numbers.

parameter. The ability of the projectile configuration to accept the incoming mass flow rate and to contain the high pressure region between the normal shock and the choking point is the primary factor for generating $I=Q$ in the subsonic combustion ram accelerator propulsive modes. The feasibility of igniting the propellant mixture, at the low entrance Mach numbers associated with the condition of constant specific volume operation, must be considered for the shock induced combustion and oblique detonation propulsive modes. Note that at a given thrust level, higher end state pressure ratios are generated by

the TCRA mode than any other ram accelerator propulsive mode in the upper left hand quadrant of the P-V plane.

The intersection point of the $I=Q$ ram accelerator Hugoniot with the $V=1$ line indicates the only location in the allowable regions of the P-V plane where the incoming and outgoing flow Mach numbers are indeterminate. This is illustrated by the convergence of the generalized Fanno curves (Fig. 2.5) at the $V=1$ line, which implies that the P-V end states for all ram accelerator propulsive modes must be the same when they are capable of operating at conditions which result in constant specific volume. The generalized Rayleigh line that lies tangent to the $I=Q$ Hugoniot also passes through the point $(1, Q+1)$, which indicates that along this ram accelerator Hugoniot, $(1, Q+1)$ is the only point where the exit velocity could be sonic. Thus, all points along the $I=Q$ Hugoniot that are to the left of the $V=1$ line correspond to subsonic exit velocities and all points to the right indicate supersonic velocities (discussed in Sec. 2.3).

Since the locus of end states described by the generalized Fanno curve of the TCRA propulsive cycle indicates points along the ram accelerator Hugoniots where the exit velocity is sonic and this curve remains at or above the $I=Q$ Hugoniot in the P-V plane (Fig. 2.5), there cannot be any ram accelerator processes which generate a value of impulse greater than Q when the end states have a lower specific volume (higher density) than the propellant mixture has in its unreacted state. Thus, the maximum impulse ram accelerator Hugoniot is characterized by $I=Q$ for a propellant mixture having a constant γ (the maximum impulse for variable γ can be determined from Eq. 2.10). In addition, the generalized Fanno curve representing the TCRA propulsive cycle forms the leftmost boundary for the region of the allowable end states in the P-V plane (on the left side of

the $V=1$ line), for any steady ram accelerator process having sonic or supersonic exit velocities.

2.5 Mach Number Limits of Ram Accelerator Operation

The detonation Hugoniot ($I=0$) shown in Fig. 2.5 represents the maximum end state pressure ratios that can be developed by any quasi-steady ram accelerator process. The upper Mach number limit of a ram accelerator propulsive cycle that has a choking point within it, and thus a constant exit Mach number, corresponds to the Mach number of the weak detonation wave that results in the same exiting flow Mach number.* The TCRA propulsive mode has an upper velocity limit that would be equivalent to the C-J detonation velocity of the gaseous propellant mixture. Projectiles that are propelled with the MCRA propulsive mode have the potential to accelerate beyond the C-J detonation velocity, though their minimum operating Mach number is greater than the minimum Mach number required for TCRA operation due to the area constriction of the nozzle throat. The actual operating velocity limits of these ram accelerator propulsive modes are expected to be sensitive to the efficiency of the supersonic diffuser and to the elevation of the chemical kinetic rates of the propellant gas as it passes through the system of shocks surrounding the projectile.^{3,21,22}

* Weak detonation waves are defined, in the stationary control volume reference frame, as supersonic combustion waves which have supersonic exit velocities. These combustion waves are intrinsically unstable in a constant area duct because the combustion process is not pressure-coupled to the leading wave front.^{15,19}

Incoming flow Mach numbers which result in the end states described by the generalized Fanno curve for a ram accelerator propulsive cycle are determined as a function of the exit Mach number from the following:

$$M_1^2 = \frac{\frac{\gamma_6 - 1}{\gamma_1 - 1} M_6^2 (Q + 1)}{V^2 \left(1 + \frac{\gamma_6 - 1}{2} M_6^2 \right) - \frac{\gamma_6 - 1}{2} M_6^2} \quad (2.21)$$

It can be seen from the above expression that in the limit as $V \Rightarrow 1$, the flow Mach number for any ram accelerator propulsive cycle at conditions which generate the impulse given by Eq. 2.10 is:

$$M_1^2 = \frac{\gamma_6 - 1}{\gamma_1 - 1} M_6^2 (Q + 1) \quad (2.22)$$

The generalized Fanno curve representing the TCRA mode (Fig. 2.5) intersects the $I=0$ Hugoniot at the C-J point of the propellant gas, and it is tangent to the $I=Q$ ram accelerator Hugoniot at the point; $(1, Q+1)$. Thus, the range of possible end states that can be generated by the TCRA mode is bounded in the P-V plane by the detonation Hugoniot and the maximum thrust ram accelerator Hugoniot ($I=Q$). The maximum thrust condition for the TCRA propulsive mode occurs at the constant specific volume line. Ram accelerator processes that operate at conditions which generate an end state having a specific volume ratio equal to unity, result in a situation where there is no residual gas velocity with respect to the tube wall at the end of the propulsive cycle.

Incoming Mach numbers of the flows resulting in end states represented by the ram accelerator Hugoniot curves are:

$$M_1^2 = \frac{(Q+1) - \frac{\gamma_6}{\gamma_1} \frac{\gamma_1-1}{\gamma_6-1} V(I+1)}{\frac{\gamma_1-1}{2} (1-V) \left(\frac{\gamma_6+1}{\gamma_6-1} V - 1 \right)} \quad (2.23)$$

The operating Mach number of any ram accelerator propulsive cycle, utilizing a given amount of heat release to generate a given level of impulse, can be determined by combining Eqs. 2.20 and 2.22, which results in the following quadratic equation for M_1^2 :

$$M_1^4 \left(\gamma_1^2 - \Phi \frac{\gamma_1-1}{2} \right) + M_1^2 (2\gamma_1(I+1) - \Phi(Q+1)) + (I+1)^2 = 0 \quad (2.24)$$

where:

$$\Phi = \frac{\gamma_1^2 (\gamma_6 - 1)}{\gamma_6^2 (\gamma_1 - 1)} \frac{(1 + \gamma_6 M_6^2)^2}{M_6^2 \left(1 + \frac{\gamma_6 - 1}{2} M_6^2 \right)}$$

Solutions using the positive root of the discriminant will yield the supersonic entrance Mach numbers and the negative root yields the subsonic solutions when they exist. Setting $I=0$ in the above expression gives the maximum Mach number that any ram accelerator propulsive cycle can attain, for a given amount of heat release. Consequently, Eqs. 2.22 and 2.24 determine the maximum Mach number range of any ram accelerator propulsive mode operating with end state specific volume ratios less than one.

2.6 Discussion of Ram Accelerator Hugoniot Analysis

The ram accelerator Hugoniot analysis determined how the end state properties of the propellant gas behave as a function of the initial Mach number, heat release, and impulse of an arbitrary ram accelerator propulsive cycle operating in a constant area tube. Resulting performance limitations indicate the widest possible bounds of operation that are consistent with the quasi-steady, 1-D flow assumptions, without considering any of the internal details of the flow processes involved. Given the acoustic speed and heat release of a particular propellant mixture, the area ratio of a nozzle for a projectile can be estimated to provide the potential for operating over a given velocity range. Conversely, for a particular projectile geometry, the maximum possible velocity that is attainable in a given propellant mixture can be determined readily from the results of the global Hugoniot analysis (Eq. 2.24). Other applications of these results are to estimate the end state Mach number of an unknown propulsive cycle and the amount of heat release provided by a given propellant mixture from experiments in which the end state pressure, acceleration and flight Mach number have been determined.

Even though the jump conditions across a 1-D control volume constrain the possible end states that can be generated in quasi-steady flow, the projectile geometry is a primary factor in the stabilization of any ram accelerator propulsive cycle. It is necessary for the area contours and flow protuberances (e.g., flame holders, fin leading edges, etc.) to interact with the propellant mixture in a manner that will initiate and stabilize the combustion process in the desirable region about the projectile, as it is accelerated throughout the intended velocity range. The maximum projectile diameter must be

appropriately sized to accept the flow at the lowest flight Mach numbers and still be able to contain the high pressure driving gas on the rear part of the projectile. The front part of the projectile (typically a nose cone) must supersonically diffuse the propellant mixture without pre-igniting it over a wide range of flight Mach numbers, and the rear part of the projectile must be contoured to either re-expand the exhaust gas supersonically behind it (MCRA) or to stabilize the combustion process at the base of the projectile (TCRA).

Supersonic combustion and superdetonative modes of propulsion require the heat addition process to occur in the region between the projectile body and the tube wall to enable the effects of the combustion process to be communicated to the projectile. The supersonic combustion of the propellant mixture around the midbody of the projectile usually results in supersonic expansion of the reacted gas back to full tube area. There is a minimum amount of supersonic diffusion of the propellant mixture required to raise its static temperature to the point where the supersonic combustion reactions can be self-initiated and stabilized by flame-holding recirculating zones or shock waves.^{18,19} The critical Mach number for shock ignition of the propellant mixture, in the region between the projectile and tube wall, is typically higher than the Mach number corresponding to conditions which result in $I=Q$ operation (Eq. 2.22); thus, the superdetonative ram accelerator propulsive modes are not expected to be able to operate at the Mach number required to generate a constant specific volume end state. Upper Mach number limits of operation are determined by either the velocity at which the net thrust drops to zero (this results in the same end state conditions as the corresponding weak detonation wave) or the point at which the propellant gas is pre-ignited ahead of the projectile throat, resulting in sonic flow at the throat and the subsequent disgoring of an overdriven detonation wave.

The manner in which the heat release is distributed over the projectile body is a major factor in determining the effective end state Mach number of any ram accelerator propulsive cycle utilizing supersonic combustion processes; thus, accurate modeling of chemically reactive viscous flow must be done to predict realistically the detailed character of the projectile flowfield. Some of the important three-dimensional flow effects that play a role in the operation of all ram accelerator propulsive modes are the shock wave-boundary layer interactions and the local flow stagnation points about the projectile. Since the theoretical Mach number limits of operation for a given projectile geometry are, in principle, determined only by the ignition properties of the propellant gas, the superdetonative ram accelerator propulsive modes may not be able to operate throughout the maximum possible operating Mach number range indicated by the ram accelerator Hugoniot analysis.

One of the most significant parameters of the projectile geometry for the TCRA propulsive mode is the ratio of maximum projectile diameter to tube diameter. For isentropic flow, the throat area contraction ratio determines the minimum mass flux that the diffuser geometry can accept without choking, this fixes the minimum supersonic flight Mach number of the projectile. The throat area contraction ratio also constrains the choices of propellant mixture composition to those that will not release more heat than is required to stabilize a normal shock behind the throat, while the projectile is operating at the minimum Mach number. Theoretical upper Mach number limits of the TCRA mode may not be obtainable in propellant mixtures that are easily ignited by the shock structure generated by the passage of the projectile at subdetonative Mach numbers. Thus, the full operating Mach number range predicted for the TCRA propulsive mode by the global 1-D model may not be attained in practice for every propellant mixture, with a particular

projectile geometry. However, the correlation of the projectile acceleration histories determined from experiments with those predicted by the global TCRA theory (i.e., the thermally choked ram accelerator wave that is determined without the inclusion of internal details of the propulsive cycle) has been found to be very good throughout most of the subdetonative velocity regime of many different propellant mixtures,^{1,9} as will be shown in the experimental results section (Chapter 5).

2.7 Mach Number Effects on Impulse of TCRA Propulsive Cycle

The amount of heat release that a gaseous propellant mixture will yield in the thermally choked ram accelerator propulsive mode is determined from the enthalpy of formation (h_{f6}) of the reaction products at the choking point. Chemical equilibria of the reaction products are determined, at a given flight Mach number, for exit flow that has the same total enthalpy as the incoming flow (i.e., $h_1 + u_1^2/2 + h_{f1} = h_6 + u_6^2/2 + h_{f6}$) and is sonic with respect to the projectile ($u_6 = c_6$). As the velocity of the flow entering the control volume (Fig. 2.1) increases, the corresponding total enthalpy increases, resulting in a higher static temperature and pressure at the thermal choking point. The pressure rise at the choke point is not sufficient to suppress the dissociation losses in the reacted propellant gas resulting from the increase in static temperature; thus, the amount of heat release decreases for the TCRA propulsive mode as the projectile is accelerated through the propellant mixture. Reducing the amount of heat release causes the thrust to decrease, as the projectile velocity increases, at a rate greater than anticipated for a propellant mixture having a constant value of Q . The solution technique for determining the Mach

number dependent heat release and its effect on the impulse of the TCRA cycle are described in the following sections.

2.7.1 Iterative Method for Impulse

The combustion algorithm of the computer program "SUPLAB" accounts for the dependence of heat capacity on local temperature and includes the effects of the increase in projectile velocity on the chemical equilibria of the combustion products. This requires an iterative numerical solution of Eqs. 2.1, 2.2, and 2.7, in which the static enthalpies h_1 and h_6 are determined as functions of temperature from tabulated JANAF data.²⁴ The iterative technique begins by computing the chemical equilibria of the combustion products for an assumed static temperature and pressure. Heat release is determined from the predicted combustion products, and then the total enthalpy of the flow exiting the control volume (with u_6 assumed to equal the local acoustic velocity) is compared with the total enthalpy of the incoming flow. The static temperature guess is then modified to raise or lower the total enthalpy of the gas at station 6 as required, and the pressure is updated from Eq. 2.1 to maintain mass conservation. The iterative procedure continues until the total enthalpies are balanced to within the desired tolerance. The thrust is then determined from Eq. 2.3, once the static temperature and pressure at station 6 are known. This approach predicts that the amount of heat released by the combustion of the propellant mixture decreases as the flight Mach number increases (due to dissociation losses) and that the zero thrust condition occurs at the C-J detonation velocity.

Chemical equilibria at a given temperature and pressure are determined from a slightly modified version of "Subroutine WEIN" listed in Strehlow [15]. This FORTRAN program determines the ideal gas equilibria of 13 reactive molecules and an

inert diluent. Reaction products considered are: O_2 , O , H_2 , H , OH , H_2O , CH_4 , CO , CO_2 , N_2 , N , NO , NO_2 and an inert specie. The C-J detonation wave parameters (C-J velocity, temperature, and pressure) predicted by the SUPLAB program for several representative gas mixtures using the above chemical species are compared in Table 2.1 with both experimental data presented in Glassman and the corresponding theoretical results of the Gordon and McBride computational program (GMcB).¹⁶ The good agreement between SUPLAB and the other data shown indicates that a sufficient number of chemical species are considered in the reaction products to account for the major properties of the burned propellant gas during TCRA operating conditions.

Table 2.1: C-J Detonation Parameters of Various Mixtures

Gas Mixture	Detonation Velocity* (m/sec)			T_6 (K)		P_6 (atm)	
	Measured	GMcB	SUPLAB	GMcB	SUPLAB	GMcB	SUPLAB
$8H_2+2O_2$	3390	3408	3401	3439	3422	17.77	17.27
$4H_2+2O_2$	2825	2841	2843	3679	3668	18.56	18.12
$2CH_4+2O_2$	2528	2639	2640	3332	3319	31.19	30.61
$1.33CH_4+2O_2$	2470	2535	2535	3725	3703	31.19	30.34

* $P_1=1$ atm, $T_1=298$ K

2.7.2 Analytical Solution for Impulse

A closed form solution for the impulse (I) of all ram accelerator propulsive cycles can be determined from Eq. 2.24 as a function of flight Mach number, M_1 , exit Mach

number, M_6 , non-dimensional heat release parameter, Q , and the effective specific heat ratios before and after combustion (γ_1 and γ_6), without including any of the internal details of the flow. This relation is as follows:

$$I = \frac{\gamma_1 M_1}{\gamma_6 M_6} (1 + \gamma_6 M_6^2) \sqrt{\left(\frac{\gamma_6 - 1}{\gamma_1 - 1} \right) \frac{Q + 1 + \frac{\gamma_1 - 1}{2} M_1^2}{1 + \frac{\gamma_6 - 1}{2} M_6^2}} - (1 + \gamma_1 M_1^2) \quad (2.25)$$

The impulse for a MCRA cycle would be determined from this equation by setting M_6 equal to the exit Mach number of the projectile nozzle. If the reacted propellant mixture is assumed to have the same thermodynamic properties throughout the theoretical operating velocity range of the projectile that it has at the C-J detonation velocity, then the analytical solution for the impulse will predict the same zero thrust velocity for the TCRA propulsive mode ($M_6=1$) as the iterative method.

Shown in Fig. 2.6 is a comparison between the two different methods for computing the impulse in the supersonic Mach number range of the TCRA propulsive mode. The fill pressure is 25 atm and the propellant mixture composition is $2.7\text{CH}_4 + 2\text{O}_2 + 5.8\text{N}_2$, which has a specific heat ratio of: $\gamma_1 = 1.369$ (this is a mixture that is used routinely in the experimental studies). The analytical solution used the heat release and effective end state specific heat ratio predicted at the C-J point by the iterative method (i.e., $Q = 4.65$ and $\gamma_6 = 1.344$). Differences in the predicted thrust levels are due primarily to the variation in heat release with projectile Mach number accounted for by the iterative method. At the Mach number of peak impulse for the iterative solution ($M_1 \approx 2.3$) the heat release parameter has a value of: $Q = 5.18$, and the end state specific heat ratio

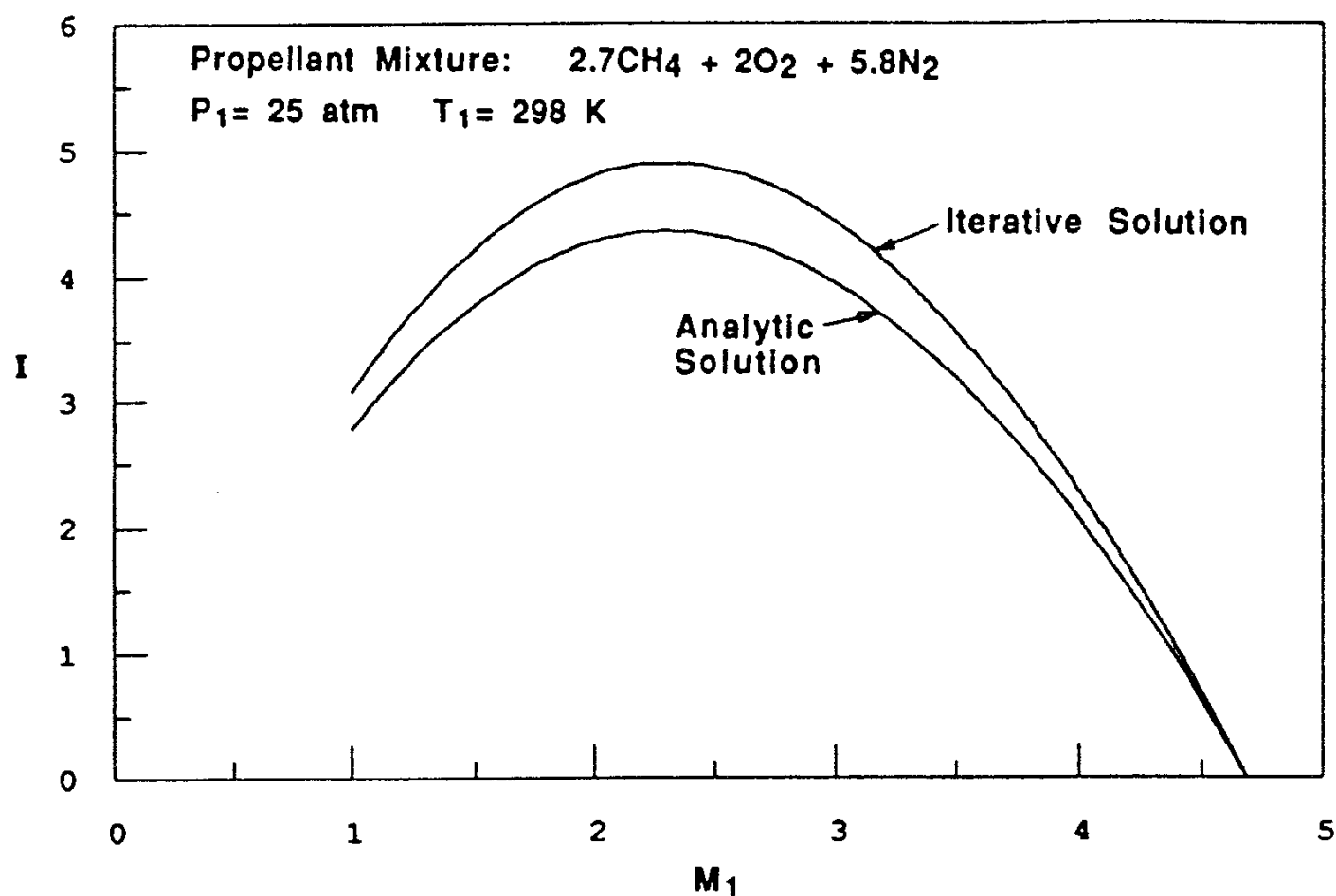


Fig. 2.6 Comparison of the impulse-Mach number profiles predicted by the iterative and analytical solutions for the thrust of the TCRA mode.

is: $\gamma_1 = 1.348$. If the instantaneous heat release and end state properties determined at any M_1 were continuously input into the analytical solution, then there would not be any difference in the impulse profiles shown in Fig. 2.6.

The closed form solution for the impulse is useful in estimating the thrust levels that can be anticipated from a particular propellant mixture; however, for a more rigorous comparison of TCRA theory with experiments, the Mach number dependence of the chemical equilibria at the thermal choking point should be accounted for. Quasi-steady flow conditions imply that the flowfield can adjust to changes in the projectile velocity

almost instantaneously, and that the impulse predicted at any Mach number is independent of the prior acceleration history.⁹ Thus, the velocity-distance history for a projectile having a given mass, m_p , can be determined from the iterative solution of the impulse-Mach number (I-M) profile by integrating the equation of motion ($F = m_p du/dx$). The SUPLAB program uses a fourth-order Runge-Kutta method that updates the thrust during each integration step as the projectile velocity increases. Integrating the theoretical velocity-distance history provides the corresponding time-distance history. The conditions at the thermal choking point, determined by SUPLAB at any Mach number, are end states of the TCRA propulsive cycle that are determined without considering any of the flow phenomena occurring within the control volume; thus, the predicted performance profiles are the result of the global TCRA theory.

CHAPTER 3

DETAILED MODEL OF THERMALLY CHOKED RAM ACCELERATOR FLOWFIELD

The TCRA mode can operate at lower Mach numbers than any other ram accelerator propulsive cycle. Projectile geometries which have proved to operate well in this propulsive mode have an area profile similar to that of the silhouette shown in Fig. 1.3, and they consist of a conical nose in front and a body that can be approximated as a truncated cone. Reference points used in the analysis of the flowfield are defined in Fig. 3.1. Flow through the control volume of the detailed theoretical model of the TCRA propulsive mode enters at station 1. The area constriction of the diffuser (nose cone) and the oblique shock waves that it generates reduce the velocity of the incoming supersonic flow to a relative minimum at the point of maximum projectile diameter, station 2 (also referred to as the "throat"). The flow then expands supersonically behind the throat until it encounters a normal shock (stations 3 and 4), which raises the static pressure and temperature of the propellant gas while rendering the flow subsonic with respect to the projectile. Behind the normal shock the subsonic flow continues to slow down relative to the projectile until it reaches the full tube area again. Station 5' indicates the point in the flow passage just before the sudden flow area expansion occurs at the base of the projectile. Combustion is assumed to be stabilized in the subsonic flow by the recirculating zone at the bluff base of the projectile (station 5), and the resulting heat

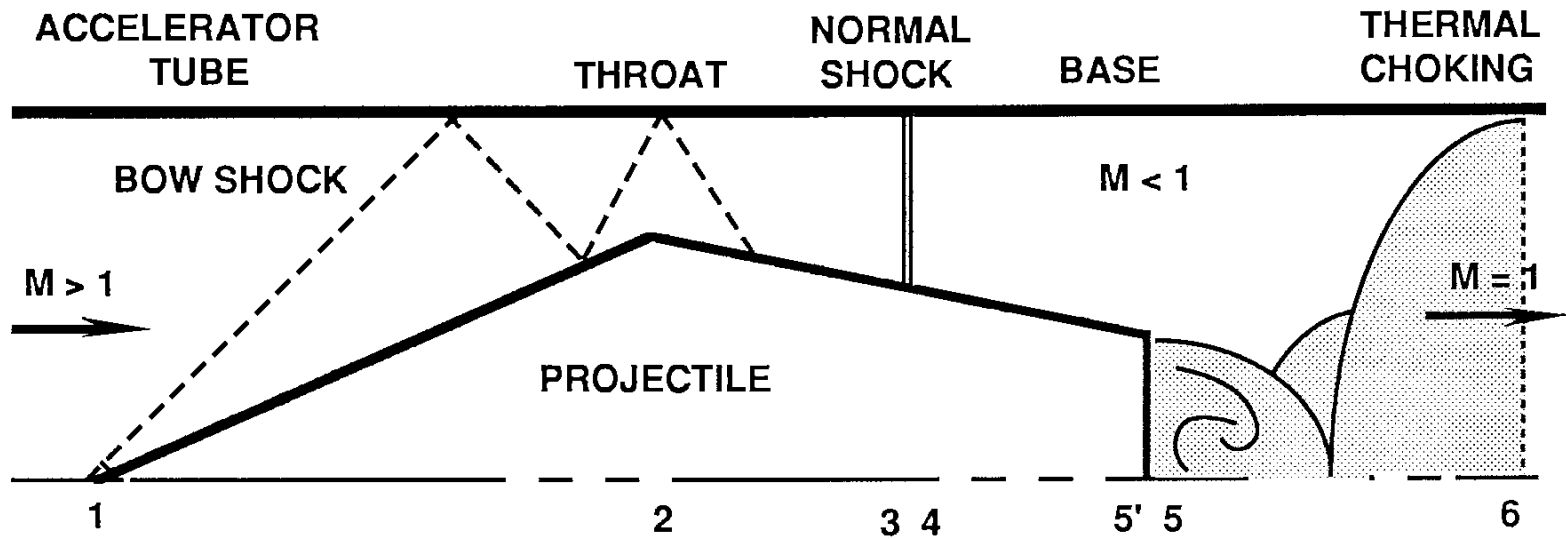


Fig. 3.1 Schematic of detailed TCRA flowfield model.

addition is assumed to thermally choke the flow at full tube area (station 6). For a projectile having isentropic flow everywhere, except across the normal shock and in the heat addition zone (sometimes referred to as an "ideal" projectile), the location of the normal shock is governed by the heat release of the propellant mixture (controlled with diluent concentration and fuel-oxygen stoichiometry) and the projectile flight Mach number.

3.1 Ideal TCRA Propulsive Cycle

Shown in Fig. 3.2 is the P-V cycle of the TCRA propulsive mode, operating at the Mach number that results in the maximum projectile thrust from a propellant mixture having a constant value of gamma ($\gamma = 1.4$). The value of the heat release parameter;

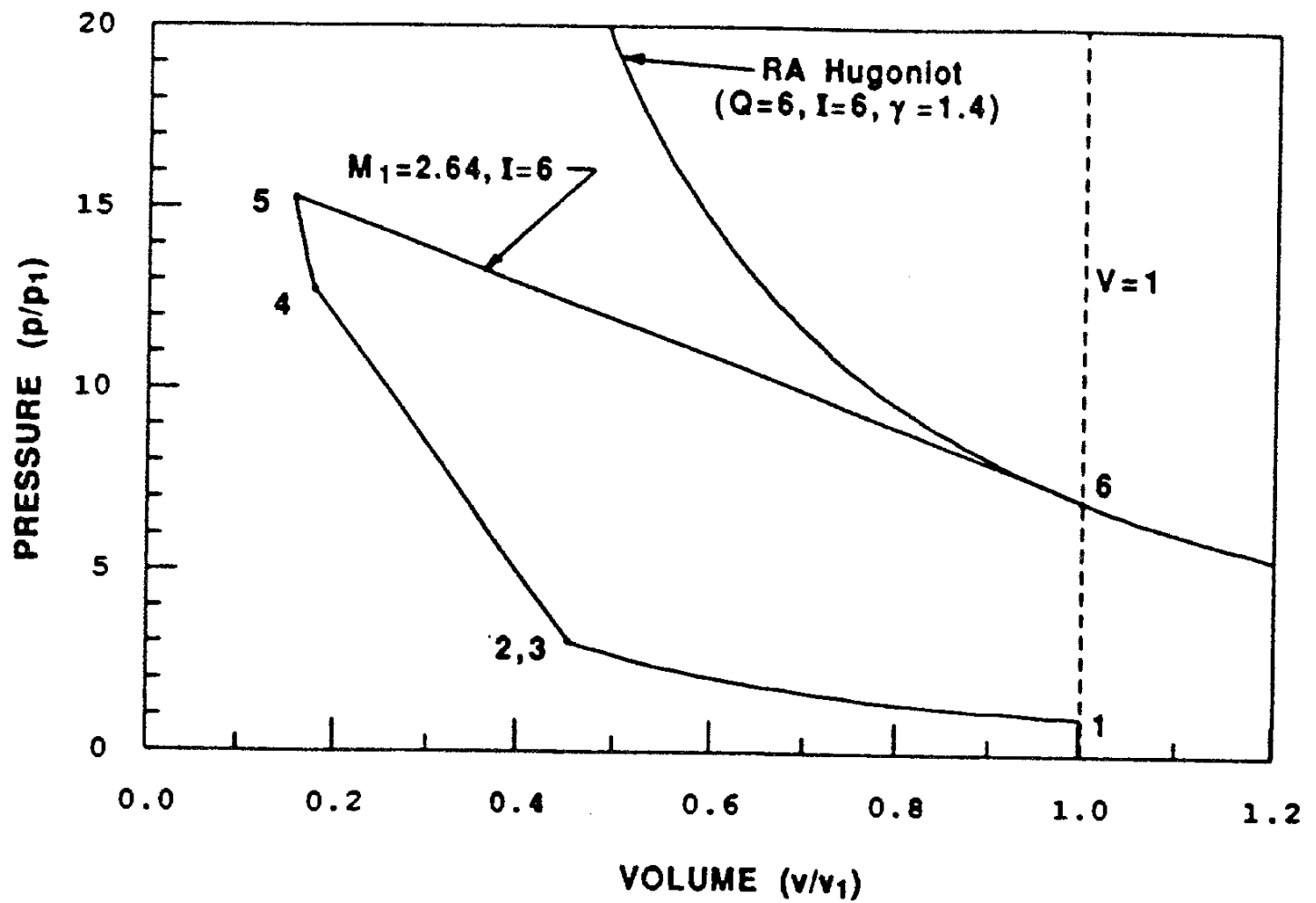


Fig. 3.2 P-V cycle of ideal TCRA propulsive mode operating at maximum thrust Mach number. The corresponding ram accelerator (RA) Hugoniot ($Q=6$, $I=6$) is also shown.

$Q=6$, was chosen for this example because it is near the value of many propellant mixtures that have been used routinely in the experiments. Thus, the impulse of the P-V cycle of the TCRA mode at the maximum thrust condition is; $I=6$. The projectile is assumed to be ideal and to have a throat-to-tube diameter ratio such that the normal shock is located exactly at the projectile throat (thus, the flow areas at stations 2 and 3 are equal, and $d_2/d_1 = 0.72$) while it is operating at the corresponding Mach number;

$M_1 = 2.64$, as given by Eq. 2.22. The rear of the ideal projectile is assumed to taper down to a point.

The numbered points on the P-V cycle of the TCRA propulsive mode (Fig. 3.2) indicate the corresponding flowfield stations as defined for Fig. 3.1. The supersonic propellant gas is isentropically compressed from station 1 to station 3, normal shock compression occurs along a *Rayleigh line* to point 4, and then the flow is subsonically compressed along an isentrope as it flows over the diverging part of the projectile to station 5, this is the point where the subsonic flow returns to full tube area. Heat addition occurs along a generalized Rayleigh line to the tangency point of the corresponding ram accelerator Hugoniot. At the flight Mach number that results in maximum thrust for the TCRA mode, the tangent point also coincides with the $V=1$ line. The total amount of work done (that is available to accelerate the projectile) by the TCRA process at this flight Mach number is the area enclosed by the P-V cycle. No work done by the unsteady expansion of the high pressure reacted gas behind the choking point can contribute to the cycle, because this work is not communicated back to the control volume.

The effects of increasing the flight Mach number on the P-V cycle of the TCRA mode are shown in Fig. 3.3, for the same propellant gas and ideal projectile geometry as before. In this case the flight Mach number ($M_1 = 4.65$) is such that the resulting impulse has a value of $I=3$. The normal shock is now behind the throat. Initial compression occurs along an isentrope to the point of maximum projectile diameter at station 2, and back again along the same isentrope to a point corresponding to station 3. Normal shock transition brings the flow to point 4, and the flow is subsonically compressed along another isentrope to station 5. Subsonic heat addition occurs along

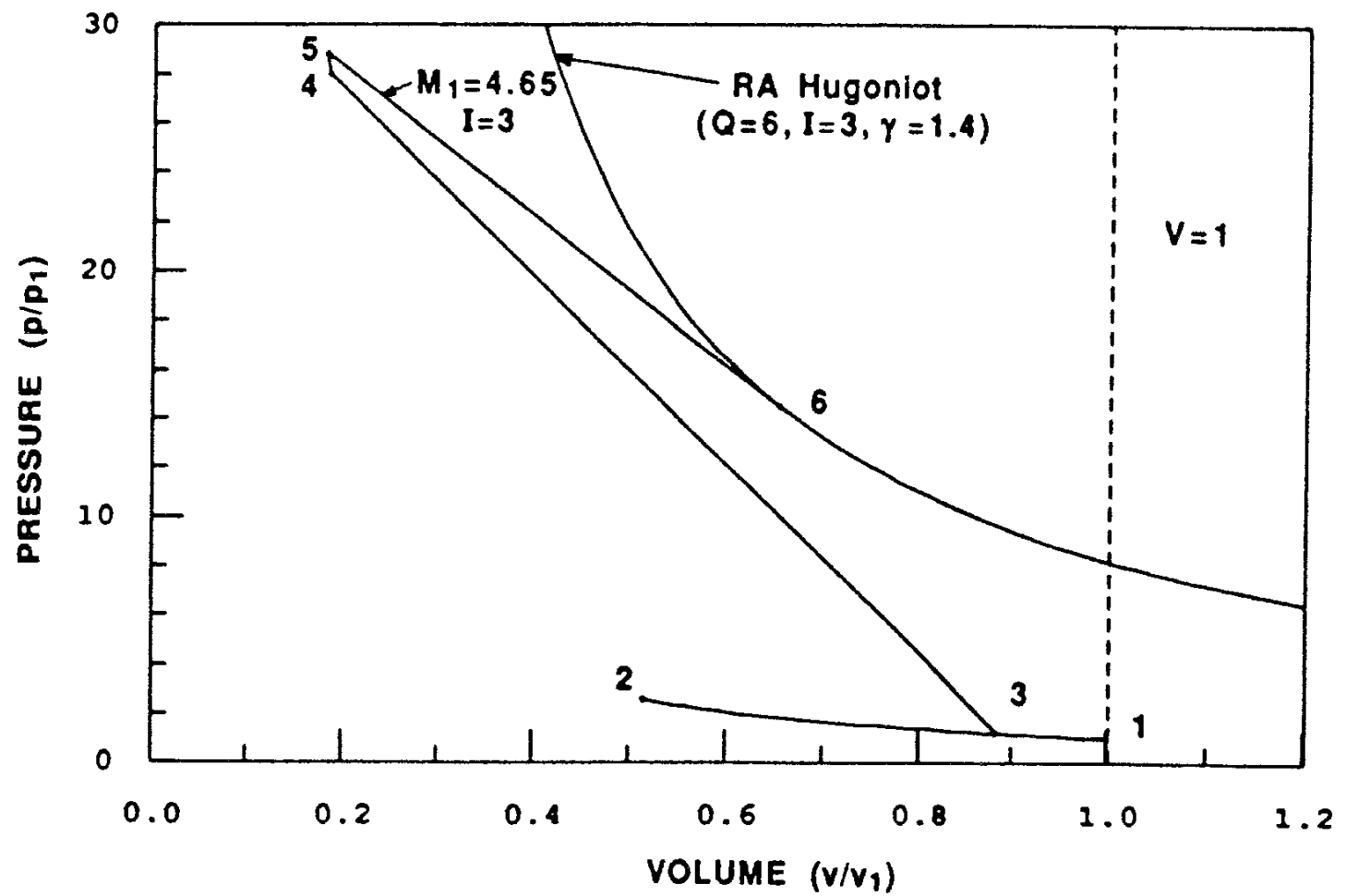


Fig. 3.3 P-V cycle of ideal TCRA propulsive mode operating at $M_1=4.65$. The corresponding ram accelerator (RA) Hugoniot ($Q=6, I=3$) is also shown.

the generalized Rayleigh line to the thermal choking point at station 6. Both the peak cycle pressure and the thermal choking pressure are greater than the previous case, as a result of the increased ram effect at the higher flight Mach number.

A vertical line (not shown) passing through the sonic point of the ram accelerator Hugoniot in Fig 3.3 would intersect the *Rayleigh line* of the normal shock process between the points 3 and 4, this line would divide the areas representing the work done by the propulsive cycle into two regions. The area that lies underneath the subsonic

branch of the generalized Rayleigh line that would be enclosed by this vertical line passing through the conditions at the thermal choking point, corresponds to work available to accelerate the projectile. The area under the part of the P-V cycle represented by the points: 1, 3 and the intersection point of the vertical dividing line with the normal shock *Rayleigh line*, corresponds to the work required to pressurize and accelerate the stationary propellant gas up to the velocity of the exhaust gas at the exit plane of the control volume (in general, the exhaust gas at the thermal choking point is moving in the direction of projectile motion in the laboratory frame of reference). As the projectile Mach number increases, the net area underneath the subsonic branch of the corresponding generalized Rayleigh line decreases, until it finally reaches zero at the C-J detonation velocity of the propellant gas. At the C-J velocity the work represented by the area underneath the corresponding supersonic branch of the generalized Rayleigh line is that which is needed to sustain the motion of the gas in the C-J detonation wave.

3.2 Discussion of Thermally Choked Propulsive Cycles

There are some important consequences which result from operating a thermally choked propulsive cycle in a constant area tube. One key point is that for adiabatic conditions, the maximum amount of entropy that can be generated by chemical reactions and/or changes in momentum flux, in a steady flow through a control volume having the same entrance and exit areas (Fig. 2.1), is that which results in the flow leaving the control volume at the local sonic velocity of the gas mixture.¹⁷ Since entropy is a thermodynamic state variable, the entropy of the end state gas at the thermal choking point is independent of the process by which the propellant mixture reached that state.

Consequently, the chemical equilibria of the exhaust products resulting from either subsonic or supersonic constant area combustion are exactly the same at the thermal choking point. Thus, for the TCRA propulsive cycle, the heat release of a propellant mixture is independent of the combustion process, as long as the reaction products reach chemical equilibrium at the thermal choking point of a flow having a given initial mass flux and total enthalpy.

Another consequence of operating a ram accelerator propulsive cycle with end state conditions that correspond to the maximum increase in entropy (TCRA) is that the impulse generated at a particular flight Mach number is independent of the disposition of the shock wave system about the body. The total entropy rise generated by the TCRA propulsive cycle (operating at a given Mach number) is due to both the subsonic heat addition process at constant area and the shock wave system that is established on the projectile body. Since the heat addition process results in thermal choking of the flow, the subsonic Mach number before combustion is fixed by the predetermined amount of heat release (as discussed in Sec. 2.7); thus, the entropy rise due to heat addition at finite Mach number is constant for a given total enthalpy of the flow.

The shock wave system about the projectile generates the remaining amount of entropy (in inviscid flow) required to establish the choked flow condition at full tube area. The oblique shock wave system in the supersonic region of the projectile depends only on geometry and flight Mach number, and it is unaffected by the heat addition process occurring in the subsonic flowfield behind the projectile. Communication between the combustion zone and the supersonic flow is established through a normal shock. In principle, the normal shock is driven to the location on the projectile body which results in the proper subsonic flow conditions at the entrance to the combustion

zone and the appropriate amount of entropy increase to compensate for all other non-isentropic phenomena. This leads to the apparent paradox that the thrust is independent of projectile geometry, which is true, as long as the geometry is such that it allows a shock system to be established that can balance the gasdynamic conservation equations across the control volume.

3.3 Component Models of the Detailed TCRA Flowfield

The detailed theory of the TCRA propulsive mode models the gasdynamic phenomena of the projectile flowfield as quasi-one-dimensional. Gas properties at the stations numbered in Fig. 3.1 are determined by applying the channel flow relations between each station, with the inclusion of a total pressure loss between stations to approximate the effects of component efficiency on the details of the flowfield.⁸ The FORTRAN program that determines the end state chemical equilibria at the thermal choking point (SUPLAB) also computes the effects of area variation on the unreacted flow. The overall total pressure loss arising from the conical shock system in the diffuser region (between stations 1 and 2) is approximated with the total pressure loss across the first two oblique shocks in supersonic flow between a wedge and a straight wall. The total pressure loss of the subsonic flow through the sudden area expansion at the base of the projectile is approximated with a model that assumes the projectile base pressure is the same as that of the flow before the area expansion.^{8,23}

These relatively simple models of the diffuser and base total pressure losses provide a way to determine the qualitative effects of non-isentropic phenomena on the theoretical location of the normal shock. There is a unique area ratio at which a normal

shock must be located to balance the entrance and exit conditions of the propellant flow through the control volume. Heat release, diffuser efficiency, base total pressure loss and flight Mach number are the factors which determine the location of the normal shock. The detailed model also provides an estimate of the static pressure and temperature at each station. These estimates indicate the flight Mach number at which pre-ignition of the propellant gas is likely to occur.

Once the chemical equilibria at the thermal choking point are known, the properties of the unreacted propellant mixture can be determined at all of the preceding stations. The Mach number at the entrance to the combustion zone (station 5) is found from the relation governing simple heat addition in a constant area duct as follows:

$$M_5^4 \left(\gamma_1^2 \chi - \frac{\gamma_1 - 1}{2} \right) + M_5^2 (2\gamma_1 \chi - 1) + \chi = 0 \quad (3.1)$$

where:

$$\chi = \frac{\gamma_6^2}{2\gamma_1^2} \left(\frac{\gamma_1 - 1}{\gamma_6^2 - 1} \right) \frac{1 + \frac{\gamma_1 - 1}{2} M_1^2}{Q + 1 + \frac{\gamma_1 - 1}{2} M_1^2}$$

The value of γ used in the computer model for the unreacted gas at the stations prior to combustion is that of the stationary propellant gas. Thus, the Mach number at station 5 is determined using the initial and final values of γ in Eq. 3.1, along with the value of the non-dimensional heat parameter (Q) predicted from the thermally choked chemical

equilibria solution.* The pressure and temperature of the unreacted propellant gas can be determined at station 5, once M_5 is known, from the ideal gas equation of state and the conservation equations of mass and momentum (Eqs. 2.1 and 2.3) as follows:

$$\frac{p_5}{p_6} = \frac{1 + \gamma_6}{1 + \gamma_1 M_5^2} \quad (3.2)$$

$$\frac{T_5}{T_6} = \left(\frac{\gamma_1}{\gamma_6} \right)^2 \frac{(\gamma_6 - 1)c_{p6}}{(\gamma_1 - 1)c_{p1}} \left(\frac{p_5 M_5}{p_6} \right)^2 \quad (3.3)$$

3.3.1 Base Total Pressure Drop

In order to determine the area ratio at which the normal shock must be to satisfy the change in flow properties across the control volume, the total pressure loss relative to the projectile in both the supersonic and subsonic regions must be estimated. The total pressure loss due to the sudden area change at the bluff base of the projectile (Fig. 3.1) is estimated by assuming the base pressure is constant across the duct (i.e., $P_5=P_5'$).^{10,23} The Mach number in the flow region just before the area change at the projectile base (M_5') is determined such that the subsonic flow can reach the full tube area at constant pressure, while satisfying the energy and mass conservation equations of channel flow.⁸ This procedure leads to the following quadratic expression for the square of the Mach number at station 5' as a function of the conditions at station 5:

* Note: γ_6 as used here, is the effective γ based on the assumption $c_{p6}=h_6/T_6$.

$$M_{5'}^4 + M_{5'}^2 \frac{2}{\gamma_1 - 1} - \left(\frac{A_1}{A_{5'}} \right)^2 \left(M_5^4 + M_5^2 \frac{2}{\gamma_1 - 1} \right) = 0 \quad (3.4)$$

The positive root of the discriminant provides the square of the proper Mach number. The total pressure loss at the projectile base ($P_{t5}/P_{t5'}$) is then calculated from the following:

$$\frac{P_{t5}}{P_{t5'}} = \left(\frac{1 + \frac{\gamma_1 - 1}{2} M_5^2}{1 + \frac{\gamma_1 - 1}{2} M_{5'}^2} \right)^{\frac{\gamma_1}{\gamma_1 - 1}} \quad (3.5)$$

3.3.2 Diffuser Total Pressure Drop

The total pressure loss of the flow in the supersonic regions of the projectile diffuser (the regions between stations 1, 2 and 3) is estimated with an oblique 2-D shock model that computes the total pressure loss across an arbitrary number of reflected shocks generated between a wedge and a flat wall. The effects of diffuser inefficiency can then be estimated by changing the wedge angle and the number of reflected shocks. This model tends to overpredict the actual total pressure loss of the conical diffuser (when using the same wedge angle as the nose cone) as the flight Mach number increases (conical flow has smaller oblique shock wave angles and a region of isentropic compression between the shock wave and cone), though it does provide a relatively simple model which qualitatively represents the effects of fixed geometry compression of a supersonic flow over a wide range of Mach numbers. The total pressure loss in the

diffuser affects both the starting Mach number* and the minimum operating Mach number of the TCRA propulsive mode.

Profiles of the total pressure ratios for the diffuser and the base flows as a function of Mach number are shown in Fig. 3.4 for a projectile accelerating throughout the operating velocity range of a propellant mixture consisting of $2.7\text{CH}_4+2\text{O}_2+5.8\text{N}_2$. Diffuser performance is based on the initial oblique shock and the first shock reflected off a flat wall that are generated by a 10° wedge traveling at the velocity of the projectile. The total pressure loss at the base is determined for a base-to-tube diameter ratio of 0.5, which is close to that of the typical experimental projectile (actual effective base-to-tube diameter ratios of the experimental projectiles vary between 0.48 and 0.6, depending on the fin thickness).

The total pressure ratio decreases both in the diffuser and at the base as the flight Mach number increases. The diffuser total pressure ratio determined in this case is much lower than would be generated by the conical shock system of a cone having the same half-angle; however, the diffuser model does indicate the qualitative effects of fixed geometry compression over a wide range of Mach numbers. The total pressure ratio at the base of the projectile is determined from a virtual M_5' which may not actually exist if the normal shock is predicted to be off the body. However, the model for the total pressure loss at the projectile base serves its purpose by providing a way to investigate the effects of an entropy increase in the subsonic portion of the flowfield on the location of the normal shock.

* The starting Mach number for a particular projectile geometry in a given gas mixture is the flight Mach number which results in sonic flow at the projectile throat. This is the minimum Mach number at which a projectile can travel through an unreactive gas mixture.

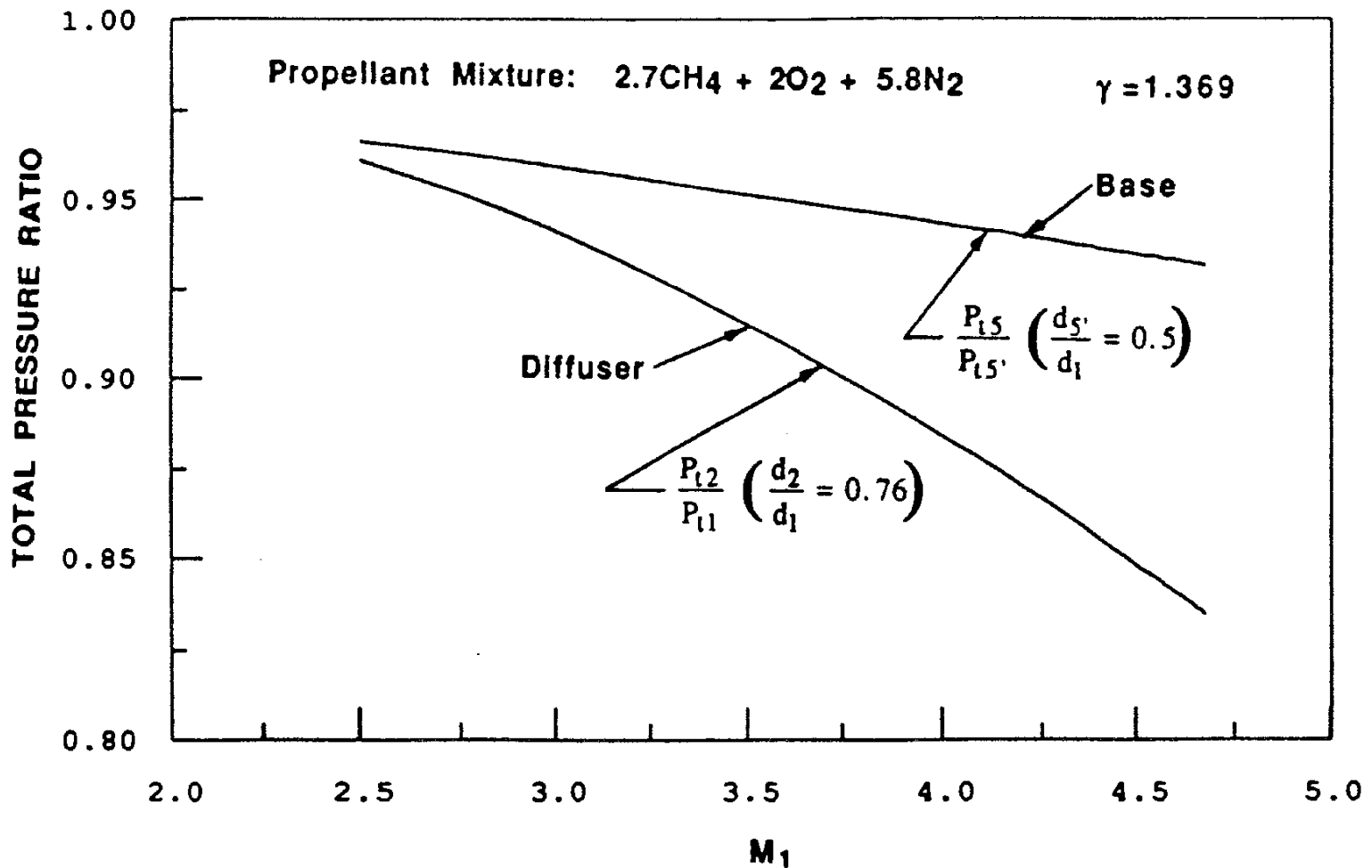


Fig 3.4 Diffuser and base total pressure ratio-velocity profiles.

3.3.3 Normal Shock Location

The flow area ratio which stabilizes the normal shock ($A_3/A_1 = A_4/A_1$) is determined iteratively, once the total pressure losses of the various components have been estimated at a given flight velocity. The iterative procedure begins by assuming the normal shock has an incoming flow Mach number (M_3) equal to M_1 , which results in an initial guess for the subsonic flow after the normal shock (M_4) which will always be higher than M_5 . An initial guess for the flow area ratio A_4/A_1 is then determined from the channel flow area relationships⁸ using M_5 , M_4 , and P_{t5}/P_{t4} . After setting

$A_3/A_1 = A_4/A_1$, a new value for M_3 is then estimated from M_1 and the predetermined value of P_{t3}/P_{t1} . A new estimate of M_4 is computed with the normal shock relations, and the iteration procedure continues until the flow area ratio for the normal shock converges. The flow area ratio which stabilizes the normal shock is then converted to the equivalent projectile-to-tube diameter ratio in order to relate the separation distance between the normal shock and the projectile throat (for a given body angle).

The effects of component efficiency on the location of the normal shock, in most of the theoretical operating Mach number range of a propellant mixture consisting of $2.7\text{CH}_4+2\text{O}_2+5.8\text{N}_2$, are shown in Fig. 3.5. The ratio of projectile-to-tube diameter at which the normal shock is predicted to be located, by the detailed TCRA model, is plotted versus Mach number for both an ideal projectile and a non-ideal projectile that includes different combinations of component total pressure losses. In the ideal case the normal shock location is predicted, at any Mach number, to be farther back on the body than is expected for the non-ideal cases, and the normal shock is predicted to fall completely off the projectile at the C-J detonation velocity limit, if it has an aftbody that tapers to a point.

The effect of including only the diffuser total pressure loss on the normal shock location profile is to move the shock slightly forward of its ideal location, as shown by the curve just above that of the ideal case in Fig. 3.5. The next curve above the ideal curve represents the location profile due only to the base total pressure loss. Note that the effect on the shock location of a small total pressure loss in the subsonic flow region of the projectile is much greater than the effect of the larger total pressure loss resulting from shock waves in the diffuser. This occurs because the supersonic total pressure loss in the diffuser reduces the flow Mach number ahead of the normal shock which, in turn, decreases the distance up the body that the shock must travel to compensate for the

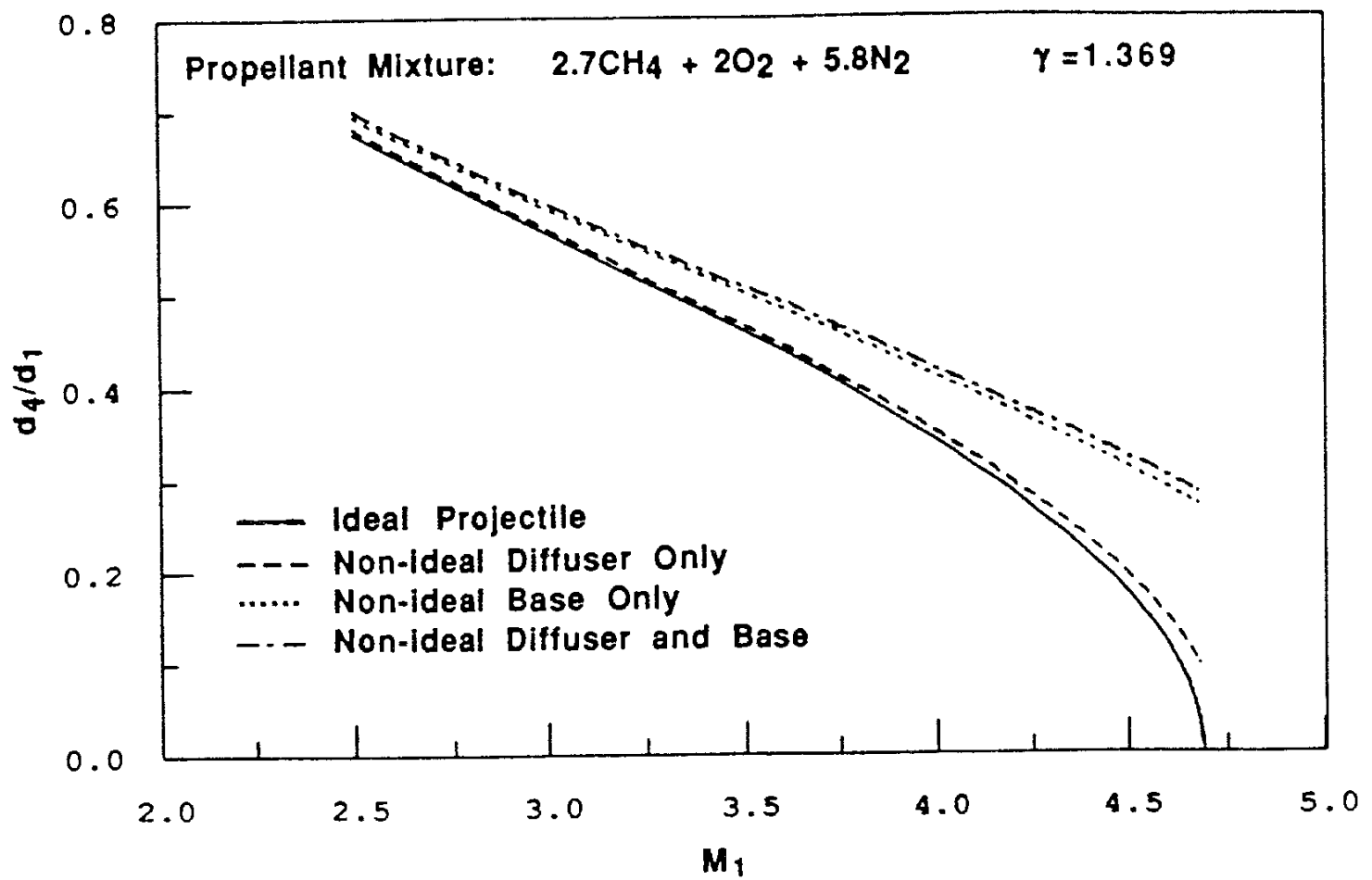


Fig 3.5 The effects of component total pressure loss on projectile-to-tube diameter ratio (d_4/d_1) at the normal shock location predicted for the TCRA propulsive mode.

corresponding entropy increase of the oblique shock waves. The subsonic total pressure loss at the base does not affect the flow conditions ahead of the normal shock; thus, the normal shock must move farther up on the body to reach a point where its incoming Mach number (M_3) is low enough to reduce the contribution of the normal shock entropy increase to the total entropy rise (as discussed in Sec. 3.2).

Combining the supersonic and subsonic total pressure losses results in a normal shock location that is about 5% farther up on the body than was predicted for an ideal

projectile operating at a flight Mach number of; $M_1 = 2.5$. The location of the normal shock at the C-J detonation velocity is predicted to be ~30% farther up on the body than ideal (if the rear of the non-ideal projectile tapered to a point); however, the thrust is still theoretically nonexistent at this velocity because the change in stream thrust across the control volume predicted by the global TCRA theory equals zero. Since a fixed amount of internally generated entropy, for a specified mass flux, must be added to the flow throughout control volume to result in thermal choking, and the amount of entropy increase due to the heat addition process is fixed by the propellant mixture composition and total enthalpy of the flow, the normal shock must move forward on the projectile body and decrease in strength to compensate for the other total pressure losses arising in the unreacted flowfield.

CHAPTER 4

EXPERIMENTAL FACILITY

The ram accelerator facility consists of a light gas gun, ram accelerator test section, final dump tank and projectile decelerator (Fig. 4.1). The 38 mm bore, 6 m long, single-stage gas gun is capable of accelerating the obturator and projectile combination (typical combined mass ~60-115 gm) to velocities up to 1300 m/sec at a maximum helium pressure of 340 atm. The muzzle of the gas gun is connected to a perforated-wall tube that passes through an evacuated tank which serves as a dump for the helium driver gas.²⁵ An instrument station located 12.7 cm from the muzzle of the helium vent tube has one pair of opposing instrument ports that allows monitoring the residual muzzle pressure behind the projectile and its time-of-passage before it enters the test section.

The 16 m long ram accelerator test section consists of eight steel tubes of equal length having a bore of 38 mm, and an outer diameter of 100 mm. There are a total of 144 instrumentation ports at 40 regular intervals along the test section of the ram accelerator. Each of the 2 m long steel tubes has five equally spaced axial instrument stations, three of which have four ports at right angles to each other and the other two stations have three ports separated by 120 degrees. This permits the simultaneous use of either three or four transducers at each station. Two of the four port stations are located 20 cm from each end of the tube segment and the third is placed at the middle of the tube. The three port stations are centered between the ones having four ports, this results in a nominal instrument station spacing of 40 cm along the length of the test section when the

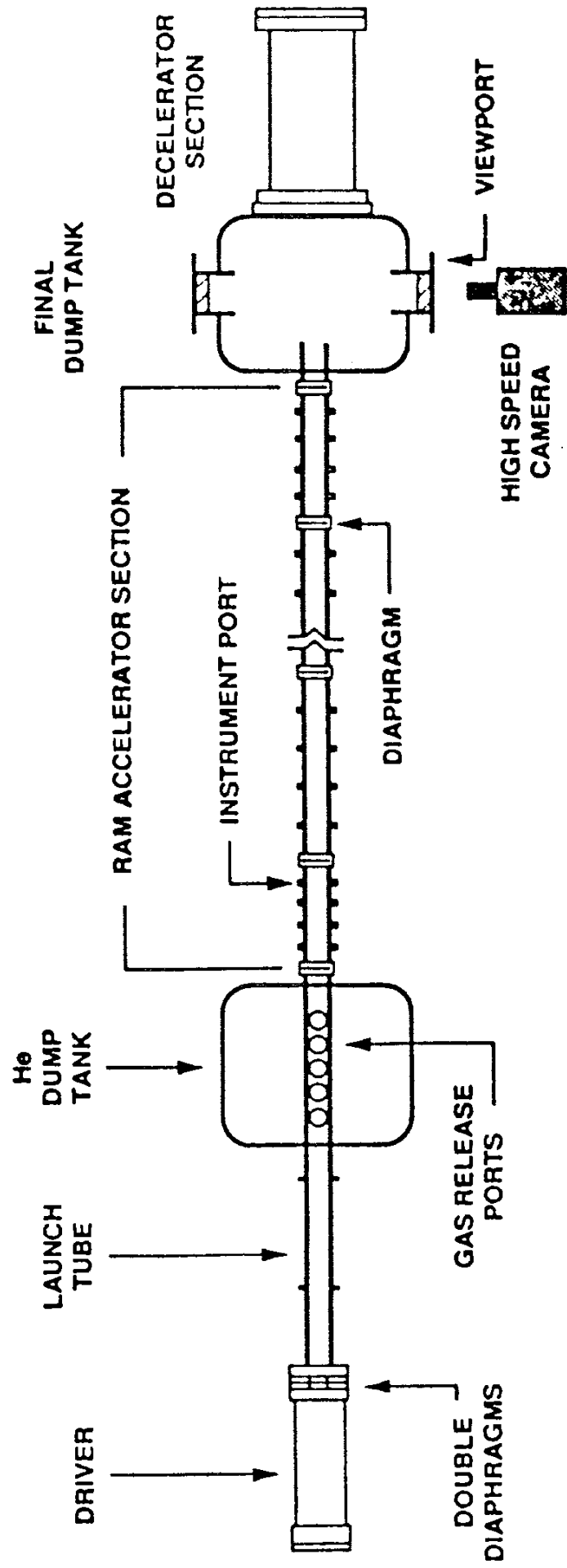


Fig. 4.1 Schematic of ram accelerator test facility.

tubes are connected together. Dimensions of the instrument ports are such that standard piezoelectric pressure transducers (6 mm diameter access hole to the sidewall of the internal bore) can be located in any of these observation stations. Remaining ports are used to mount electromagnetic transducers and fiber-optic light guides. Unused ports are sealed with a blank steel plug having the exterior dimensions of the standard pressure transducers. Track-and-hold circuits of the 1 MHz digital data acquisition system, used to acquire the data, can be triggered by the output from any of the sensors located along the test section. Multiplexing permits monitoring of over 100 separate input signals on the 32 available data channels.

The maximum static pressure that be contained by the steel tubes (4140 alloy, hardened to Rockwell C32-36) of the ram accelerator test section is ~5500 atm (based on thick tube wall theory³⁶ using the minimum outer diameter at the tube ends; O.D. = 63.5 mm, and a yield stress of ~8600 atm). The highest static pressures that are generated in the experiments result from overdriven detonation waves being pushed ahead of an unstarted projectile. Peak overdriven detonation pressure ratios of ~50 have been measured in the experiments. To maintain a safety factor of at least two, during the worst case scenario, the fill pressure is limited to 50 atm. Thin Mylar diaphragms, ranging in thickness from 0.2 mm to 1.6 mm, are placed in the tube joints to seal each end of the ram accelerator test section and to separate segments filled with different propellant mixtures.

The end of the ram accelerator test section is connected by a 0.76 m long drift tube of similar bore to a 2.4 m long evacuated dump tank, through which the projectile is allowed to fly freely. Two instrument stations, each having one pair of opposing instrument ports, are located in the drift tube to provide final velocity measurements and to examine

the pressure field about the projectile as it exits the test section. The first station in the drift tube is 35.8 cm from the end of the ram accelerator test section and the interval to the second instrument station is 34.9 cm. The final dump tank has a pair of 25 cm diameter viewing ports for high-speed photography and additional velocity measurements.²⁵ Free-flying projectiles are brought to a stop in tightly packed rug remnants contained in a mild steel catcher tube attached to the far end of the dump tank. The catcher tube has internal dimensions of 20 cm I.D. by 1 m long, and its tube wall thickness is 2.5 cm. The far end of the catcher tube is closed off by means of a 15 cm thick plate of 4150 steel alloy.

4.1 Ram Accelerator Test Section Instrumentation

Data from the experiment are collected and stored with a Lecroy data acquisition system (DAS) and the data are processed on an IBM-compatible 386 type micro-computer using the Lecroy Wave-Form Catalyst software. Major components of the DAS are two Lecroy CAMAC crates (Model #1434), five Quad 10-bit transient digitizing modules (Model #8210) with ten memory modules (Model #8800A), three Quad 12-bit transient digitizing modules (Model #6210), and two CAMAC to GPIB interfaces (Model #8910A). Digitizing modules can be configured to provide 32 data channels with a minimum memory time window of 16 msec at a sampling rate of 1 MHz. Maximum amplitude range for data storage is ± 5 volts with a digitization level of 10 mV. Triggering of the DAS is accomplished with the output signals from either an electromagnetic transducer or pressure sensor that can be located at any instrument station along the ram accelerator test section.

4.1.1 Electromagnetic Sensors

Time-of-passage of the projectiles at each instrument station is determined with an electromagnetic (EM) transducer that detects an annular magnet placed at the throat of the projectile. The EM sensors consist of ~20 turns of 32 gauge copper coil wire wrapped around a solid polycarbonate core having an O.D. of 2 mm.^{27,28} The sensing coil is inserted into a one-piece protective stainless steel casing which can withstand the high pressure transients of the experiments. Typical output signal intensity of the EM sensors, due to the passage of the projectile throat magnet, is ~5 mV and the typical signal width is ~15 μ sec. Signals are amplified 100 times with amplifiers having a 2 MHz bandwidth, and then multiplexed through a summing amplifier and digitally stored by the DAS.²⁸ Output from 43 different EM stations are stored on 6 digitizing channels in this manner. Multiplexed sensors are situated at stations that are typically 0.8 m to 2 m apart, which results in a minimum temporal separation of ~320 μ sec for a projectile velocity of ~2500 m/sec. During normal TCRA operation, this has been found to be more than sufficient temporal separation to distinguish the axial location of a particular EM signal from the string of signals that result from multiplexing individual sensors.

4.1.2 Pressure Transducers

Pressure sensors are used to monitor the pressure field generated by the passing projectile and the associated combustion activity. The primary piezoelectric pressure transducers used in the experiment are manufactured by PCB Piezotronics Inc., with model number 119M39-402M99. They have a natural resonant frequency of ~450 KHz and vary in sensitivity from 9 to 18 mV/atm. These pressure transducers have a

6800 atm maximum operating pressure rating and are designed to have a 1 μ sec rise time. The ability of the transducers to follow the transient behavior of the pressure waves about the projectile have made them invaluable in interpreting the gasdynamic phenomena generated by the projectile passage. Output signals from various stations are input into a multiplexer which isolates the individual signals and monitors each sensor for ~ 2 msec after the projectile has passed. The pressure sensors which are multiplexed together are situated at stations that are spatially separated by 3 m to 5 m, this multiplexing configuration allows monitoring of up to four transducers on a single DAS channel for projectile velocities up to 2500 m/sec.

4.1.3 Optical Fiber Probes

Luminosity probes have been developed which monitor the light emissions from the phenomena occurring in the vicinity of the projectile. The luminosity probe design has a 1 mm diameter optical fiber pulled through a small hole in a blank instrument plug. This fiber has a polymethyl-methacrylate core, fluorine polymer cladding, and a black plastic jacket. The jacket is stripped from the last 3 cm of the fiber, the bare acrylic fiber is coated with epoxy before it is inserted through the steel plug, and its sensor face is sanded flush to the bottom surface of the probe and polished.²⁹ The acceptance angle of the flush mounted fiber is 56° ; thus, the luminosity data must be interpreted as emanating from within the viewing cone of the sensor.³⁰ Nevertheless, the correlation of the luminosity data with the EM and pressure signals has provided valuable information on the combustion phenomena that occur in the vicinity of the projectile.

The optical fiber guides the in-tube light to a photodiode whose output is logarithmically amplified. The PIN diode has a surface area of $\sim 5 \text{ mm}^2$, this can

accommodate the ends of up to four different fiber-optic cables to effect an optical multiplexing of the observed light transmitted from the experiment. Attenuation factors for the individual fiber-optic probes (due to fiber-optic cable length and surface condition of the viewing window) are calibrated with several reference light sources (He-Ne laser, mercury arc lamp, and 6 VDC incandescent lamp) when the output from different optical fibers are to be quantitatively compared.³⁰ Qualitative comparison of the outputs from different stations is based on the relative intensity levels of the luminosity data at various locations in the region of the projectile.^{21,22}

4.2 Propellant Gas Handling Procedures

4.2.1 Propellant Gas Mixing

The gas mixing system has the capability of remotely filling the ram accelerator test section with propellant mixtures having up to five different components. Calibration of the steady mass flow rates of various gases through the orifice of a micro-metering valve (Whitey Model #SS22RS4) is accomplished by timing the pressure rise in the test section volume at several different dome regulator pressure settings upstream of the orifice. Hand regulators use nitrogen gas within the operating bunker to remotely control the pressure settings ahead of the metering valves.²⁵ (The plumbing lines for the constituents of the propellant mixture are kept outside of the operating bunker to avoid exposing personnel to combustible gases.) Measured mass flow rates are repeatable to within 0.5% for this calibration procedure. Pressure settings for the desired propellant mixture are interpolated from the individual mass flow rate calibrations. Individual gases

are metered and brought together through several T junctions to mix inside the long runs of stainless steel tubing (typical $L/D \gg 1000$) which route the propellant mixture to the desired tube segments. Gas chromatography of the propellant mixtures is able to validate the relative mole fractions of the individual components to within $\sim 2\%$.

Regulating the pressure above the metering valves provides a steady mass flow rate through their orifices as long as the back pressure on the downstream side remains below the critical choking pressure (unchoking of the orifice occurs when the back pressure is greater than $\sim 1/2$ the upstream pressure). Typical back pressures are less than 3 atm above tube fill pressure when three gases are combined at the flow rates associated with minimum dome regulator pressure settings of 70 atm. This allows the test section to be loaded with steady mass flow rates with fill pressures up to ~ 32 atm. The dome regulator settings required to charge the test section with a gaseous propellant mixture at 50 atm have to be set at or above 106 atm to minimize variations in propellant composition between experiments. Because of the lack of fine control of the hand regulators, the pressure at the dome regulators can only be adjusted to within 0.7 atm of the desired pressure setting for each component of the propellant mixture. This results in a maximum mixture variation between experiments of $\sim 2\%$ for propellant mixtures which are loaded in the test section while all dome regulator pressure settings are greater than 70 atm. Propellant fill pressures are monitored with 0.5% accurate vibration-resistant gauges which have been calibrated with a mirrored 0.25% accurate test gauge over the anticipated fill pressure range of the ram accelerator experiments. The observed nonlinearity of the test section pressure gauges introduces a maximum uncertainty in fill pressure of ± 0.7 atm for every stage.

4.2.2 Gas Handling Procedure for Experiments

All of the ram accelerator experiments begin by evacuating the test section segments, launch tube, and dump tanks of the facility down to ~1 torr. Hand regulators set the pressure on the dome regulators to within ± 0.7 atm of the desired upstream metering valve pressure setting, and the flowing gases are brought together and allowed to mix as they flow out the dump line until the pressure transients from valve switching have died away (typically, one minute is a sufficient amount of time). When the mass flow rates of each gas component have stabilized the propellant mixture is then routed to the appropriate tube segment. Gauges measuring the propellant fill pressure are monitored with a video camera as the propellant mixture is being loaded. After the ram accelerator stages have been loaded, the breech of the light gas gun is charged with helium to the appropriate pressure in order to bring the projectile-obturator combination up to the desired entrance velocity. The DAS is triggered by the pressure pulse which is generated by the nose cone of the projectile as it passes the first instrument station in the test section. After exiting the test section, the projectile free-flies past the observation window where a high-speed photograph is taken to discern the condition of the projectile before it is suddenly decelerated in the catcher tube. Subsequent re-evacuation of the system removes the combustion products and helium driver gas before the recycle procedure begins.²⁵

4.3 Experimental Projectile Configuration

A schematic of the nominal projectile geometry that has been used in the majority of the experimental work to date is illustrated in Fig. 4.2. It is fabricated of magnesium alloy (ZK60 AT5) or aluminum alloy (7075 T6) in two hollow pieces that thread together (nose cone and body). The nominal projectile shown has a measured volume of 66 cm^3 and has been manufactured with different internal dimensions that result in a range in total mass of 45 to 100 gm (depending on projectile material). Four fins serve to center the projectile in the tube and the octagonal cross section of the body is simply a machining convenience. Thin rubberized magnetic sheets are mounted in the nose-body joint and in the base of the body. When the projectile passes by the electromagnetic transducers in the accelerator tube, the magnetic material induces signals which are used to determine the time-distance history of the projectile and, hence, its velocity.^{27,28}

4.3.1 Nose Cone

The primary variables considered in the design of the nose cone are the cone half-angle and mass distribution. Nose cones with large half-angles ($>15^\circ$) tend to reduce the upper operating Mach number limit of the TCRA propulsive mode due to pre-ignition of the propellant mixture by one of the conical shock waves. Experiments have indicated that nose cones with too small a half-angle ($<10^\circ$) result in excessively long noses that move the projectile's center of gravity (CG) too far forward, this reduces the upper velocity potential due to asymmetric pressure forces on the nose arising from a canted projectile. Wide operating Mach number ranges have been observed with projectiles having nose cone half-angles between 10° and 12.5° . The depth and half-angle of the

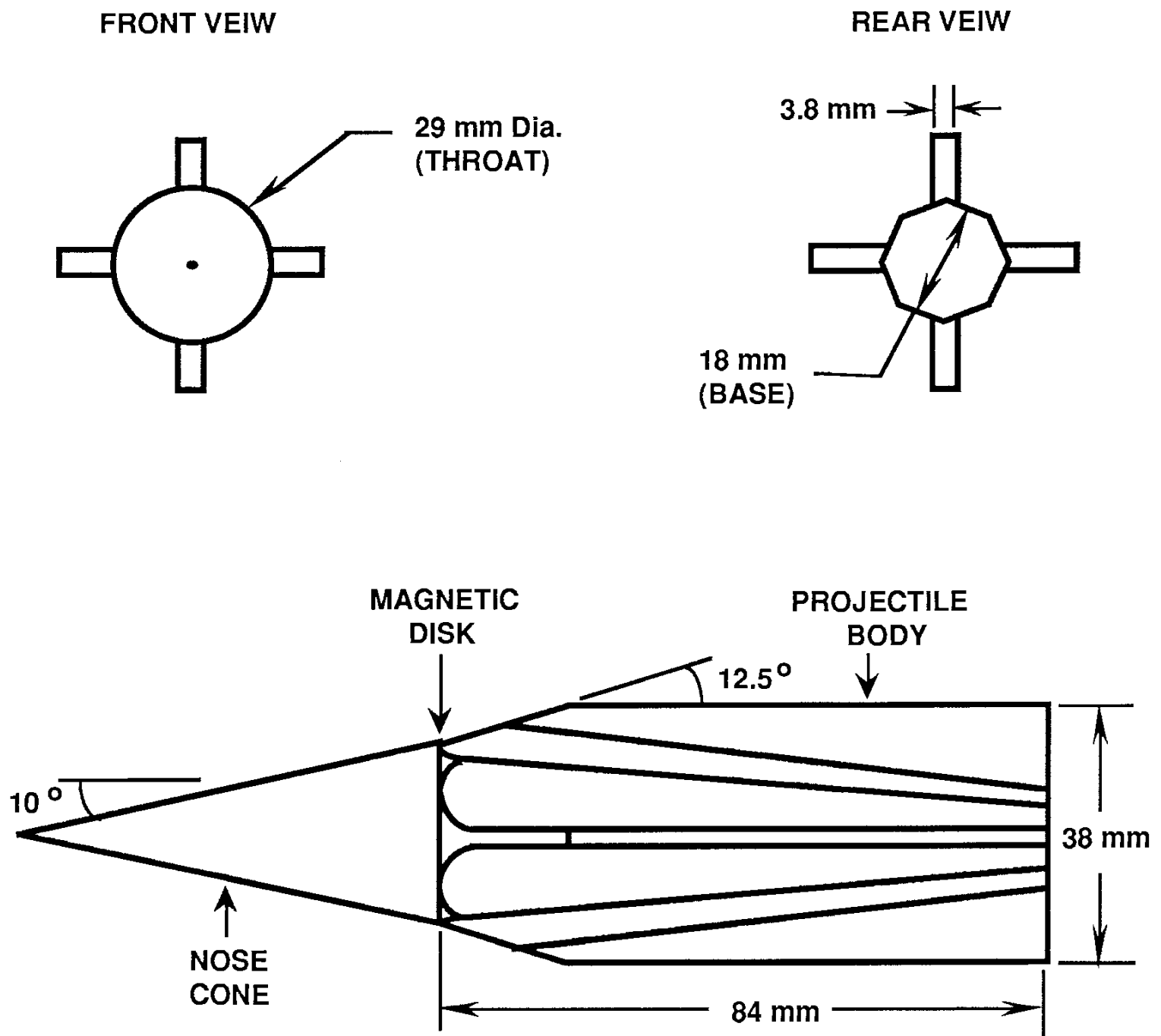


Fig. 4.2 Schematic of experimental projectile and its nominal dimensions.

internal coning of the nose affect both its CG and its wall thickness. Current nose cones have a smaller internal angle than the outside angle in order to provide a wall thickness which decreases toward the nose tip. This results in a linear variation in wall thickness which provides the nose cone with greater resistance to implosion than a cone made with the same amount of material having a constant wall thickness. The depth of internal coning is the primary factor in determining the CG of the nose cone, consequently, it is a factor in the location of the overall CG of the assembled projectile.

4.3.2 Body Configuration

The configuration of the projectile body has many degrees of freedom to explore. Material properties, CG, external geometry and aerodynamic effectiveness are all factors considered in the design of the appropriate body configuration. Desirable mechanical properties of the body material are: high impact and abrasion resistance, high strength to density ratio, low chemical reactivity in a reducing atmosphere (most propellant mixtures used to date are fuel rich) and high temperature capability. Resistance to destabilizing forces arising from asymmetric pressure fields about the projectile is enhanced by maintaining an overall projectile CG behind the point where the leading edge of the fins are in contact with the tube wall. Strong durable fins reduce the amount of fin wear that the projectile experiences as it accelerates through the test section.

Primary body variables that interact with the flow around it are: the fin dimensions and their leading edge configuration, body length, and the effective throat and base diameters (actual cross-sectional area equated to a circle having the same area). The leading edges of the fins affect the area profile in the region behind the throat and they

interact with the system of reflected conical shock waves generated between the cone and tube wall. Fin thickness is a significant contributor to the flow area profile along the body and the strength of the centering fins. The body length determines fin length (for a given leading edge geometry) and the separation distance between the recirculating zone at the base and projectile throat. Body length and nose cone half-angle determine the turning angle of the flow around the nose-body joint for different projectiles having the same base and throat cross-sectional areas.

The nose cone base diameter normally sets the maximum diameter of the projectiles used in the experiments, and this determines the throat-to-tube flow area ratio. Details of the external shape of the leading edges of the fins and the projectile body geometry at the nose-body joint govern the actual area profile in the throat region (defined here as the region between the projectile throat and the point where the fins first contact the tube wall, the effective flow area is nearly constant throughout this region for the nominal projectile configuration). Throat area ratio and aerodynamic efficiency have significant effects on both the starting Mach number and the static temperature of the propellant gas flowing through the throat region. The turning angle of the flow over the nose-body joint is expected to be a factor in the separation of the flow over the rear part of the projectile body and is under current computational and experimental investigations.

4.4 Data Reduction Technique

The velocity and acceleration of the projectile at any point in the ram accelerator tube are determined from the time-distance ($t-x$) data generated by the EM sensors. Experimental mean projectile velocity is determined from the central differences of the $t-x$

data table. This results in an approximation to the velocity at a point midway between the instrument stations. The maximum uncertainty in the experimentally determined mean projectile velocity is given by the sum of the uncertainties in measuring both the separation distance between EM sensors and the transit time. The maximum relative uncertainty in knowing the separation distances between instrument stations is $\sim 0.5\%$, if the displacements due to a 1 mm thick Mylar diaphragm in every joint are ignored (worst case scenario). The relative uncertainty in measuring the transit time between transducers is proportional to the projectile velocity and is due primarily to a finite sampling rate and random EM signal distortions. Analog EM signals are digitized at a sample rate of 1 MHz, this contributes a maximum uncertainty level of $\sim 0.5 \mu\text{sec}$ in the measurement of the arrival time of the projectile at any instrument station.

A more serious factor limiting the time resolution of the projectile history during an experiment is the distortion of the EM sensor signal itself. Shown in Fig. 4.3 are the outputs from four different EM sensors located at the same instrument station. Signals are time synchronized and all are displayed on the same vertical scale (500 mV/div). Each major division on the horizontal scale indicate a 20 μsec time interval. Ideally, the time-of-passage of the center of the magnet is determined from the intersection of the line-of-symmetry of the signal with the time axis. Interpretation of the asymmetric and distorted signals is not always so straightforward. Normal procedure is to take the time nearest the midpoint of the ascending signal (or descending if the polarity of the throat magnet is reversed) as the time-of-passage. The times of projectile magnet passage (relative to the trigger time) taken from the EM signals shown are: 4.138, 4.137, 4.137, and 4.136 msec, from the upper trace to the lower trace, respectively.

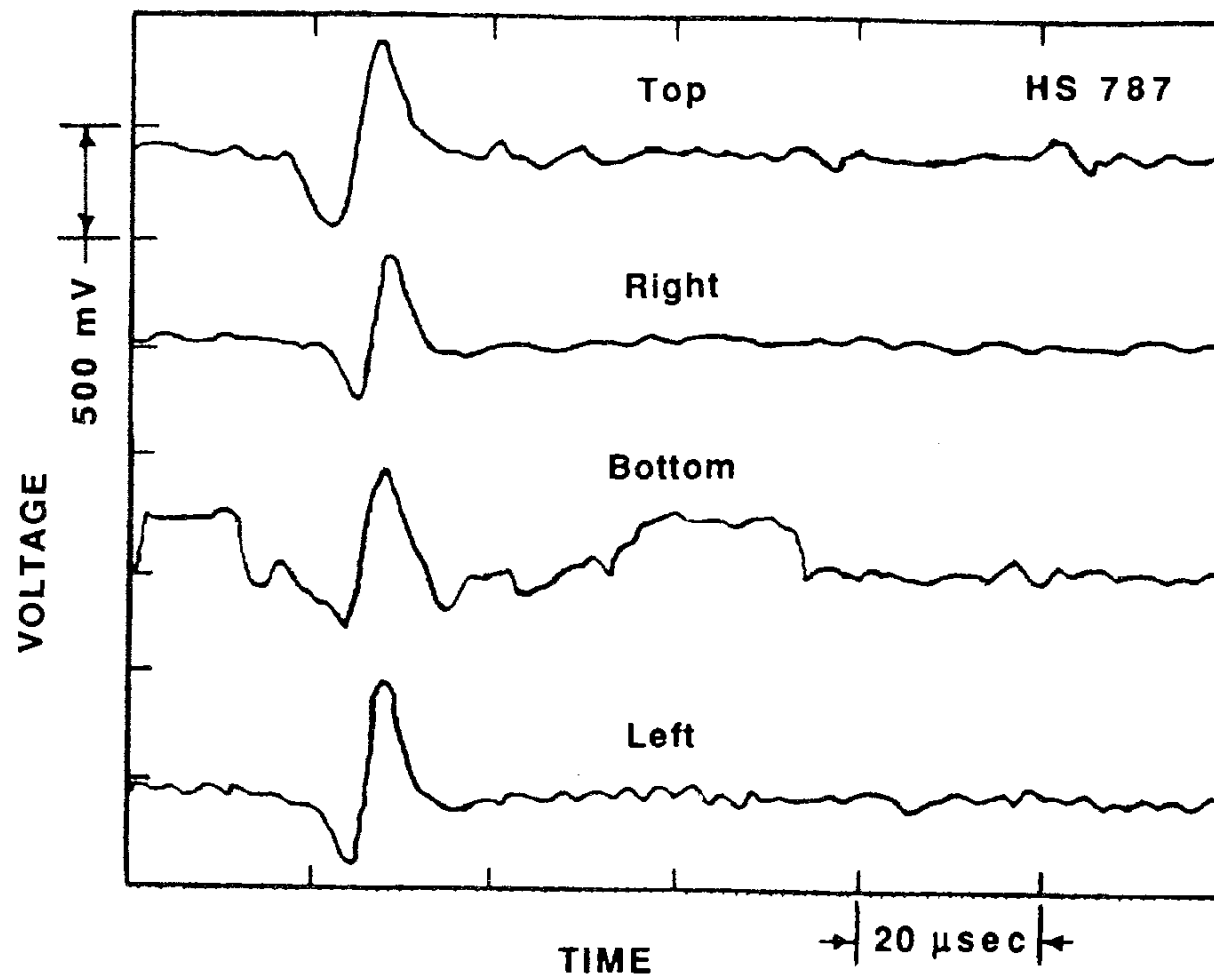


Fig. 4.3 Experimental data from coaxial EM sensors.

Additional complications in interpreting the EM signals arise from the shielding effects of the electrically conducting probe casing (316 stainless steel). The diffusion of the magnetic field through the protective casing delays the true signals and results in a slight phase shift which displaces their lines of symmetry.^{27,28} However, since all the probes are of uniform construction and the projectile does not change velocity between adjacent instrument stations at an extreme rate, the accuracy of the mean velocity determined from the output of adjacent probes is not affected seriously by differences in this small time lag. (Experiments have shown this phase shift to be $\sim 2 \mu\text{sec}$ at projectile velocities of $\sim 1500 \text{ m/sec}$.²⁸)

The EM data shown in Fig. 4.3 are representative of the variations in signal quality that are observed during routine experiments conducted in the current ram accelerator facility. The maximum discrepancy in determining the time-of-passage of the projectile between these signals is 2 μ sec, which accounts for the digitizing limitations of the DAS and the typical level of signal distortions. Thus the overall uncertainty in measuring the transit time (Δt) between any two EM stations is $\sim 4 \mu$ sec. The linear relationship of the relative uncertainty, due to measurement errors, for the experimentally determined mean velocity (\bar{u}) is as follows:

$$\frac{\Delta \bar{u}_{EM}}{\bar{u}} = \frac{\Delta x}{\bar{x}} + \frac{\Delta t}{\bar{x}} \bar{u} \quad (4.1)$$

where Δx is the uncertainty in the measurement of the separation distance between adjacent instrument stations and \bar{x} is the nominal instrument spacing.

For an accelerating projectile, the mean velocities will always under-predict the actual projectile velocity at the midpoint. The magnitude of the relative velocity error resulting from ignoring the effects of the acceleration on the velocity-distance (\bar{u} - x) profile of an experiment is related to projectile velocity as follows:

$$\frac{\Delta u_{\ddot{x}}}{\bar{u}} = \sqrt{1 + \left(\frac{\ddot{x}_0 \bar{x}}{2 \bar{u}^2} \right)^2} - 1 \quad (4.2)$$

where \ddot{x}_0 is the average acceleration level between sensors. A plot of the relative mean velocity error resulting from ignoring acceleration is shown in Fig. 4.4 (bottom curve), for a projectile undergoing a steady acceleration of $\ddot{x}_0 = 50,000$ g through a tube having

a uniform instrument spacing of $\bar{x} = 40$ cm. Note that the effects of acceleration on the experimental mean velocity, at projectile velocities above 1000 m/sec, results in relative mean velocity errors much less than 0.5%.

The total relative uncertainty in the mean velocity measurements of the experiments is the sum of errors given by Eqs. 4.1 and 4.2. For an experimental uncertainty in instrument spacing of; $\Delta x = 1$ mm, the variation of the total relative uncertainty in mean velocity, determined with the previously mentioned instrument spacing and acceleration conditions, is shown by the middle curve in Fig. 4.4 for the velocity range of 1000-3000 m/sec. Since the uncertainty resulting from ignoring accelerations up to 50,000 g is much smaller than the uncertainty in measuring the mean velocity, the \bar{u} -x history of the projectile, determined from the first center differences of the raw t-x data table, is not significantly distorted by the routine acceleration levels (15,000 g to 30,000 g) experienced in the current ram accelerator experiments. Thus, the actual projectile velocity at the midpoints between adjacent stations is adequately represented, within the bounds of the measuring uncertainty, by the experimental mean velocity.

Comparisons of theoretical predictions to experimental results for the projectile's velocity and acceleration histories are presented in four different formats: t-x, \bar{u} -x, \ddot{x} -u and I-M. Experimental \ddot{x} -u and I-M histories are determined from a polynomial curve fit to the \bar{u} -x data. Henceforth, the velocity-distance profile determined by this curve fit is designated by u or u(x) to distinguish it from the raw mean velocity \bar{u} . The order of the polynomial is determined from the sequence of Chebyshev polynomials that results in a curve (typically 5th to 8th order) having the minimum standard deviation in u-x history

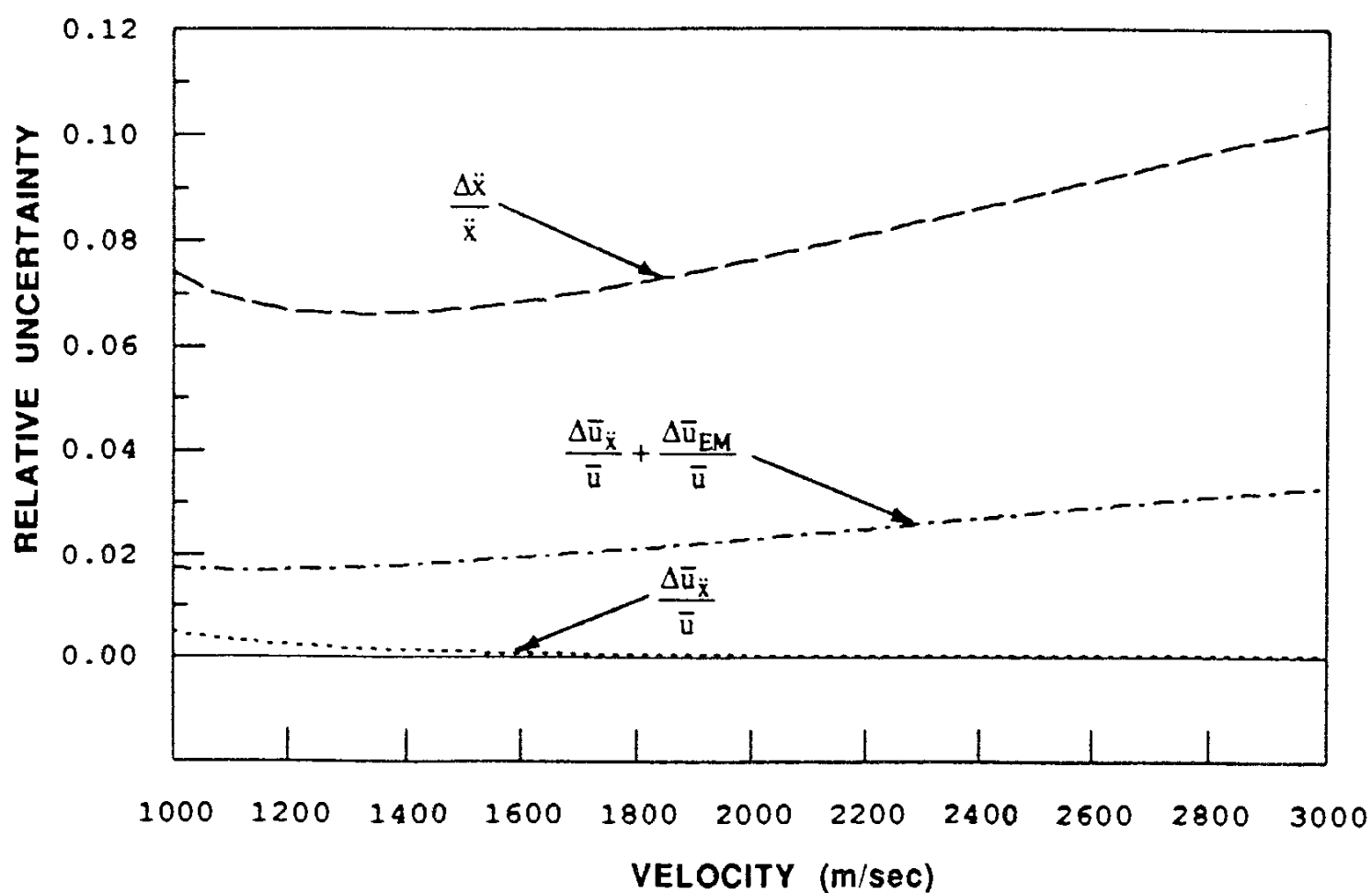


Fig. 4.4 Relative uncertainty in velocity and acceleration measurements.

with respect to the experimental \bar{u} - x profile.³² Projectile \ddot{x} - u profiles are determined by differentiating these polynomials [$\ddot{x}(x) = u(x)du(x)/dx$] and plotting the results against the corresponding velocity, $u(x)$. (This data reduction scheme follows the trends in \ddot{x} - u behavior better than the alternative approach of fitting a curve to the original t - x data and doubly differentiating the resulting curve to obtain projectile acceleration.) Experimental I-M profiles, based on the projectile mass, propellant fill pressure and the acoustic speed of the propellant mixture, are the non-dimensional version of the \ddot{x} - u curves.

The velocity uncertainty in the polynomial u - x history of a particular experiment is the sum of the polynomial's mean deviation, σ , and the total mean velocity error due to experimental measuring uncertainties. The corresponding relative uncertainty in the

acceleration profile, deduced from an experiment having a peak acceleration level of \ddot{x}_0 , can be determined to the first order as a function of velocity as follows:

$$\frac{\Delta\ddot{x}}{\ddot{x}} \approx \frac{\sigma}{u} + 2\frac{\Delta x}{\bar{x}} + 3\frac{\Delta t}{\bar{x}}u + \frac{1}{2}\left(\frac{\ddot{x}_0\bar{x}}{u^2}\right)^2 \quad (4.3)$$

The relative acceleration error is plotted versus velocity in Fig. 4.4 (upper curve) for a typical polynomial mean deviation of $\sigma = 20$ m/sec and the same experimental conditions as before ($\bar{x} = 0.4$ m and $\ddot{x}_0 = 50,000$ g). This curve shows that even for these extreme experimental conditions, the data reduction scheme described above, using the current instrumentation of the ram accelerator test section, has the ability to determine the instantaneous acceleration experienced by a 3000 m/sec projectile to within ~10%.

CHAPTER 5

EXPERIMENTAL RESULTS AND DISCUSSION

Over 800 experiments have been conducted in the ram accelerator facility at the University of Washington since it first became operational in 1985. The ability to initiate the thermally choked propulsive mode has been demonstrated with projectile entrance velocities as low as 700 m/sec, which is an easily achieved muzzle velocity for many conventional launching systems. Projectiles have been successfully accelerated to velocities over 2600 m/sec in multi-stage experiments using propellant fill pressures up to 44 atm. To investigate the applicability of the global TCRA theory (resulting from the Hugoniot analysis) and the detailed TCRA flowfield model to accelerating projectiles, the theoretical models are compared with the results of three representative experiments that accelerated projectiles in the velocity range of 1130-1760 m/sec, using a propellant mixture having a C-J detonation velocity of 1700 m/sec.

A reliable method for igniting the propellant mixture as the projectile enters the ram accelerator test section has been developed, and a brief summary of the process is provided here. More detailed descriptions of the method and apparatus of the ignition process can be found in U.S. Patent No. 4,982,647 [Ref. 35]. The establishment of a subsonic flow region behind and on the rear part of the projectile body has proved essential for enabling the combustion process to be initiated and stabilized. This is accomplished with a passive method (no external ignitors or timing constraints) which requires the obturator and projectile to remain in contact as they puncture the entrance

diaphragm to the test section. Upon entering the propellant mixture a shock wave is pushed onto the rear of the projectile by the obturator, which is glued to the projectile base. The high pressure gas generated by the shock on the rear of the projectile separates the obturator and decelerates it behind the projectile.

Some of the kinetic energy that the obturator has as it enters the test section, goes to raising the static enthalpy of the propellant gas behind the shock. Enough energy transfer occurs to raise the gas temperature to the point where self-ignition of the propellant mixture begins between the obturator and projectile base. The volume expansion of the gas due to the chemical heat addition process increases the rate of obturator deceleration as it moves the shock wave farther up on the projectile body. To prevent the shock wave from being pushed through the projectile throat during the initial ignition process, the obturator must either recede quickly or reduce the amount of the tube area blockage that it presents. An analysis of the unsteady flow effects of heat addition on the dynamics of the separation sequence of the projectile and obturator was performed by Burnham [26]. Analysis and experiments have shown that fill pressure, obturator mass, projectile mass, entrance Mach number and the flammability of the propellant mixture are the primary variables that affect the reliability of the ignition process.³¹ It has been found that the ignition of the propellant gas begins behind the projectile, and the thermally choked propulsive mode is normally fully established within ~0.5 m of the test section entrance for fill pressures above 25 atm.

5.1 Performance Profiles of TCRA Propulsive Mode

The effects of experimental uncertainties in propellant mixture composition and fill pressure can be accounted for by determining two performance histories predicted by the global TCRA theory (determined from the SUPLAB computer program), based on inputs from both extremes of possible experimental error. The curves bounding the range of theoretical performance profiles, generated from various experimental input values that are within the measurement uncertainty, are determined by using the combination of possible errors in the propellant mixture composition and fill pressure which result in the highest and lowest predicted acceleration levels. The corresponding bounding curves indicate the maximum range in performance that the global TCRA theory predicts from the available data on fill pressure and propellant composition. This manner of displaying the theoretical results indicates the potential variability in experimental performance that may arise from small fluctuations in these propellant mixture parameters.

Theoretical $t-x$, $\bar{u}-x$ and $\ddot{x}-u$ histories are shown in Figs. 5.1, 5.2 and 5.3, respectively, along with the experimental data from a single-stage shot (HS 752),* using a nominal propellant mixture of $2.7\text{CH}_4 + 2\text{O}_2 + 5.8\text{N}_2$ (based on gas chromatography) at a fill pressure of 23.4 atm. The corresponding highest and lowest theoretical acceleration levels result from using the following propellant mixture compositions and fill pressures as inputs to the SUPLAB computer program: $2.65\text{CH}_4 + 2\text{O}_2 + 5.7\text{N}_2$ at

* Experiments are referred to as "hot shots" when their purpose is to accelerate subcaliber projectiles through the test section while the tubes are filled with gaseous combustible mixtures. The corresponding identification numbers begin with the acronym, HS, and the experiments have been numbered sequentially since the first hot shot; HS 1.

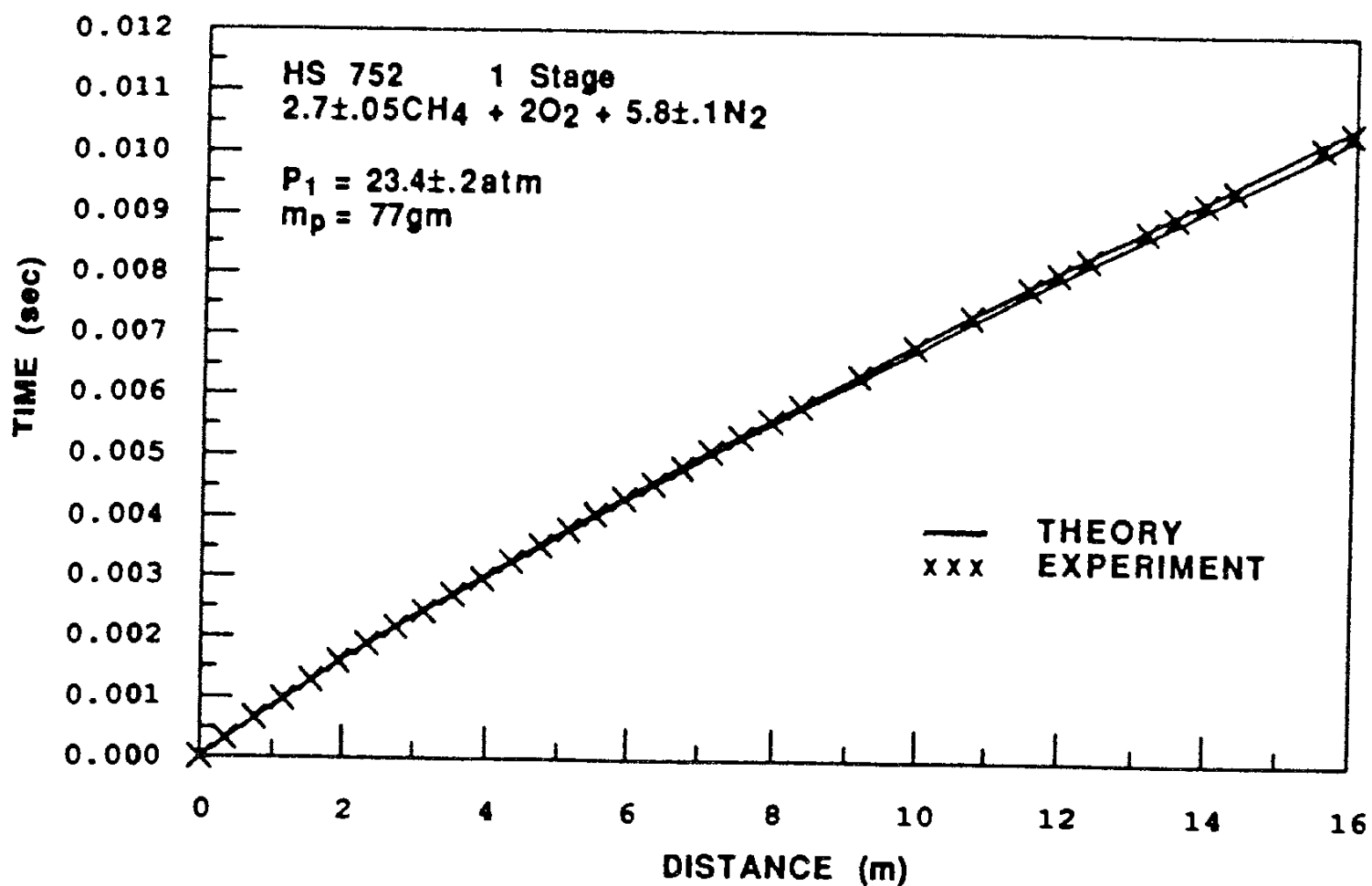


Fig. 5.1 Time-distance profiles of experiment and global TCRA theory, the limits of uncertainty in the propellant mixture parameters were used as inputs for the theory.

23.6 atm and $2.75\text{CH}_4 + 2\text{O}_2 + 5.9\text{N}_2$ at 23.2 atm, respectively. Extremes in the uncertainty of the propellant composition are due to the limited accuracy of the gas chromatography analysis. The exterior dimensions of the projectile used in this experiment were exactly the same as those shown in Fig. 4.2, except that the thickness of the fins was reduced to 2.5 mm. This aluminum projectile had a mass of 77 gm. The entrance velocity was 1130 m/sec ($M_1 = 3.1$) and the projectile accelerated through 16 m of propellant mixture before it left the test section at 1730 m/sec ($M_1 = 4.8$). The

peak acceleration determined from this experiment was $\sim 20,000$ g and the average acceleration level was 5500 g.

The two solid curves shown in Fig. 5.1 are the theoretical t-x histories determined by running the SUPLAB computer program with all the propellant mixture parameters input with values from the extreme ends of the uncertainty range for this experiment (HS 752). The crosses in Fig. 5.1 indicate the experimental t-x data. Experimental uncertainty in measuring the time of projectile magnet passage is not indicated because it is smaller than the dimensions of the plotting symbols. It can be seen that the theoretical t-x profiles are not very sensitive to small variations in the propellant mixture parameters. Close agreement between the t-x profiles of theory and experiment indicate that predicting the arrival time of an accelerating projectile at a particular point in the test section can be accomplished with a high degree of certainty using only the global theory for the TCRA propulsive mode.

The effects of propellant mixture composition and fill pressure uncertainties are more evident in the \bar{u} -x profile of the above experiment. Shown in Fig. 5.2 are the bounding theoretical velocity curves from the above t-x plots along with the mean velocities determined from the first central differences of the experimental t-x data table. A representative error bar for the mean velocity uncertainty is shown on a data point 1 m from the entrance to the test section. Since the theoretical model is based on the Hugoniot analysis in Chapter 2, the excellent agreement between the theoretical and experimental velocity profiles for this experiment indicates that the performance of the TCRA propulsive mode is governed mainly by the thermodynamics of the process rather than the details of the flow phenomena occurring about the projectile, much like the results of Chapman-Jouguet theory in predicting experimental detonation wave velocities.^{15,16}

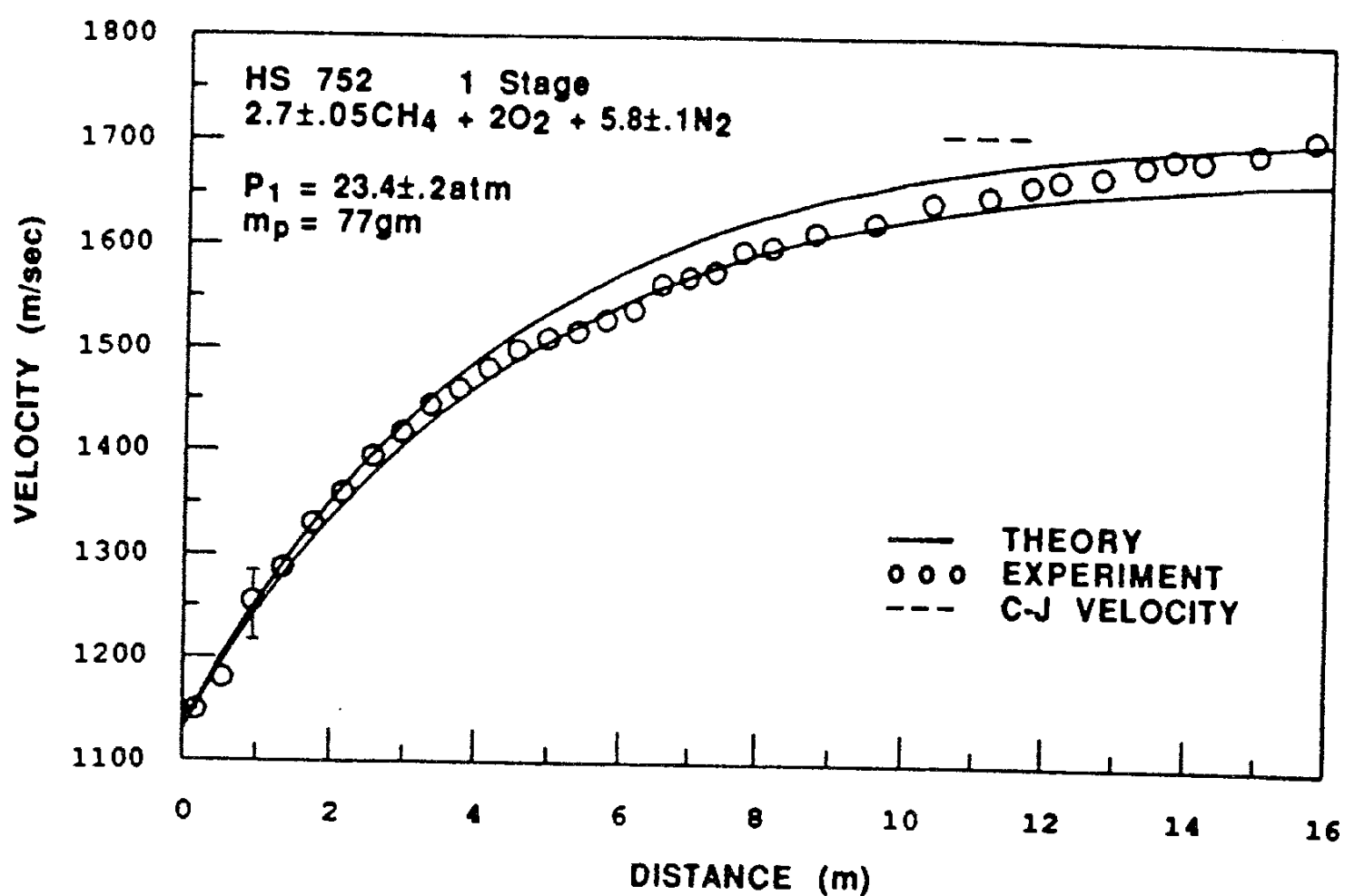


Fig. 5.2 Velocity-distance profiles of experiment and global TCRA theory, the limits of uncertainty in the propellant mixture parameters were used as inputs for the theory.

Close agreement in the velocity profiles predicted by the global TCRA theory and those determined from the experiments has been demonstrated for several different projectile configurations operating in various propellant mixtures.^{1,9,13,14}

A comparison of the \ddot{x} - u history, determined from the previously described experiment (HS 752), to the corresponding theoretical prediction is shown in Fig. 5.3. The effect of the uncertainty in propellant fill pressure and composition on the predicted

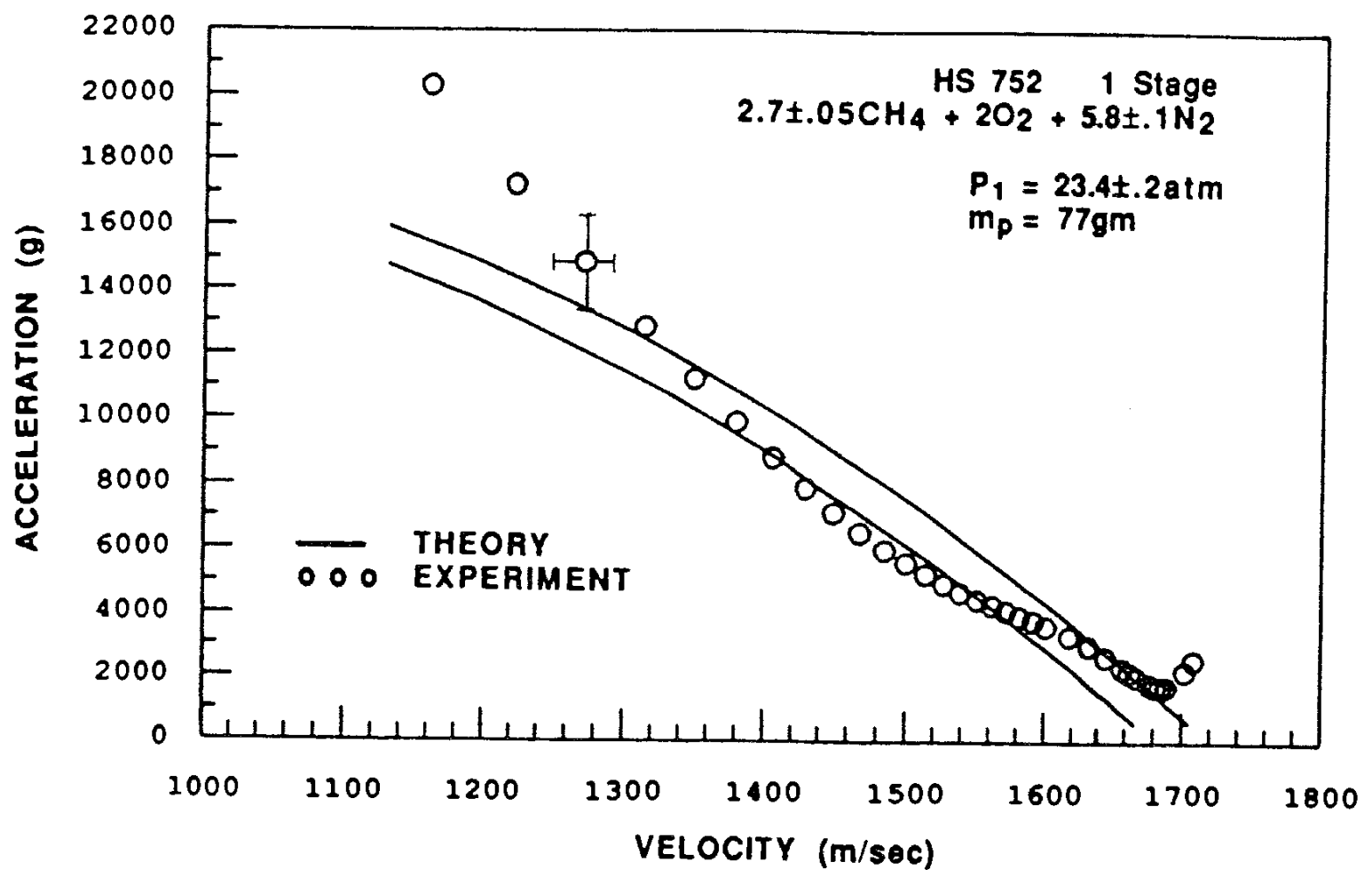


Fig. 5.3 Acceleration-velocity profiles of experiment and global TCRA theory, the limits of uncertainty in the propellant mixture parameters were used as inputs for the theory.

acceleration profile of the TCRA mode is indicated by the separation distance between the two theoretical curves. The maximum experimental uncertainty in the projectile acceleration, due to the previously described data reduction scheme and possible measuring errors, is represented with a vertical error bar affixed to the third data point from the beginning of the run, and the accompanying horizontal error bar indicates the maximum uncertainty in projectile velocity. It can be seen that the \ddot{x} - u profiles of the TCRA theory and experiment agree very well over the majority of the velocity range

achieved in this experiment, supporting the assumption that the projectile is accelerated with a propulsive cycle that is stabilized by a thermal choking point at full tube area. Consequently, acceleration levels needed as input for analyzing the g-loading effects on the projectile structure and internal cargo can be estimated from the global TCRA theory.

Small variations in the external body configurations of projectiles have proved to have little effect on the acceleration profiles determined from ram accelerator experiments in the subdetonative velocity regime. Shown in Table 5.1 are the parameters of three different experiments conducted in the propellant mixture previously discussed ($2.7\text{CH}_4 + 2\text{O}_2 + 5.8\text{N}_2$). The primary differences in the experimental projectile configurations were in the body length, fin thickness and total projectile mass (Table 5.1). Nose cone angles, throat areas, base areas and fin leading edge geometries were maintained at the nominal values shown in the projectile schematic (Fig. 4.2). These three experiments (HS 751, HS 752 and HS 754) had projectile entrance Mach numbers to the ram accelerator test section of ~ 3.1 , and the projectiles left the test section at a Mach number of ~ 4.8 . The C-J detonation Mach number of this propellant mixture is: $M_{\text{CJ}} = 4.68$.

Table 5.1: Variations in Experimental Parameters

Experiment Number	Mass (gm)	Fill Pressure (atm)	Body Length (mm)	Fin Width (mm)
HS 751	70	21.4	71	3.8
HS 752	77	23.4	84	2.5
HS 754	79	25.1	84	3.8

Shown in Fig. 5.4 are the results of the three experiments (HS 751, HS 752 and HS 754) discussed above. Experimentally determined impulse versus Mach number profiles are compared with a single theoretical I-M profile that is based on the nominal propellant mixture composition. Representing the thrust and velocity in non-dimensional units allows the results of these experiments to be compared directly with theory, in spite of the slight differences in projectile mass and propellant fill pressure. Results show excellent agreement at Mach numbers below ~ 4.4 (94% M_{CJ}), which supports the claim

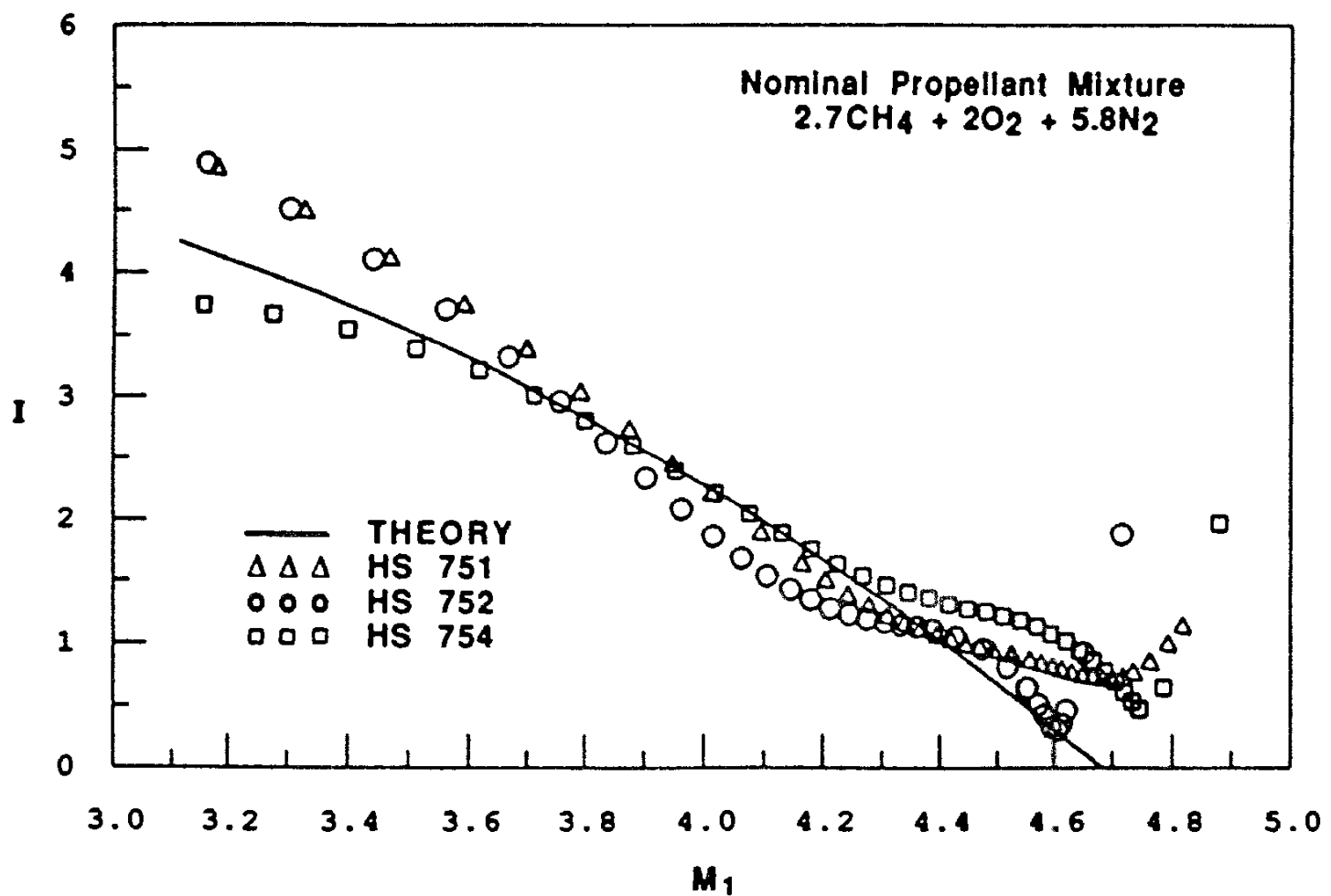


Fig. 5.4 Impulse-Mach number profiles of three experiments and the global TCRA theory.

in Sec. 3.2 that the thrust was independent of the projectile geometry, as long as that geometry can sustain the necessary shock structure to balance the requirements of the gas conservation equations across the control volume.

Note the non-zero thrust levels as the projectile approaches the C-J detonation Mach number for the experimental acceleration profiles shown in Fig 5.4. Many experiments have demonstrated that the projectiles encounter a thrust minimum near C-J velocity, and then accelerate continuously beyond it with increasing thrust at superdetonative velocities.^{13,14} This anomalous acceleration behavior (in the context of TCRA theory) is an experimental discovery which indicates the existence of a propulsive cycle that can operate smoothly through the C-J detonation velocity of a propellant mixture. This mode has come to be referred to as the “transdetonative” propulsive cycle. Continuous acceleration through the C-J point of a propellant mixture has proved to be a naturally occurring phenomenon that is relatively insensitive to projectile geometry; however, propellant mixture composition does appear to play a role in establishing the transdetonative propulsive mode. The sensitivity of the transdetonative mode to variations in propellant mixture and projectile geometry is a subject currently under computational and experimental investigation.

5.2 Sensor Data From Coaxial Instrumentation Ports

Representative sensor data, from an instrumentation station located 1 m from the entrance to the ram accelerator test section, are shown in Fig. 5.5 (HS 789). Experimental data were collected at a four port instrument station which was monitored simultaneously with a pressure transducer, fiber-optic probe and an EM sensor. The

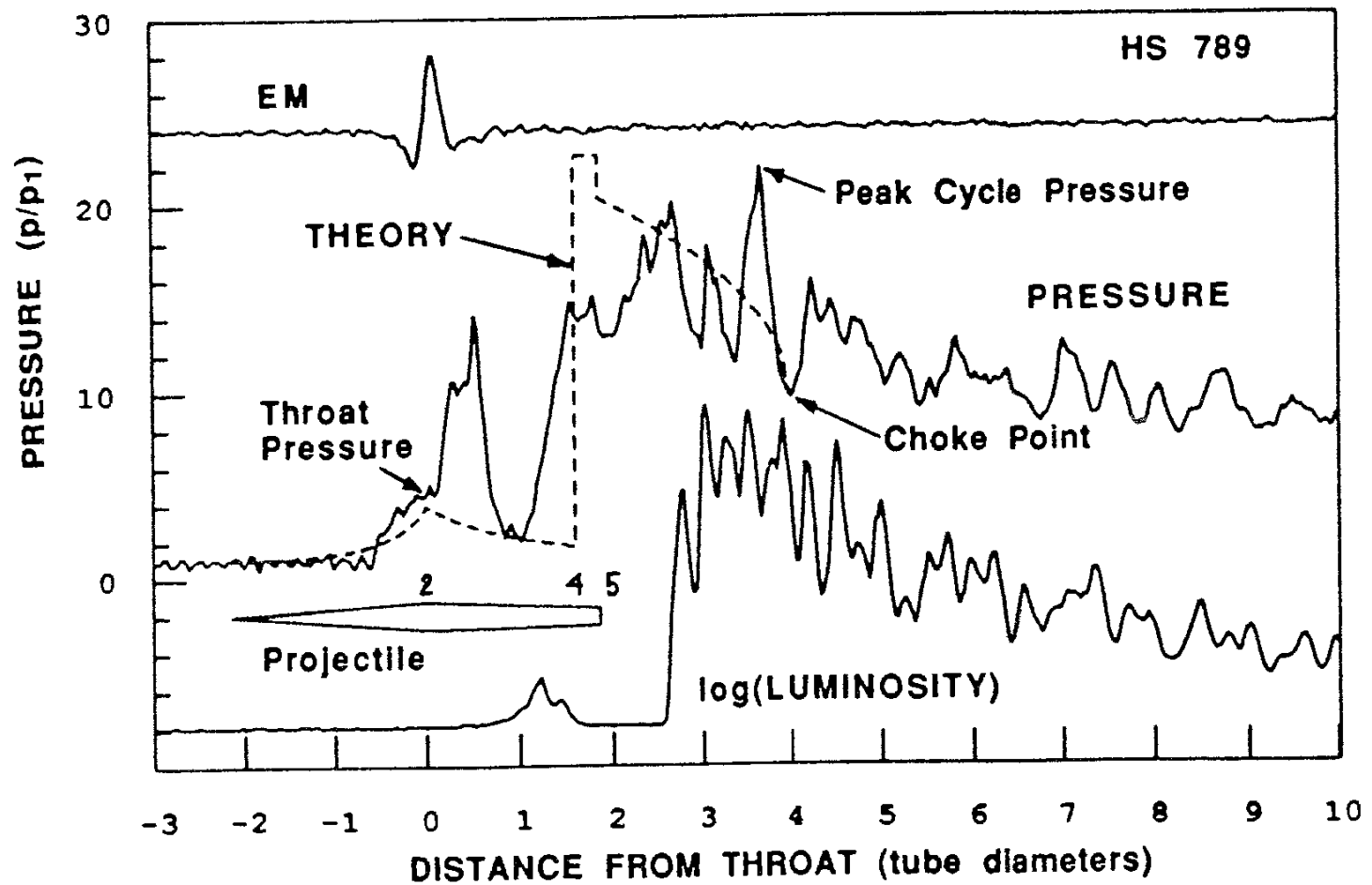


Fig. 5.5 Pressure, EM and luminosity data from coaxial instrumentation ports. Corresponding theoretical pressure profile is also shown.

propellant mixture ($2.7\text{CH}_4 + 2\text{O}_2 + 5.6\text{N}_2$) differed slightly in composition from the one noted in the previous section. The flight Mach number of the projectile was ~ 3.6 as it passed this station and the propellant fill pressure was ~ 40 atm. Luminosity, pressure and EM data have been time-synchronized and converted to a non-dimensional distance scale (tube diameters) by multiplying the time intervals ($1 \mu\text{sec}$) between experimental data points with the projectile velocity, and dividing the result by the tube diameter. The zero reference was located at the projectile throat; thus, the units of the non-dimensional

distance scale indicate the approximate separation distance* between the data and the projectile throat. The time-of-passage of the projectile throat is determined from the time at the line-of-symmetry between the minimum and maximum peaks of the EM signal (discussed in Sec. 4.5), which is displayed in arbitrary amplitude units. The experimental projectile configuration had exactly the same dimensions as the projectile used in HS 751 (Table 5.1). Also shown in Fig. 5.5 is the profile view of the projectile geometry used in the theoretical detailed TCRA model, it has been aligned with the zero reference point of the non-dimensional distance scale.

The experimental wall pressure profile is shown in Fig. 5.5 along with the streamwise average pressure profile predicted by the detailed model of the TCRA mode (dashed lines). The calibration factor of the pressure sensor was applied to its voltage output and the resulting amplitudes were normalized to the tube fill pressure. Only the pressure data can be read directly from the vertical scale. The first rise in the experimental pressure profile is the result of impingement on the tube wall by the initial conical shock wave. A gradual pressure rise follows to the point where another shock wave strikes the tube wall (the first one reflected from the nose cone), resulting in an abrupt pressure increase. Expansion waves, originating from the process of turning the flow around the nose-body joint (throat), reduce the pressure on the tube wall behind the projectile throat. The next abrupt pressure increase is believed to indicate a normal shock wave followed by subsonic flow, this is suggested because there are no signs of the reflected shock system over the projectile body that is normally expected when it is traveling at supersonic velocities with respect to the flow.^{31,38} The tube wall pressure

* The exact separation distance would be determined by accounting for the projectile acceleration on the time intervals between data points, this would be a very small correction for this experiment and has not been included.

trace has a slight dip in it at the projectile base, and increases to a peak behind the projectile in a region of strong pressure oscillations, the pressure then decays with pressure oscillations that are, in general, less extreme than those observed ahead of the point of peak cycle pressure.

Logarithmic amplification of the voltage output from the PIN photodiode allows the fiber-optic probes to remain unfiltered for maximum sensitivity, without saturating the DAS with the high intensity output due to combustion luminosity. The light data trace [$\log(\text{luminosity})$] shown in Fig. 5.5 does not have an absolute calibration reference; however, the relative intensity of the light output at various points in the flowfield is presumed to indicate the relative temperature of the gas. Regions in the flow where the propellant mixture begins to undergo changes in composition are assumed to be indicated by an abrupt increase in light intensity. The sources of luminosity in the flowfield behind the projectile are assumed to be the blackbody radiation emitted by soot particles generated from fuel rich combustion and/or spectral line radiation.^{29,30} Shock luminosity, such as that shown in Fig. 5.5, has routinely been observed on the projectile body while it is accelerating at low Mach numbers ($M_1 < 4$). The amplitude ratio of the logarithm of peak combustion luminosity to the logarithm of peak shock luminosity (Fig. 5.5) corresponds to a relative intensity ratio of $\sim 10^6$. Shock luminosity on the body tends to increase relative to that of the combustion zone as the projectile Mach number increases.^{21,22} Whether this phenomenon is the result of the increasing shock strength exciting radiative energy modes of the unreacted propellant gas or actually the beginning signs of shock-boundary layer ignition of the propellant mixture has not yet been ascertained. Spectroscopic and thin-film thermocouple studies have been initiated

which will help interpret the luminosity detected in the tube as the projectile passes the sensor stations.^{29, 37}

5.2.1 Identification of Thermal Choking Point

Methods for positively determining the point of thermal choking have not yet been developed. Validation of the existence of a thermally choked point comes from the close agreement between the performance predictions of the global TCRA theory and experimental performance profiles, as previously discussed. In order to establish a combustion zone length and a criterion for locating the sonic point from pressure data, the thermal choking point is assumed to be located where the extreme oscillations in the pressure field behind the projectile change character suddenly. This point is indicated in Fig. 5.5, the amplitudes of the pressure oscillations decrease significantly behind this point as the flow undergoes an unsteady expansion process in the constant area tube.

Using this criterion for the sonic point is justified in two ways. First; the acoustic phenomenon associated with the combustion activity between the thermal choking point and the projectile body can only be communicated to the projectile from within the subsonic flow region; thus, if the pressure oscillations observed behind the projectile are an acoustic phenomenon¹⁰ that is coupled between the projectile and the sonic point, then the possibility for the pressure waves to be reinforced (or resonate) by reflections of waves off the tube wall and the projectile ceases at the sonic point, afterwards, the flow undergoes an unsteady expansion process in a constant area tube with pressure oscillations of relatively low intensity. Second; the observed luminosity behind the projectile begins to drop significantly at the point where the extreme oscillations in the

pressure field change character, this indicates that the temperature of the gas is decreasing as is expected from the unsteady expansion of the burnt propellant mixture.

5.2.2 Pressure Profile of Detailed TCRA Flowfield

The primary purpose of the detailed TCRA model is to determine the flow conditions at the stations referenced in Fig. 3.1. Relatively simple models of the flow between stations have been used to provide a continuous pressure trace that qualitatively displays the predicted trends in the pressure field between stations. Key station numbers (2, 4 and 5) have been placed at their corresponding locations on the profile view of the theoretical projectile shown in Fig. 5.5. The throat-to-tube diameter ratio (0.76), the base-to-tube diameter ratio (0.5) and the body length (71 mm) of the theoretical projectile were the same as those of the experimental projectile. The theoretical area ratio profile between the throat and base was assumed to be that of a cone frustum having the corresponding projectile dimensions, the distortions to this area profile resulting from the thickness of the fins were ignored.

The theoretical pressure profile between stations 1 and 2 is determined by linearly distributing the overall total pressure loss from the diffuser model in the axial direction over the forebody of the nose cone. Each axial theoretical pressure value is then computed from the quasi-1-D channel flow relations with the inclusion of the appropriate fraction of the diffuser total pressure loss. This provides an approximate pressure profile in the flow region of the nose cone, and results in flow conditions at the throat (station 2) which exactly satisfy the gasdynamic conservation equations of the detailed TCRA model. Isentropic expansion is assumed to occur in the region of supersonic flow behind the projectile throat (between stations 2 and 3).

Behind the normal shock the flow is assumed to undergo isentropic, subsonic compression until it reaches the point just before it passes through the sudden area expansion at the projectile base. The total pressure loss predicted over the bluff projectile base is then applied to the subsonic flow, resulting in a sudden static pressure drop at the base. This is not an "expansion shock," the sudden pressure drop reflects the streamwise average change that the flow must undergo in order to attain the predicted conditions at the entrance of the combustion zone, which are dictated by thermally choking the flow in a constant area duct with the prescribed amount of heat release (Sec. 3.3).

In order to provide a continuous pressure trace between the conditions predicted at stations 5 and 6 by the detailed TCRA model, the pressure profile in the heat addition zone was determined by adding the total amount of heat release, as computed by SUPLAB from the thermally choked chemical equilibria, in small increments to the subsonic flow behind the projectile until the thermal choking point was reached. The total amount of heat release was distributed equally in 50 equidistant increments behind the projectile and the changes in γ were ignored for the theoretical pressure profile shown. The length of the combustion zone in the detailed model was chosen to coincide with the point where the extreme oscillations in the pressure field behind the projectile suddenly change in frequency and amplitude, as previously discussed.

This model for the heat addition process is consistent with the heat addition profile behind a C-J detonation wave, predicted for flows having finite kinetic rates.¹⁵ Since a detonation wave results from bulk ignition of the flow and the combustion process behind the TCRA projectile is assumed to be the result of turbulent mixing phenomena in the wake of a flame holder, the assumption of a linear distribution of heat release is very simplistic; however, the resulting pressure profile of the combustion zone

does show the qualitative effects of adding heat to a subsonic flow in a constant area duct, and the pressure profile terminates at the theoretical end state pressure ratio of the TCRA propulsive mode. It can be seen from the experimental pressure profile (Fig. 5.5) that the predicted pressure ratio at the thermal choking point of the theoretical model agrees very well with the measured pressure ratio at the point where the flow is assumed to be sonic with respect to the projectile.

5.2.3 Discussion of Experimental and Theoretical Pressure Profiles

The limitations of the quasi-1-D flowfield model are apparent in Fig. 5.5 by the lack of detailed wave character in the theoretical pressure profile. However, the superposition of the theoretical pressure profile onto the experimental data does provide a convenient way to compare the predicted pressure ratios at various stations to the tube wall pressure data. The theoretical throat pressure ratio (station 2) is ~20% lower than that determined at the tube wall as the projectile magnet passed the instrument station. Since the flow at the projectile surface experiences a drop in static pressure as it turns around the projectile throat, the streamwise average prediction of the theoretical model is expected to underpredict the actual tube wall pressure at this point.

The pressure ratio predicted across the normal shock in the theoretical model is ~40% higher than the tube wall pressure ratio measured at the corresponding shock wave; however, the location of the shocks are in good agreement for this particular case. Shapiro [20] shows photographs and pressure data of supersonic flow as it transitions to subsonic flow in a duct. These data show that the normal shock, in viscous duct flow, is actually composed of a system of oblique and normal shock waves, which eventually render the flow subsonic with approximately the same pressure ratio as predicted for a

single normal shock. Thus, the experimental normal shock (Fig. 5.5) may indicate the leading shock of a complicated compression wave system (between the projectile body and the tube wall) that eventually results in subsonic flow behind the projectile.

Note that the tube wall pressure ratio reaches a relative maximum in the region where the luminosity sharply increases (approximately one tube diameter from the projectile base), and has almost the same pressure ratio as that predicted for the subsonic flow at the entrance to the heat addition region (station 5). This correlation may indicate the point where the subsonic compression of the flow ends, and the region where the flow at the tube wall begins to be influenced by the heat addition process (or the leading edge of the flame front). The subsonic wake at the base of the projectile prevents the streamlines of the flow at its surface from converging immediately behind the projectile; thus, the flow is expected to require a certain amount distance behind the projectile to attain the conditions predicted for the entrance to the combustion zone (station 5).

It is necessary to collect more experimental data at various Mach numbers, in conjunction with running computer programs capable solving the Navier-Stokes equations in chemically reacting flow, to substantiate the interpretations presented in this section of the pressure and luminosity data in the subsonic flow regions. However, Euler and Navier-Stokes computer codes for axisymmetric flow have reproduced the experimental tube wall pressure profiles very well in the regions where the projectile is supersonic with respect to the propellant gas.^{31,38} The quasi-1-D model does provide insight into the general properties of the flowfield and, considering the relative simplicity of the detailed TCRA model, the agreement between theory and experiment shown in Fig. 5.5 is good for the pressure profile and the location of the normal shock.

5.3 Pressure-Velocity Profiles in Ram Accelerator

The repeatability of the pressure measurements in the experiments using the nominal methane, oxygen and nitrogen propellant mixture ($2.7\text{CH}_4+2\text{O}_2+5.8\text{N}_2$) is shown in Figs. 5.6, 5.7 and 5.8. Experimental pressure ratios, determined at particular points in the tube wall pressure profiles of all pressure transducers in the ram accelerator test section, are plotted against the projectile velocity at each station determined from the polynomial fit to the \bar{u} -x data, $u(x)$, as discussed in Sec. 4.5. The results from the three previously discussed experiments (HS 751, HS 752 and HS 754) are shown together with the theoretical pressure ratio-velocity profile predicted at the corresponding points in the flowfield. Pressures measured at the tube wall at every instrument station along the test section have been corrected for the individual calibration factors, normalized to the tube fill pressure and plotted against projectile velocity.

5.3.1 Throat Pressure Ratio vs Velocity

Experimental throat pressure ratio-velocity profiles are shown in Fig. 5.6. Each pressure ratio is from the point in the tube wall pressure profile that corresponds to the time-of-passage for the throat magnet, this point is indicated on the pressure profile shown in Fig. 5.5. Theoretical throat pressure ratios were determined from the model for total pressure loss in the diffuser, based on the effects of the nominal propellant gas ($\gamma = 1.369$) flowing over a 10° wedge with two oblique shocks (Sec. 3.3.2) and a throat-to-tube flow area ratio of 0.42. Note that the theoretical pressure ratio at the throat decreases with increasing projectile velocity, this occurs because the ratio of throat Mach number to flight Mach number decreases with increasing projectile velocity, and the total

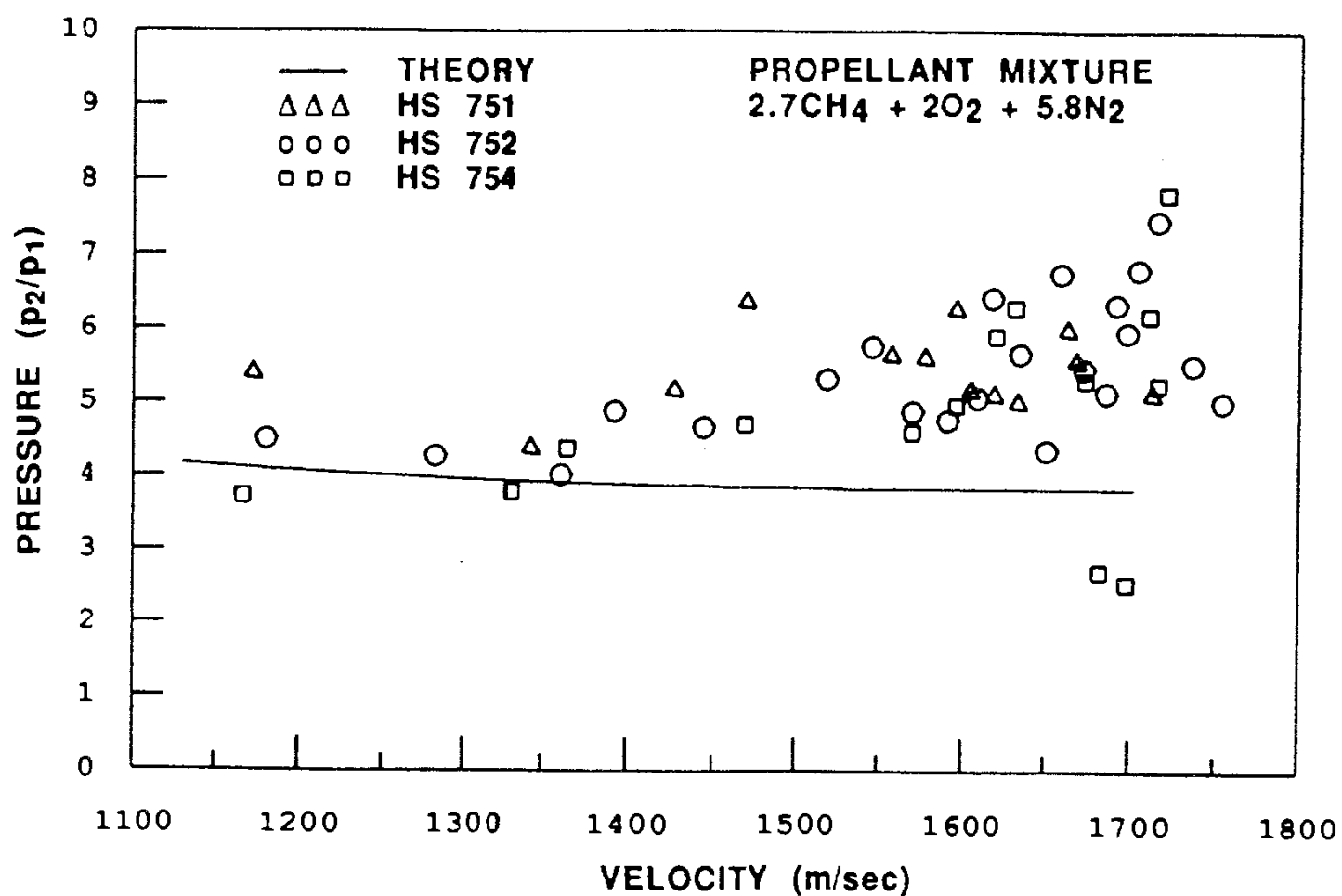


Fig. 5.6 Experimental and theoretical throat pressure ratio vs velocity.

pressure loss in the diffuser is not large enough to alter this trend the range of Mach numbers shown.*

The trend of the experimental data for the throat pressure ratios, measured at the tube wall, is to increase with increasing flight Mach number. The pressure transducer in the tube wall normally measures a relatively gradual increase in static pressure between the first sharp pressure rise in the pressure profile (Fig. 5.5) and the location of the

* In isentropic flow the pressure ratio at the throat approaches unity as the flight Mach number approaches infinity. The Mach number dependence of the total pressure loss model, consisting of two oblique shocks off a 10° wedge, results in a minimum throat pressure ratio of 3.81 at $M_1=4.67$. The average static pressure ratio of the flow at the throat then begins to increase as the flight Mach number increases.

projectile throat magnet. The first abrupt increase in wall pressure indicates the impingement effects of the leading conical shock wave (emanating from the nose cone), and its immediate reflection back toward the projectile, the pressure increase that follows results from the continued compression of the flow behind a reflected conical shock wave. As the projectile Mach number increases, the point where the initial conical shock strikes the tube wall moves closer to the throat, and the pressure ratios behind this shock and at the projectile throat increase with increasing projectile Mach number.

The divergence of the theoretical throat pressure ratio history from the trend in the experimental data indicates that the 3-D effects of the conical shock wave system, in the flow region of the nose cone and throat, have a large influence on the magnitude of the throat pressure ratio measured at the tube wall. Results of an axisymmetric, Euler solving computer program³¹ show that the pressure at the projectile's surface is usually lower than the tube wall pressure at the throat, for projectile geometries having cone angles and effective area ratios similar to those of the experimental projectile. Thus, the average static pressure of the supersonic flow in the throat passage is expected to be less than the corresponding tube wall pressure. The model for the total pressure loss of the nose cone diffuser serves its purpose for investigating the sensitivity of the theoretical normal shock location to diffuser inefficiencies, but it only provides a coarse estimate of what the tube wall and surface pressures are at the projectile throat.

5.3.2 Experimental Pressure Ratios at Thermal Choking Point

Pressure ratios at the thermal choking point, determined from the wall pressure profile of each transducer in the ram accelerator test section, are shown in Fig. 5.7 as a function of projectile velocity for the same three experiments as before. The thermal

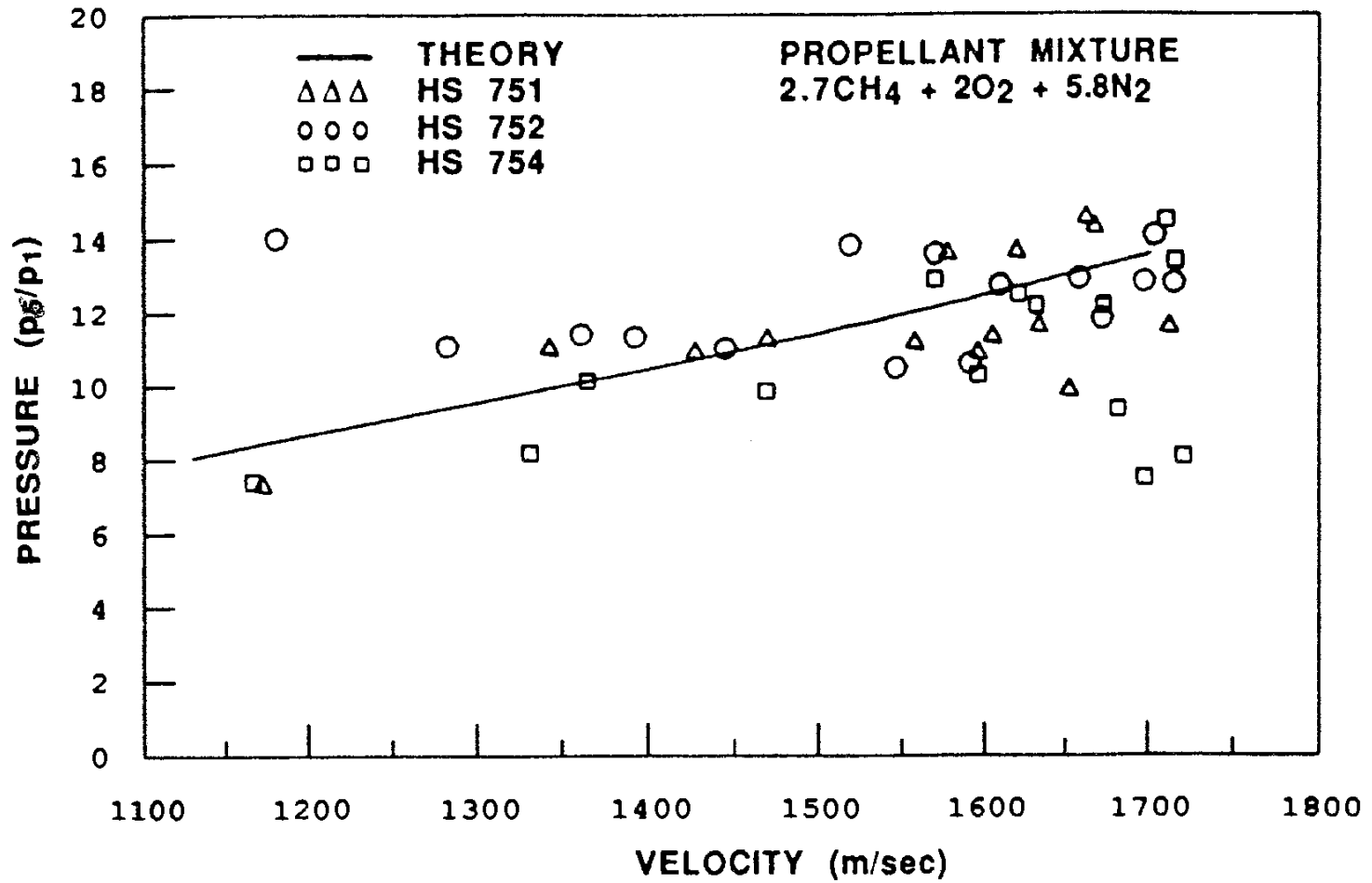


Fig. 5.7 Experimental and theoretical choke point pressure ratio vs velocity.

choking point is assumed to be where the amplitude of pressure oscillations behind the projectile dampen suddenly, as previously discussed. The theoretical curve is from the static pressure ratio history predicted for the choke point of the global TCRA theory. The repeatability of the experiments and the correlation of the thermal choking pressure amplitudes with theory support the assumption that the projectile is accelerated with a thermally choked propulsive cycle. There is good agreement between the theory and experiment indicating that the end state pressure ratio of the TCRA propulsive cycle is

determined by the thermodynamics of the ram accelerator process, not by the details of the flow phenomena occurring around the projectile.

5.3.3 Peak Combustion Pressure Ratio vs Velocity

The noisiest experimental pressure ratio-velocity data occur at the point of peak pressure behind the projectile, which is also the peak cycle pressure under normal operating conditions. Since these pressure ratios are determined in the region where the combustion of the propellant mixture usually takes place, they are referred to as the peak combustion pressure ratios. Maximum tube wall pressures measured between the projectile base and the thermal choking point are plotted versus velocity in Fig. 5.8 for the three experiments discussed above. The projectile base pressure predicted from the detailed TCRA flowfield model is also plotted for comparison. Theoretically, the peak cycle pressure occurs at the projectile base for Mach numbers below ~ 3.5 , and at higher Mach numbers the peak cycle pressure is behind the normal shock (see Fig. 5.5). Only the theoretical base pressure ratio is plotted because it represents the streamwise average static pressure that the subsonic flow must have prior to heat addition in the full tube area.

The trend in the experimental data is for the pressure ratio to decrease with increasing projectile velocity; however, the theoretical peak cycle pressure steadily increases as the flight Mach number increases, and is $\sim 30\%$ higher than experiment by the time the projectile has reached the C-J detonation velocity. It is unclear as to why the experimental peak cycle pressure tends to decrease or remain nearly the same throughout most of the operating Mach number range of the TCRA propulsive mode. Increasing the flight Mach number should increase the ram compression effect on the propellant mixture in the subsonic region between the thermal choking point and the projectile body.

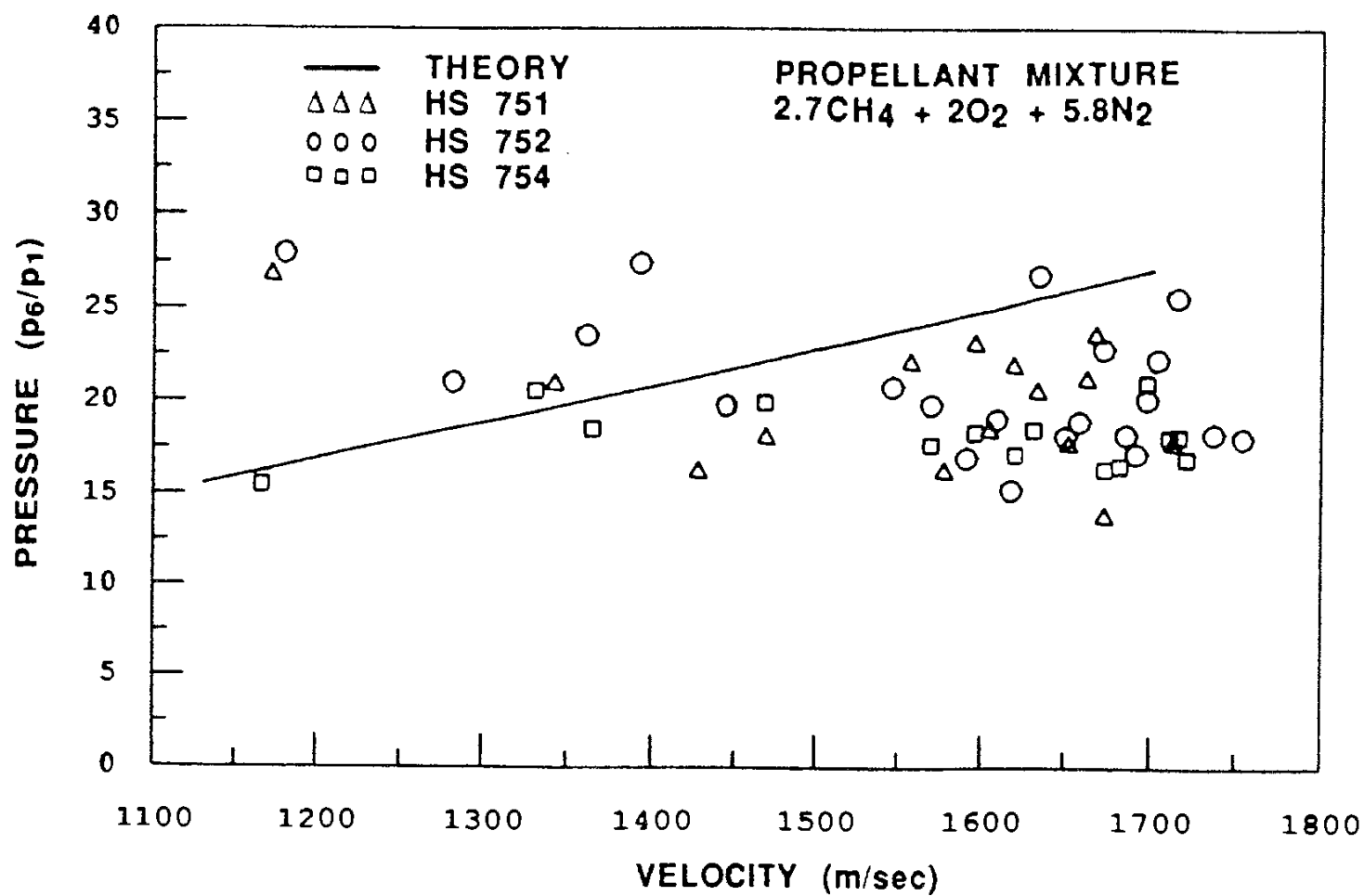


Fig. 5.8 Experimental peak combustion pressure ratio-velocity profiles and detailed TCRA model.

One possible explanation for the lack of increasing peak combustion pressure ratios with increasing projectile velocity is that there is a mixture of supersonic and subsonic flow in the wake of the projectile after the normal shock falls off the body. The heat addition process could be occurring in both the supersonic and subsonic regions in the flowfield of the combustion zone (between stations 5 and 6). In this situation, the maximum pressure in the combustion region would not be subject to the subsonic pre-combustion conditions that must exist before the flow can be thermally choked at full tube area with the prescribed amount of heat release. Alternatively, chemical reactions may be

taking place which release a portion of the available heat into the flow over the projectile body before it has returned to the full tube area. This would increase the subsonic Mach number (and reduce the pressure ratio) predicted by the detailed TCRA model at the entrance to the constant area combustion region (station 5). Neither of the above scenarios for explaining the trends in the peak combustion pressure of the experiments would affect the end state conditions predicted by the global TCRA theory. Since the current pressure instrumentation of the test section is limited to monitoring only the tube wall pressure, it will probably require Navier-Stokes solving computer programs to resolve the flow phenomena occurring behind the projectile.

5.3.4 Normal Shock Location vs Velocity

One other important feature of the detailed TCRA flowfield model is to be compared with experiment. Shown in Fig. 5.9, in non-dimensional length units (tube diameters), is the separation distance between the normal shock location and the projectile throat that was predicted by theory and determined from the data of the three experiments previously mentioned (HS 751, HS 752 and HS 754). Also shown are two horizontal lines (dashed) that indicate the non-dimensional lengths of the various projectile bodies used in these experiments, three plotting symbols have been placed on the left hand sides of the horizontal lines to indicate what the projectile lengths were for the corresponding experimental data. The time interval between the time-of-passage for the throat magnet and the time at the peak of the first strong shock after the throat spike in the tube wall pressure profile, is multiplied by projectile velocity and normalized to tube diameter to get a non-dimensional separation distance that is independent of the projectile length.

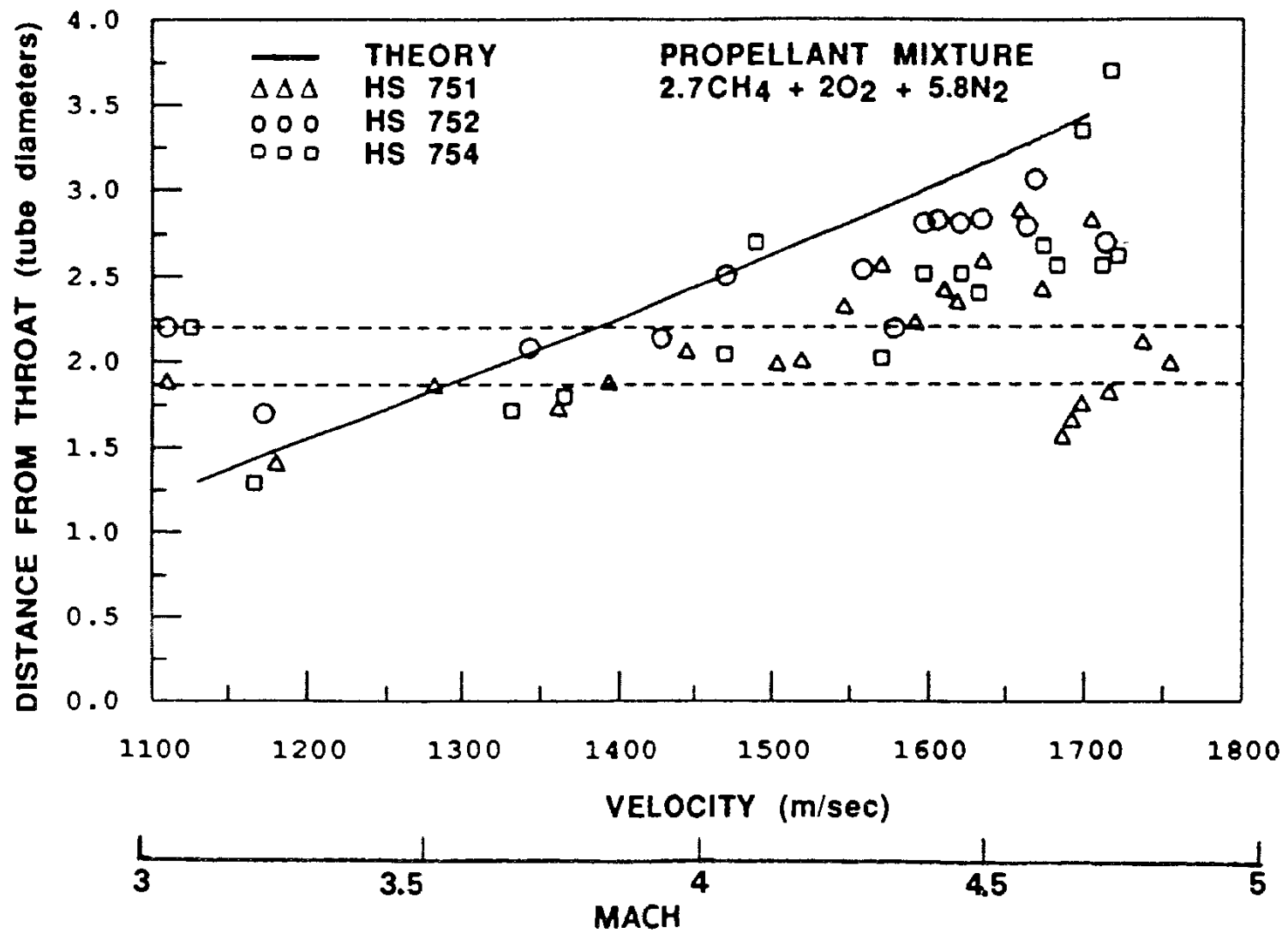


Fig. 5.9 Experimental and theoretical normal shock location vs velocity.

The theoretical normal shock separation distance is based on a projectile body that consists of a rearward facing cone having a 4° half angle. The base of the cone has the dimensions of the projectile throat diameter (29 mm) which results in a theoretical body length of ~5 tube diameters. This theoretical body is the same as that shown in Fig. 5.5, except that the rear of the projectile continues to taper down to a point. Diffuser and base total pressure losses (from the models previously discussed) were included to determine the shock location as a function of velocity for the area profile of this theoretical projectile.

The experimental normal shock tends to move backward as the projectile velocity increases throughout the experimental velocity range shown in Fig. 5.9. The predicted separation distance between the projectile throat and normal shock is generally greater than the that determined from the experimental data. Around Mach 4, the experimental normal shock seems to move off the projectile, and it continues to fall behind at a rate greater than predicted as the flight Mach number continues to increase. The experimental data for projectiles having a body length of 84 mm (HS 752 and HS 754) indicate that the normal shock is always behind the projectile at the C-J detonation velocity (1700 m/sec), and it is usually located within one tube diameter of the base. In the experiment using a projectile body length of 71 mm (HS 751) the normal shock appeared to recede behind the projectile to a distance of about one tube diameter, and then move back onto the body as the C-J velocity was approached. There is a relatively large amount of scatter in the experimental normal shock location data, though it is apparent that the general trend is for the shock to move rearward and off the projectile as the flight Mach number increases throughout the subdetonative velocity regime.

The detailed TCRA model has only a limited ability to predict the normal shock location, as shown by the data in Fig. 5.9. This is partially due to the experimental projectile's lack of a continuous body area profile that would offer a physical presence on which the normal shock could be located. After the normal shock has fallen off the body, the supersonic flow will tend to turn toward the center of the tube at the corresponding Prandtl-Meyer angle, this results in streamlines that form a virtual tail cone at the projectile base.³¹ The normal shock system may be stabilized on this virtual tail cone and continue to recede as the projectile velocity increases. Adding a virtual tail cone to the bluff base of the projectile body provides a mechanism for matching the predicted normal

shock-velocity profile to experiment. For the data shown in Fig. 5.9, it was found that a 15° tail cone, having a length of about one tube diameter, would kink the theoretical shock profile downward at the velocity predicted for shock fall-off, and the resulting curve would pass through the data points with nearly the same slope as the trend in the data. Thus, the normal shock-velocity profile predicted by the detailed TCRA flowfield model is very sensitive to the body geometry and provides only a coarse indication of where the experimental shock is positioned with respect to the projectile throat.

The geometry of the flow passages between the fins of the projectile complicate the interpretation of the normal shock data because of the 3-D flow effects. There is always a question about the orientation of the projectile as it passes by the pressure transducers, the details of the flowfield measurements are expected to depend on how close the projectile fins were to the instrument port when the data were collected. Thus, the projectile orientation with respect to the sensors could be a significant factor in determining the apparent location of the normal shock (when it is on the body) and the resultant scatter in the experimental data.

Another interpretation of what appears to be a normal shock is that the corresponding pressure rise actually results from the last oblique shock wave reflected off the projectile body. As the velocity increases, the oblique wave angle will decrease and the point where the shock reflects off the body will move farther back, eventually it will fall off the projectile and the oblique shocks will interact with the recirculation zone. The subsequent recompression shocks will couple with the combustion process, resulting in a region of mixed supersonic and subsonic flow ahead of the thermal choking point. The corresponding experimental normal shock location determined from this situation would be at the point where the first recompression shock strikes the tube wall.

Insight into the behavior of the normal shock system on accelerating projectiles has been gained from unsteady flow calculations. The results of 2-D, unsteady computation modeling of the TCRA propulsive mode have indicated that heat addition is likely to occur in the region of mixed supersonic and subsonic flow behind the projectile when it is accelerating near the C-J detonation velocity.³¹ Unsteady flow effects tend to lower the total temperature of the overall flowfield, which reduces the dissociation losses in the reacted propellant mixture. More heat release is then available which would tend to drive the normal shock farther up on the body than predicted from the quasi-steady analysis.^{26,31} Computer codes for coupling the combustion process to the unsteady, viscous flowfield of the thermally choked propulsive cycle are needed to better understand the complex flow phenomena that occur when the normal shock has fallen off the projectile body.

CHAPTER 6

SUMMARY AND CONCLUSIONS

A Hugoniot analysis of the ram accelerator process has been presented, which determines the effects of heat addition and momentum change on the end state of a propellant gas. This quasi-steady analysis applies to all ram accelerator propulsive modes operating in a straight-walled tube. Regions of accessible end states in the P-V plane were identified, which indicate that there are not any fundamental reasons why a properly shaped projectile cannot operate at or beyond the C-J detonation velocity of a propellant mixture. The generalized Rayleigh lines were shown to be tangent to the ram accelerator Hugoniots at the sonic point, and these lines represent the history of end states that the propellant mixture undergoes during the subsonic heat addition process of the thermally choked propulsive mode. The history of P-V end states generated by a ram accelerator propulsive cycle having a fixed exit flow Mach number was determined from the generalized Fanno curves. The thermally choked propulsive mode was shown to have a theoretical upper velocity limit corresponding to the C-J detonation velocity of the propellant mixture. In contrast, the upper theoretical velocity limit for a ram accelerator propulsive cycle that uses a fixed geometry nozzle was at the velocity of the corresponding weak detonation wave that has an exiting flow Mach number equal to the exiting flow Mach number of the propulsive cycle.

Since the TCRA propulsive mode operates with an end state condition corresponding to the maximum amount of entropy that can be generated in the propellant

mixture (thermally choked), details of the flow phenomena ahead of the choke point do not affect the resulting chemical equilibria. Thus, the predicted amount of heat addition and projectile thrust at a given flight Mach number are independent of the disposition of the shock wave system about the projectile. The good agreement with global TCRA theory (based on the Hugoniot analysis) for both the experimental performance profiles ($t-x$, $\bar{u}-x$ and $\ddot{x}-u$) and the thermal choking pressure-velocity history indicates that the performance of the TCRA propulsive mode is governed only by the thermodynamics of the process, not by the details of the projectile geometry.

A detailed flowfield model for the TCRA propulsive mode was presented which determined the streamwise average conditions of the flow at various stations on the projectile. Experimental throat pressure ratio data, determined at the tube wall, were consistently higher than predicted by the theoretical supersonic diffuser model which applied the total pressure losses from two oblique wedge shocks to estimate the average static pressure and Mach number of the flow at the projectile throat. The trend in the experimental data was for the throat pressure to increase with increasing projectile velocity, whereas the theory predicts a decreasing pressure trend, these discrepancies indicate that conical flow effects are important for determining the tube wall and projectile surface pressures in the throat region.

The total pressure losses arising from the supersonic diffuser and the sudden area expansion at the projectile base, as determined by the detailed TCRA flowfield model, were found to move the normal shock closer to the throat than predicted in the ideal lossless case. Total pressure losses in the subsonic regions of the flow have a greater effect on normal shock location than the total pressure losses in the supersonic regions of the flowfield. The experimental normal shock location data showed that the first strong

shock detected at the tube wall, after the passage of the projectile throat, tended to move back on the projectile body as its velocity increased. The experimental normal shock falls off the projectile at Mach numbers above ~ 4 , and it continues to recede behind to a distance of approximately one tube diameter away from the projectile base at the C-J detonation velocity. The theoretical normal shock was always predicted to be located farther back on the projectile body than the experimentally observed normal shock.

The peak combustion pressure data showed that the maximum pressure remains nearly constant or decreases slightly throughout the subdetonative velocity range of the propellant mixture investigated, whereas the detailed TCRA model predicts that the maximum pressure in the combustion zone (at the projectile base) steadily increases as the velocity increases. This discrepancy is likely the result of the normal shock not being able to stay on the projectile body as the flight Mach number increases. Heat addition in the resulting region of mixed supersonic and subsonic flow would tend to reduce the pre-combustion static pressure required for the flow to thermally choke.

One-dimensional modeling of the TCRA flowfield provides insight into how the thermodynamic properties of the propellant mixture change as it passes around the projectile. The inability of the detailed theory to accurately predict the maximum cycle pressure determined at the tube wall and the location of the experimental normal shock indicates that these phenomena depend strongly on 3-D flow effects and the details of the combustion process. The unsteady viscous flowfield of the TCRA is a complicated mixture of supersonic and subsonic flows in a reactive combustible gas. It will require sophisticated computer algorithms to resolve the phenomena resulting from the interaction of the propellant mixture with the projectile, as it is being propelled through the tube by the thermally choked propulsive cycle. However, the experimental performance of

projectiles being accelerated at velocities below the C-J detonation velocity can be predicted very well with the relatively simple global TCRA theory.

BIBLIOGRAPHY

1. A. Hertzberg, A.P. Bruckner and D.W. Bogdanoff (1988) "Ram Accelerator: A New Chemical Method for Accelerating Projectiles to Ultrahigh Velocities," *AIAA J.* **26**:195-203.
2. A. Hertzberg, A.P. Bruckner, D.W. Bogdanoff and C. Knowlen (1987) "The Ram Accelerator and Its Applications: A New Approach for Reaching Ultrahigh Velocities," Proc. 16th International Symposium on Shock Tubes and Waves, H. Groenig (ed.), Technische Hochschule Aachen, FRG, pp. 117-28.
3. C. Knowlen, A.P. Bruckner, D.W. Bogdanoff and A. Hertzberg (1987) "Performance Capabilities of the Ram Accelerator," AIAA Paper 87-2152, AIAA/SAE/ASME/ASEE 23rd Joint Propulsion Conference, San Diego, CA, June 29 - July 2.
4. D.C. Brackett and D.W. Bogdanoff (1989) "Computational Investigation of Oblique Detonation Ramjet-in-Tube Concepts," *J. Propulsion* **5**(3):276-81.
5. S. Yungster, S. Eberhardt, and A.P. Bruckner (1989) "Numerical Simulation of Shock-Induced Combustion Generated by High-Speed Projectiles in Detonable Gas Mixtures," AIAA-89-0673, 27th Aerospace Sciences Meeting, Reno, NV, January 9-12.
6. S. Yungster, A.P. Bruckner (1989) "A Numerical Study of the Ram Accelerator Concept in the Superdetonative Velocity Range," AIAA Paper No. 89-2677, AIAA/ASME/SAE/ASEE, 25th Joint Propulsion Conference, July 10-12.
7. G.L. Dugger, ed. (1969) Ramjets (New York: American Institute of Aeronautics & Astronautics, Vol. 6, AIAA Selected Reprint Series).

8. G.C. Oates (1988) Aerothermodynamics of Gas Turbine and Rocket Propulsion, rev. & enl. (Washington, DC: American Institute of Aeronautics & Astronautics), pp. 19-60, 133-8, 177-208.
9. A.P. Bruckner, C. Knowlen, A. Hertzberg, and D.W. Bogdanoff (1990) "Operational Characteristics of the Thermally Choked Ram Accelerator," *J. Propulsion & Power*, in press.
10. G.C. Oates, ed. (1985) Aerothermodynamics of Aircraft Engine Components, (Washington, DC: American Institute of Aeronautics & Astronautics), pp. 59-78, 135-41.
11. A.P. Bruckner, D.W. Bogdanoff, C. Knowlen and A. Hertzberg (1987) "Investigation of Gasdynamic Phenomena Associated with the Ram Accelerator Concept," AIAA 19th Fluid Dynamics, Plasma Dynamics and Lasers Conference, Honolulu, HI, AIAA Paper 87-1327, June 8-10.
12. A.P. Bruckner, C. Knowlen, K.A. Scott and A. Hertzberg (1988) "High Velocity Modes of the Thermally Choked Ram Accelerator," AIAA Paper No. 88-2925, AIAA/ASME/SAE/ASEE 24th Joint Propulsion Conference, Boston, MA, July 11-14.
13. A.P. Bruckner, A. Hertzberg, and C. Knowlen (1990) "Review of Ram Accelerator Propulsion Modes," 27th JANNAF Combustion Subcommittee Meeting, Warren Air Force Base, Cheyenne, WY, November 5-9.
14. A. Hertzberg, A.P. Bruckner, and C. Knowlen (1991) "Experimental Investigation of Ram Accelerator Propulsion Modes," *Shock Wave International Journal*, in press.

15. R.A. Strehlow (1984) Combustion Fundamentals (New York: McGraw-Hill), pp. 114-39, 302-36, 360-4.
16. I. Glassman (1987) Combustion, 2d ed. (Orlando, FL: Academic Press), pp. 182-92, 198-226.
17. L.D. Landau and E.M. Lifshitz (1984) Fluid Mechanics (Oxford: Pergamon Press), pp. 319-32, 337-41, 347-53, 480-96.
18. S. Yungster (1989) "Numerical Simulation of Shock-Induced Combustion for Application to the Ram Accelerator Concept" (Ph.D. Dissertation, University of Washington).
19. D.T. Pratt, J.W. Humphrey, and D.E. Glenn (1991) "Morphology of Standing Oblique Detonation Waves," *J. Propulsion & Power*, in press.
20. A.H. Shapiro (1953) The Dynamics and Thermodynamics of Compressible Fluid Flows (New York: Ronald Press, Vol. 1 and Vol. 2), pp. 73-262, 689-98, 1153-59.
21. A. Kull, E. Burnham, C. Knowlen, A.P. Bruckner, and A. Hertzberg (1989) "Experimental Studies of the Superdetonative Ram Accelerator Mode," AIAA Paper No. 89-2632, AIAA/ASME/SAE/ASEE 25th Joint Propulsion Conference, July 10-12.
22. E.A. Burnham, A.E. Kull, C. Knowlen, A.P. Bruckner, and A. Hertzberg (1990) "Operation of the Ram Accelerator in the Transdetonative Velocity Regime," AIAA/SAE/ASME/ASEE 26th Joint Propulsion Conference, Orlando, FL, July 16-18.
23. L.P. Barclay (1972) "Pressure Losses in Dump Combustors," Wright-Patterson AFB, Ohio: Technical Report AFAPL-TR-72-57.

24. J. Stull, ed. (June 1971) JANAF Thermochemical Tables, 2d ed. NSRDS-NBS 37.
25. I.L. Stonich (1986) "Experimental Investigation of the Ram Accelerator Principle: Instrumentation and Data Acquisition" (M.S.A.A. thesis, University of Washington).
26. E.A. Burnham (1989) "Experimental and Numerical Analysis of the Thermally Choked Ram Accelerator Starting Process" (M.S.A.A. thesis, University of Washington).
27. D.W. Bogdanoff, C. Knowlen, D. Morakami, and I. Stonich (1990) "A Magnetic Detector for Projectiles in Tubes," *AIAA J.* **28**(11):1942-44.
28. E.C. Christofferson (1989) "A Magnetic Transducer Detection System for High Speed Projectiles in Tubes" (M.S.A.A. thesis, University of Washington).
29. A.E. Prochko (1991) "Preliminary Spectral Analysis of the Ram Accelerator" (M.S.A.A. thesis, University of Washington).
30. K.A. Scott (1988) "Experimental Investigation of Ram Accelerator Concept Using an Optical Probe" (M.S.A.A. thesis, University of Washington).
31. P. Kaloupis (1990) "An Unsteady Total Variational Diminishing Axisymmetric Numerical Model for the Ram Accelerator Subsonic Combustion Thermal Choking Propulsion Mode" (M.S.E. thesis, University of Washington).
32. R.R. Bate, D.D. Mueller, and J.E. White (1971) Fundamentals of Astrodynamics (New York: Dover Publications Inc.), pp. 123-31.

33. A. Kull (1990) "Preliminary Investigations of Superdetonative and Transdetonative Ram Accelerator Propulsion Modes" (M.S.E. thesis, University of Washington).
34. A. Hertzberg, A.P. Bruckner and D.W. Bogdanoff (1990) "Apparatus and Method for the Acceleration of Projectiles to Hypervelocities," United States Patent No. 4,938,112.
35. A. Hertzberg, A.P. Bruckner, D.W. Bogdanoff and C. Knowlen (1991) "Method and Apparatus for Initiating Stable Operation of a Ram Accelerator," United States Patent No. 4,982,647.
36. O.W. Eshbach (1974) Handbook of Engineering Fundamentals, 3d ed. (New York: Wiley and Sons), pp. 541, 542.
37. R.J. McIntosh (1991) "A Microsecond Response Thermocouple in the Ram Accelerator" (M.S.A.A. thesis, University of Washington).
38. M.J. Nusca (1990) "Numerical Simulation of Reacting Flow in a Thermally Choked Ram Accelerator," 27th JANNAF Combustion Subcommittee Meeting, Warren AFB, Cheyenne, WY, November 5-9.
39. P.J. Wilbur, C.E. Mitchell, and B.D. Shaw (Nov.-Dec. 1983) "The Electrothermal Ramjet," *Journal of Spacecraft & Rockets*, pp. 603-10.

APPENDIX A

DERIVATION OF EXPERIMENTAL UNCERTAINTY RELATIONS

The velocity and acceleration of the projectile at any point along the ram accelerator test section can be determined with reasonable accuracy from the experimental t-x data table. The uncertainty in measuring the time-of-passage of the projectile throat magnet (Δt), the average spacing of the instrument stations (\bar{x}), and the uncertainty in knowing the separation distance between sensors (Δx) are the primary factors which govern the overall uncertainty in the performance profiles. The rate of change of acceleration with respect to distance is another source of error that is intensified by large instrument spacing intervals and low projectile velocities. Expressions for the uncertainty in the \bar{u} -x and \ddot{x} -u profiles are derived here.

Assuming that the acceleration does not change significantly between two instrument stations, the uncertainty in the mean velocity due to ignoring the average acceleration \ddot{x}_0 over the distance interval of the EM transducers can readily be determined. The square of the exact velocity $u(x)$ as a function of distance is as follows:

$$u(x)^2 = u_0^2 + 2\ddot{x}_0 x \quad (\text{A.1})$$

where u_0 is the velocity at the first sensor station and x is the distance from the first station. The velocity at the next instrument station is then:

$$u(\bar{x})^2 = u_0^2 + 2\ddot{x}_0\bar{x}$$

For constant acceleration the mean velocity \bar{u} between adjacent stations is the same as the first central difference of the t-x data (if t and x are known exactly). The mean velocity is then:

$$\bar{u} = \frac{u_0 + u(\bar{x})}{2} = \frac{u_0 + \sqrt{u_0^2 + 2\ddot{x}_0\bar{x}}}{2}$$

After solving for u_0 from above and substituting it into Eq. A.1, the exact velocity at the midpoint between the instrument stations is found to be:

$$u\left(\frac{\bar{x}}{2}\right) = \bar{u} \sqrt{1 + \left(\frac{\ddot{x}_0\bar{x}}{2\bar{u}^2}\right)^2}$$

Normalizing the difference between the exact and mean velocities results in the following expression (Eq. 4.2 in text) for the relative uncertainty in velocity at the midpoint between sensors:

$$\frac{\Delta u_{\bar{x}}}{\bar{u}} = \sqrt{1 + \left(\frac{\ddot{x}_0\bar{x}}{2\bar{u}^2}\right)^2} - 1 \quad (\text{A.2})$$

For an instrument spacing of $\bar{x}=0.4$ m and an average acceleration level of $\ddot{x}_0=50,000$ g, the value of the squared term underneath the square root sign of Eq. A.3 is much less than unity when the projectile has a velocity of 1000 m/sec or above.

Therefore, the uncertainty in mean velocity when ignoring the acceleration can be approximated as:

$$\Delta u_{\bar{x}} \approx \frac{\bar{u}}{8} \left(\frac{\ddot{x}_0 \bar{x}}{\bar{u}^2} \right)^2 \quad (\text{A.3})$$

The first central difference of the t-x data table indicates the projectile velocity at the midpoint with a relative uncertainty due to measuring errors as follows:

$$\frac{\Delta u_{EM}}{\bar{u}} = \frac{\Delta x}{\bar{x}} + \frac{\Delta t}{\bar{x}} \bar{u} \quad (\text{A.4})$$

The overall experimental uncertainty in midpoint velocity is the sum of Eqs. A.2 and A.4.

A polynomial $u(x)$ is fit to the experimental \bar{u} -x data which provides an expression for projectile velocity as a continuous function of distance with a mean deviation σ . This polynomial represents the actual projectile velocity (u_p) with an average uncertainty that is the sum of the mean deviation and the overall experimental error in determining the velocity at the midpoints between instrument stations. The actual projectile velocity at any point in the test section can be expressed as follows:

$$u_p \approx u(x) + \sigma + \Delta u_{EM} + \Delta u_{\ddot{x}} \quad (\text{A.5})$$

The relative uncertainty in projectile velocity is then:

$$\frac{\Delta u}{u(x)} \approx \frac{\sigma}{u(x)} + \frac{\Delta x}{\bar{x}} + \frac{\Delta t}{\bar{x}} u(x) + \frac{1}{8} \left(\frac{\ddot{x}(x)\bar{x}}{u(x)^2} \right)^2 \quad (\text{A.6})$$

where the expression $\ddot{x}(x)$ is used to emphasis that the projectile acceleration varies with distance. The contribution of acceleration effects to the velocity uncertainty is maximized if the peak acceleration of an experiment is used for $\ddot{x}(x)$ in Eq. A.6.

The actual projectile acceleration can be expressed in terms of the acceleration determined from the polynomial u-x history as follows:

$$u_p \frac{du_p}{dx} \approx u(x) \frac{du(x)}{dx} \left(1 + \frac{\Delta u}{\bar{u}} \right) \left(1 + \frac{d(\Delta u)}{dx} \frac{dx}{du} \right) \quad (\text{A.7})$$

Keeping only the first order terms in the above equation results in the following expression for the uncertainty in projectile acceleration:

$$\Delta \ddot{x} \approx \ddot{x}(x) \left(\frac{\Delta u}{\bar{u}} + \frac{d(\Delta u)}{du} \right) \quad (\text{A.8})$$

Assuming that a constant acceleration \ddot{x}_0 can be used to estimate the projectile acceleration effects on the velocity uncertainty, differentiating the expression for overall velocity uncertainty (Eq. A.5) results in the following:

$$\frac{d(\Delta u)}{dx} \approx \frac{\Delta x}{\bar{x}} + 2 \frac{\Delta t}{\bar{x}} u - \frac{3}{8} \left(\frac{\ddot{x}_0 \bar{x}}{u^2} \right)^2 \quad (\text{A.9})$$

The worst case error in acceleration is determined by adding the absolute values of the terms in Eqs. A.6 and A.9 together while assuming the maximum acceleration level was maintained throughout the experiment. This results in the following expression (Eq. 4.3 in text) for the overall relative uncertainty in projectile acceleration:

$$\frac{\Delta\ddot{x}}{\ddot{x}} \approx \frac{\sigma}{u} + 2 \frac{\Delta x}{\bar{x}} + 3 \frac{\Delta t}{\bar{x}} u + \frac{1}{2} \left(\frac{\ddot{x}_0 \bar{x}}{u^2} \right)^2 \quad (\text{A.10})$$

The uncertainties in the experimental \bar{u} - x and \ddot{x} - u profiles, due to ignoring the projectile acceleration when determining the initial \bar{u} - x data table, are small for the acceleration levels of the current experiments (Fig. 4.4), so the assumption of constant acceleration in the derivation of Eq. A.10 does not significantly affect the expression for the overall relative uncertainty in projectile acceleration when the projectile is traveling at velocities above 1200 m/sec (see Fig. 4.4).

Biographical Note

Carl Knowlen was born November 8, 1957 in Turlock, CA. After graduating from Cheney High School, he worked for a year in a lead-silver refinery before serving a 3 year enlistment with the US Army as a meteorological observer. After an honorable discharge in 1979, he began full time studies at Spokane Falls Community College, two years later he transferred to the University of Washington where he received his Aeronautical and Astronautical Engineering degree in June, 1983. The ram accelerator concept was just emerging as he began graduate school, he worked on the early theoretical modeling of various ram accelerator propulsive modes and was one of the original construction crew of graduate students that set up the initial experimental facility. He received his Master of Science in Aeronautics and Astronautics in March, 1985. A one year break from his graduate studies was taken so he could concentrate full time on the ram accelerator experiments, this contributed to the development of the "starting" process which initiates and stabilizes the thermally choked propulsive cycle. He has worked, since January 1987, on developing hypersonic propulsive concepts as well as his doctoral research on the thermally choked ram accelerator at the University of Washington.